



**HAL**  
open science

# Vibrations of a beam with a unilateral spring. Periodic solutions - Nonlinear normal modes

H. Hazim

► **To cite this version:**

H. Hazim. Vibrations of a beam with a unilateral spring. Periodic solutions - Nonlinear normal modes. Mathematics [math]. Université Nice Sophia Antipolis, 2010. English. NNT : . tel-00520999

**HAL Id: tel-00520999**

**<https://theses.hal.science/tel-00520999>**

Submitted on 24 Sep 2010

**HAL** is a multi-disciplinary open access archive for the deposit and dissemination of scientific research documents, whether they are published or not. The documents may come from teaching and research institutions in France or abroad, or from public or private research centers.

L'archive ouverte pluridisciplinaire **HAL**, est destinée au dépôt et à la diffusion de documents scientifiques de niveau recherche, publiés ou non, émanant des établissements d'enseignement et de recherche français ou étrangers, des laboratoires publics ou privés.

UNIVERSITÉ DE NICE-SOPHIA ANTIPOLIS - UFR Sciences  
École Doctorale Sciences Fondamentales et Appliquées

## THÈSE

Pour obtenir le titre de  
**Docteur en Sciences**  
de l'UNIVERSITÉ de Nice-Sophia Antipolis

Spécialité : **MATHÉMATIQUES**

présentée et soutenue par

**Hamad Hazim**

# **Vibrations of a beam with a unilateral spring. Periodic solutions - Nonlinear normal modes**

Thèse dirigée par **Bernard Rousselet**

Soutenue le 05 Juillet 2010

M. Hedy Attouch	Professeur, Université de Montpellier II	Rapporteur
M. Yann Brenier	Directeur de recherche, UNSA	Examineur
M. Neil Ferguson	Senior Lecturer, University of Southampton, U.K.	Examineur
M. Alain Léger	Directeur de recherche, L.M.A. CNRS, Marseille	Rapporteur
Mme. Francesca Rapetti	Maître de Conférence, HdR, UNSA	Examineur
M. Bernard Rousselet	Professeur, UNSA	Directeur
M. Jérôme Buffe	Responsable Ingénierie Mécanique, Thales Alenia Space	Invité

Laboratoire J.-A. Dieudonné  
Université de Nice  
Parc Valrose, 06108 Nice Cedex 2







# Remerciements

*Je voudrais, en premier lieu, remercier mon directeur de thèse, Bernard Rousselet, Professeur à l'UNSA, pour ce qu'il m'a apporté durant ces trois années, mais aussi pour sa patience, pour le temps qu'il m'a consacré et évidemment pour son bon encadrement lors de la thèse.*

*Je tiens à remercier Professeur Alain Léger, pour le temps qu'il a consacré à la lecture de ce mémoire et à la rédaction du rapport. Je le remercie également pour ses commentaires constructifs et ses suggestions, en particulier durant les journées du GDR 2501 d'acoustique. Merci également au Professeur Hedy Attouch pour avoir accepté de rapporter sur cette thèse, pour ses suggestions et pour sa présence au sein du jury.*

*Je souhaite également remercier les examinateurs, M.Yann Brenier, directeur de recherche à l'UNSA, M. Neil Ferguson, senior lecturer at the University of Southampton, M. Jérôme Buffe, responsable ingénierie Mécanique à Thales Alenia Space et Mme Francesca Rapetti, Maître de conférence et HdR à l'UNSA, pour avoir accepté d'être présents aujourd'hui.*

*Je remercie la direction de la société Thales Alenia Space, France, pour le financement de cette thèse. En espérant que le travail présenté soit au niveau de leur attente. Je ne peux pas passer sur cet aspect sans citer les efforts de mon directeur et de Mme Samia Gill pour établir ce contrat de recherche.*

*Je remercie aussi Mme Stéphanie Behar, responsable Cellule Expertise Mécanique et M. Jérôme Buffe qui ont suivi la thèse du côté de Thales Alenia Space. Ce travail n'aurait pas été accompli de cette façon sans leur support, notamment sur la partie expérimentale. Je tiens également à remercier M. Grégory Ladurrée qui s'occupait de cette thèse avant son départ pour l'ESA.*

*Mes remerciements vont aussi à M. Gérard Vanderborck, M.Bernard Grangier, M. Marc Constancio et M.Roger Thannberger de Thales Underwater System, Sophia Antipolis, pour leur aide et pour le bon déroulement des essais expérimentaux.*

*Je remercie M. Stéphane Junca, Maître de conférence à l'UNSA, avec lequel j'ai eu la chance de travailler et de discuter surtout sur la partie analytique.*

*Je suis reconnaissant au Professeur Gérard Iooss pour ses conseils, ses explications et sa disponibilité.*

*Je suis aussi reconnaissant à M. Abdul Habbal, Maître de conférence à l'UNSA, qui m'a profondément soutenu durant la préparation de cette thèse, et à M. Mohammad El Kadi, Maître de conférence à l'UNSA, qui m'a beaucoup aidé sur différents aspects, notamment au début lors de mon arrivé au laboratoire.*

*J'exprime ma gratitude envers tout les membres du laboratoire Jean Alexandre Dieudonné, Professeurs, Maîtres de conférence, Ingénieurs, personnes administratives et techniciens, pour m'avoir accueilli durant ces trois ans. Je remercie les responsables de l'école doctorale EDSFA et du CED pour le bon suivi des doctorants ainsi que pour toutes les formations proposées.*

*I gratefully thank Doctor Neil Ferguson and all members of the Institute of Sound and Vibrations Research, Southampton, U.K., where I spent around two months. This period was very important for the success of the experimental part of the thesis.*

*Je tiens à remercier mes professeurs de l'université libanaise à Tripoli où j'ai eu mon premier diplôme en mathématiques.*

*Durant ces trois ans, j'ai eu la chance de rencontrer plusieurs amis avec lequel j'ai partagé des bons moments. Notamment (Sans ordre :- ) Sarrage (10 ans?!), Hanzoul (habibi), Hayssam (ahla 3alam), Akhi Osman (Tibe.. :-)), Ahed (Rafik), Soleiman (3ala rassi), Jérôme (sympa co-bureau essa-essa-essatement), Thang (co-bureau très force! magnifisse!), Luca (amico!), Nikolas (amigo!), Sami, Federicco (il mio caz.. maestro d'italiano :-)), Nahla, Houssam (l'Ingénieur l khadoum), Taleb, Claire (pré-rapporteur de tout :)), Nadia, Isabelle (mach 3 en fr) et Wassila (atyab couscous :-)). Je n'oublie pas les collègues doctorants et ancien doctorants du laboratoire J.A.D que j'ai eu l'honneur de les connaître.*

*Je suis reconnaissant à mon oncle Ali Assaad et sa famille qui m'ont accueilliet m'ont soutenu surtout au début de mon arrivée en France, merci!*

*A propos de Cristina, c'est une amie exceptionnelle que j'ai eu la chance de la connaître. Elle était toujours et continue à être à mon côté. Je te remercie pour tout le bien que tu m'as apporté (Ch, Laz, am1, am2, ma, lat etc... :-)). Ti auguro tutti le fortune nel tuoi progetti!*

*Mes "11" soeurs et frères étaient mon support solide depuis toujours, notamment Fida et Oussama, avec lesquels j'ai vécu la période la plus difficile au Liban, grazie! Ca ne sera pas complet si je ne cite pas (dans l'ordre décroissant :) Louàa, Samar, Inad, Abed, Racha, Bassel, Malak, Asraa, Sara et ma nièce Nathalia et bien sure son père Mouamar.*

*Finalement, cette thèse est dédiée aux personnes qui la méritent, ma mère et mon père! C'est un petit cadeau négligeable devant la vie qu'ils ont sacrifié pour élever cette grande famille.*





# Contents

<b>1</b>	<b>Numerical and experimental study for a beam with unilateral elastic contact under a support excitation</b>	<b>23</b>
1.1	Introduction . . . . .	23
1.1.1	State of the problem . . . . .	23
1.1.2	State of the art . . . . .	24
1.1.3	The present contribution . . . . .	24
1.2	Modelling . . . . .	25
1.2.1	Partial differential equation of the motion . . . . .	25
1.2.2	Adimensional analysis . . . . .	26
1.2.3	Finite Element approximations . . . . .	27
1.2.4	Existence of the solutions . . . . .	27
1.3	Experimental validations . . . . .	27
1.3.1	Experimental setup and instruments . . . . .	28
1.3.2	Highlights on the linear states of the system . . . . .	30
1.3.3	Characterization of the Solithane snubber . . . . .	30
1.3.4	Parameters identifications and model adjustments . . . . .	32
1.4	Beam in a one sided contact with a spring . . . . .	33
1.4.1	Comparison in the frequency domain . . . . .	33
1.4.2	Comparison in the time domain . . . . .	33
1.4.3	Numerical predictions . . . . .	33
1.4.4	Frequency sweep . . . . .	34
1.4.5	Conclusion . . . . .	35
1.5	Beam in contact with a pre-Stressed spring . . . . .	41
1.5.1	Comparison in the frequency domain . . . . .	41
1.5.2	Numerical predictions . . . . .	42
1.5.3	Conclusion . . . . .	43
1.6	Beam in contact with a spring in the presence of backlash . . . . .	53
1.6.1	Comparison in the frequency domain . . . . .	53
1.6.2	Numerical predictions . . . . .	53
1.6.3	Conclusion . . . . .	53
1.7	General conclusion and perspectives . . . . .	58
1.8	Acknowledgment . . . . .	58
<b>2</b>	<b>The vibration of a beam with a local unilateral elastic contact</b>	<b>59</b>
2.1	Introduction . . . . .	61
2.2	Numerical modelling . . . . .	62

2.3	Experimental validation . . . . .	63
2.4	Beam piecewise linear system dynamics . . . . .	64
2.4.1	The two linear states . . . . .	64
2.4.2	Characterization of the spring support stiffness . . . . .	64
2.5	Comparison of simulations with experiments . . . . .	65
2.5.1	Comparison in the frequency domain . . . . .	66
2.5.2	Magnitude-Energy dependence . . . . .	66
2.6	Numerical simulations . . . . .	67
2.7	The effect of the unilateral spring position . . . . .	68
<b>3</b>	<b>A numerical method to compute nonlinear normal modes of mechanical systems</b>	<b>83</b>
3.1	Introduction . . . . .	85
3.1.1	State of the Art . . . . .	85
3.1.2	In this paper . . . . .	86
3.2	Mechanical system and normal modes . . . . .	87
3.2.1	Normal Modes of the linearized system . . . . .	87
3.2.2	Nonlinear Normal Modes (NNM) of the nonlinear system . . . . .	87
3.3	Nonlinear normal modes: mathematical formulation . . . . .	88
3.3.1	Nonlinear differential system . . . . .	88
3.3.2	Formulation . . . . .	89
3.4	Theoretical investigation in the smooth case . . . . .	89
3.4.1	Useful theorems . . . . .	89
3.5	An algorithm to compute the nonlinear normal modes . . . . .	91
3.5.1	A relaxed problem . . . . .	91
3.5.2	The algorithm . . . . .	91
3.5.3	Energy dependence . . . . .	91
3.5.4	Calculation of the gradient in the smooth case . . . . .	93
3.6	Numerical results . . . . .	95
3.6.1	Mass-spring model with a cubic spring . . . . .	95
3.6.2	Mass-spring model with a unilateral spring . . . . .	99
3.6.3	Cantilever beam with a unilateral spring . . . . .	104
3.7	Conclusion and perspectives . . . . .	107
<b>4</b>	<b>The method of multiple scales for a model of a unilateral contact</b>	<b>109</b>
4.1	Introduction . . . . .	109
4.2	One degree of freedom nonlinear forced oscillator . . . . .	110
4.2.1	The method of multiple scales - First order approximation . . . . .	110
4.3	One degree of freedom nonlinear autonomous oscillator . . . . .	113
4.3.1	A stationary approximate solution [Permanent regime] . . . . .	117
4.3.2	Stability of the approximate solution . . . . .	118
4.3.3	Numerics . . . . .	118
4.4	Nonlinear normal mode of systems with unilateral contact . . . . .	120
4.4.1	Equation of motion in the eigenvector space . . . . .	120
4.4.2	The method of multiple scales . . . . .	121

4.4.3	Nonlinear normal mode of the autonomous system with unilateral contact . . . . .	123
4.4.4	Bounds on the remainders . . . . .	126
4.4.5	Comparison between the numerical solutions and the asymptotic expansions . . . . .	128
4.4.6	Nonlinear normal mode of a beam with a unilateral spring . . . . .	132
4.5	Nonlinear normal modes and forced systems . . . . .	135
4.5.1	Multiple scales expansion of forced system with unilateral contact .	135
4.5.2	Bounds on the remainder . . . . .	137
4.5.3	Approximate steady state solution . . . . .	141
4.5.4	Stability of the approximate solution . . . . .	142
4.5.5	Alternative Calculation of the nonlinear normal modes with an excitation force . . . . .	142
4.5.6	Numerical results of a cantilever beam with a unilateral elastic contact	144
4.6	conclusion . . . . .	147

## List of Figures

1.1	Beam system in unilateral contact with a bumper modeled as a linear spring.	25
1.2	Schematic of the cantilever Beam and the unilateral contact, the snubber was modelled as a linear spring. . . . .	28
1.3	Photo of the cantilever aluminum beam on a shaker with four accelerometers.	29
1.4	The cantilever aluminum beam in contact with the Solithane snubber at the free end. The whole system is based on a shaker which produces a harmonic motion of support given as an imposed acceleration $a(s) = -\frac{a}{\omega^2}d(s)$ . . . . .	29
1.5	The frequency contents of the measured (dashed line) and the predicted (solid line) acceleration for an excitation at 45 Hz and for a magnitude of $2g$ . The data are measured above the elastic support, the frequency axis is normalized by the excitation frequency. . . . .	35
1.6	The frequency contents of the measured (dashed line) and the predicted (solid line) acceleration for an excitation at 65 Hz and for a magnitude of $2g$ . The data are measured above the elastic support, the frequency axis is normalized by the excitation frequency. . . . .	36
1.7	The frequency contents of the measured (dashed line) and the predicted (solid line) acceleration for an excitation at 78 Hz and for a magnitude of $2g$ . The data are measured above the elastic support, the frequency axis is normalized by the excitation frequency. . . . .	36

1.8	The frequency contents of the measured (dashed line) and the predicted (solid line) acceleration for an excitation at 160 Hz and for a magnitude of $2g$ . The data are measured above the elastic support, the frequency axis is normalized by the excitation frequency. . . . .	37
1.9	the predicted (a) and the measured (b) acceleration for an excitation at 45 Hz and for a magnitude of $2g$ ; the data are measured above the elastic support .	37
1.10	the predicted (a) and the measured (b) acceleration for an excitation at 65 Hz and for a magnitude of $2g$ ; the data are measured above the elastic support .	37
1.11	the predicted (a) and the measured (b) acceleration for an excitation at 78 Hz and for a magnitude of $2g$ ; the data are measured above the elastic support .	38
1.12	the predicted (a) and the measured (b) acceleration for an excitation at 160 Hz for a magnitude of $2g$ ; the data are measured above the elastic support .	38
1.13	The numerical displacement of the free end of the beam for an excitation at 45 Hz and 65 Hz, the magnitude of excitation is $2g$ . . . . .	38
1.14	The numerical displacement of the free end of the beam for an excitation at 78 Hz and 160 Hz, the magnitude of excitation is $2g$ . . . . .	39
1.15	The predicted force time signal for an excitation at 45 Hz and 65 Hz, the magnitude of excitation is $2g$ . The force is induced by the spring contact. . .	39
1.16	The predicted force time signal for an excitation at 78 Hz and 160 Hz, the magnitude of excitation is $2g$ . The force is induced by the spring contact. . .	40
1.17	Frequency sweep of the system with unilateral contact (solid line) compared to the sweep of the cantilever beam without contact (dashed line). The first natural frequency of the linear system is shifted to the right to become the first nonlinear frequency. The harmonics of this nonlinear frequency also appear as well as the subharmonics of the second nonlinear frequency. . . .	40
1.18	Frequency sweep around the position of the first linear normal mode and the corresponding nonlinear normal modes with its harmonics. . . . .	41
1.19	The frequency contents of the measured (dashed line) and the predicted (solid line) acceleration for an excitation at 465 Hz and for a magnitude of $1g$ . The data is measured above the elastic support, the frequency axis is normalized by the excitation frequency. The response contains a single peak which mean that the system responds linearly. . . . .	43
1.20	The input imposed acceleration frequency contents measured on the shaker for an excitation at 465 Hz and a magnitude of $1g$ , it is not a single sine wave excitation as there is some noise. The small peaks appears also in the response corresponding to this excitation. . . . .	44
1.21	The frequency contents of the measured (dashed line) and the predicted (solid line) acceleration for an excitation at 90 Hz and for a magnitude of $0.5g$ . The data is measured above the elastic support, the frequency axis is normalized by the excitation frequency. The response contains a single peak which mean that the system responds linearly. . . . .	44
1.22	The input imposed acceleration frequency contents measured on the shaker for an excitation at 90 Hz and a magnitude of $0.5g$ , it is not a single sine wave excitation as there is some noise. The small peaks appears also in the response corresponding to this excitation. . . . .	45

1.23	The frequency contents of the measured (dashed line) and the predicted (solid line) acceleration for an excitation at 160 Hz and for a magnitude of $5g$ . The data is measured above the elastic support, the frequency axis is normalized by the excitation frequency. The response contains all the harmonics which means that the system responds nonlinearly. . . . .	45
1.24	The frequency contents of the measured (dashed line) and the predicted (solid line) acceleration for an excitation at 90 Hz and for a magnitude of $3g$ . The data is measured above the elastic support, the frequency axis is normalized by the excitation frequency. The response contains all the harmonics which means that the system responds nonlinearly. . . . .	46
1.25	The frequency contents of the measured (dashed line) and the predicted (solid line) acceleration for an excitation at 220 Hz and for a magnitude of $8g$ . The data is measured above the elastic support, the frequency axis is normalized by the excitation frequency. The response contains all the harmonics which means that the system responds nonlinearly. . . . .	46
1.26	The frequency contents of the measured (dashed line) and the predicted (solid line) acceleration for an excitation at 465 Hz and for a magnitude of $15g$ . The data is measured above the elastic support, the frequency axis is normalized by the excitation frequency. The response contains all the harmonics which means that the system responds nonlinearly. . . . .	47
1.27	The numerical displacement of the free end of the beam for an excitation at 90 Hz, the magnitude of excitation is $0.5g$ . The signal corresponds to a linear system with a positive mean. . . . .	47
1.28	The numerical displacement of the free end of the beam for an excitation at 465 Hz, the magnitude of excitation is $1g$ . The signal corresponds to a linear system with a positive mean. . . . .	48
1.29	The numerical displacement of the free end of the beam for an excitation at 45 Hz, the magnitude of excitation is $3g$ . The signal corresponds to a nonlinear system with a positive mean. . . . .	48
1.30	The numerical displacement of the free end of the beam for an excitation at 90 Hz, the magnitude of excitation is $3g$ . The signal corresponds to a nonlinear system with a positive mean. . . . .	49
1.31	The numerical displacement of the free end of the beam for an excitation at 160 Hz, the magnitude of excitation is $5g$ . The signal corresponds to a nonlinear system with a positive mean. . . . .	49
1.32	The predicted force time signal for an excitation at 90 Hz, the magnitude of excitation is $0.5g$ . The force is induced by the spring contact, it is linear with the same period as the corresponding acceleration and it is permanently positive. . . . .	50
1.33	The predicted force time signal for an excitation at 465 Hz, the magnitude of excitation is $1g$ . The force is induced by the spring contact, it is linear with the same period as the corresponding acceleration and it is permanently positive. . . . .	50

1.34	The predicted force time signal for an excitation at 45 Hz, the magnitude of excitation is $3g$ . The force is induced by the spring contact, it is nonlinear with the same period as the corresponding acceleration and it is permanently positive. . . . .	51
1.35	The predicted force time signal for an excitation at 90 Hz, the magnitude of excitation is $3g$ . The force is induced by the spring contact, it is nonlinear with the same period as the corresponding acceleration and it is permanently positive. . . . .	51
1.36	The predicted force time signal for an excitation at 465 Hz, the magnitude of excitation is $15g$ . The force is induced by the spring contact, it is nonlinear with the same period as the corresponding acceleration and it is permanently positive. . . . .	52
1.37	The frequency contents of the measured (dashed line) and the predicted (solid line) acceleration for an excitation at 45 Hz and for a magnitude of $2g$ for $5mm$ of backlash. The data is measured above the elastic support, the frequency axis is normalized by the excitation frequency. The response contains all the harmonics which means that the system responds nonlinearly. . . . .	54
1.38	The frequency contents of the measured (dashed line) and the predicted (solid line) acceleration for an excitation at 65 Hz and for a magnitude of $3g$ for $5mm$ of backlash. The data is measured above the elastic support, the frequency axis is normalized by the excitation frequency. The response contains all the harmonics which means that the system responds nonlinearly. . . . .	54
1.39	The frequency contents of the measured (dashed line) and the predicted (solid line) acceleration for an excitation at 110 Hz and for a magnitude of $13g$ for $5mm$ of backlash. The data is measured above the elastic support, the frequency axis is normalized by the excitation frequency. The response contains all the harmonics which means that the system responds nonlinearly. . . . .	55
1.40	The numerical displacement of the free end of the beam for an excitation at 65 Hz, the magnitude of excitation is $3g$ . The signal corresponds to a nonlinear system. . . . .	55
1.41	The numerical displacement of the free end of the beam for an excitation at 110 Hz, the magnitude of excitation is $13g$ . The signal corresponds to a nonlinear system. . . . .	56
1.42	The predicted force time signal for an excitation at 65 Hz, the magnitude of excitation is $3g$ . The force is induced by the spring contact. . . . .	56
1.43	The predicted force time signal for an excitation at 110 Hz, the magnitude of excitation is $13g$ . The force is induced by the spring contact. . . . .	57
1.44	Frequency sweep of the system with unilateral spring in a backlash position (solid line) compared to the sweep of the linear free beam (dashed line). Both curves overlay at the frequency where the beam loses contact with the spring. This frequency point depends on the excitation magnitude. . . . .	57
2.1	A schematic of the experimental setup. . . . .	63
2.2	Left: Solar array of a satellite under a test on a shaker. Right: A solar array from the folded to the final position . . . . .	69

2.3	beam system with an unilateral spring under a periodic excitation . . . . .	69
2.4	The rig used for the experiments: a linear clamped-free beam in contact with a rubber support (enlarged photograph on the right). . . . .	70
2.5	Predicted (solid) and measured displacements (dashed) (dB) for an excitation at 32 Hz applied to the beam with unilateral support stiffness. The displacement is normalized by the peak value and is measured immediately above the support and the frequency axis is normalized by the excitation frequency. . . . .	70
2.6	Predicted (solid) and measured displacements (dashed) (dB) for an excitation at 124 Hz applied to the beam with unilateral support stiffness. The displacement is normalized by the peak value and is measured immediately above the support and the frequency axis is normalized by the excitation frequency. . . . .	71
2.7	Predicted (solid) and measured displacements (dashed) (dB) for an excitation at 100 Hz applied to the beam with unilateral support stiffness. The displacement is normalized by the peak value and is measured immediately above the support and the frequency axis is normalized by the excitation frequency. . . . .	71
2.8	Measured excitation force (a) and its frequency contents (b), measured acceleration response (c) and its frequency content (d) for an excitation at 32 Hz. Strictly the force is not harmonic. . . . .	72
2.9	Measured excitation force (a) and its frequency contents (b), the measured acceleration response (c) and its frequency content (d) for an excitation at 124 Hz. Strictly the force is not harmonic. . . . .	73
2.10	The predicted displacements for an excitation at 32 Hz; the displacement is measured immediately above the support. The high unilateral stiffness yields almost a positive displacement. . . . .	74
2.11	The predicted displacements for an excitation at 124 Hz, the displacement is measured immediately above the support. . . . .	74
2.12	The predicted displacements for an excitation at 100 Hz, the displacement is measured immediately above the support. . . . .	75
2.13	The normalized mean square responses (mean square displacement divided by the mean square excitation force) in each harmonic for inputs at three different mean square force levels. The excitation frequency is 32 Hz, the acceleration is measured immediately above the support. . . . .	75
2.14	The predicted displacements for a sine excitation at 32 Hz, The acceleration magnitude is $a = 1 \text{ m/s}^2$ . The displacement is measured immediately above the support. . . . .	76
2.15	The predicted displacements for a sine excitation at 124 Hz. The acceleration magnitude is $a = 1 \text{ m/s}^2$ . The displacement is measured immediately above the support. . . . .	76
2.16	The frequency content of the predicted numerical displacement for sine excitation at 32 Hz, the displacement is measured immediately above the support. The excitation frequency is split into all its harmonics. . . . .	77
2.17	The predicted elastic force of the spring support for an excitation at 32 Hz. The acceleration magnitude is $a = 0.1 \text{ m/s}^2$ and the spring is only in contact at times where the beam displacement is negative. . . . .	77

2.18	The predicted elastic force of the spring support for an excitation at 124 Hz. The acceleration magnitude is $a = 0.1m/s^2$ and the spring is only in contact at times where the beam displacement is negative. . . . .	78
2.19	beam system with an unilateral spring under a periodic excitation . . . . .	78
2.20	Predicted (solid) and measured displacements (dB) for an excitation at 122 Hz applied to the beam with unilateral support stiffness. The displacement is measured immediately above the support and the frequency axis is normalized by the excitation frequency. . . . .	79
2.21	The time signal and its FFT of the input force for an excitation at 122 Hz. . . . .	80
2.22	Predicted (solid) and measured displacements (dB) for an excitation at 32 Hz applied to the beam with unilateral support stiffness. The displacement is measured immediately above the support and the frequency axis is normalized by the excitation frequency. . . . .	81
3.1	A mass-spring model with a cubic component. . . . .	95
3.2	The displacements of the six nodes for the fourth nonlinear normal mode, the period is $T_{n2} = 3.93$ s and the corresponding frequency is $f_{n2} = 0.254$ Hz. All the components have the same period and they reach their maximum at the same time. 66 steps in $\epsilon$ to reach this nonlinearity, The value of the functional $J_\epsilon$ at the last iteration is $10^{(-6)}$ and the average CPU time is 0.06 s for a calculation of the function and the gradient. The total CPU time is 6.6 minutes. . . . .	97
3.3	The displacements of the fifth node (a) and the first node (b) of the linear system (dashed line) and of the nonlinear system (solid line) for the second nonlinear normal mode. . . . .	97
3.4	The displacements of all nodes as function of the fifth one, the curves are not straight lines and their shapes depend on the form of the nonlinearity. . . . .	98
3.5	The second nonlinear frequency of the system as function of the nonlinearity (a), the FFT of the displacement for an integration time of 50 nonlinear period (b). . . . .	98
3.6	The phase space (solid line) compared to the corresponding linear phase space (dashed line) of the fifth node (a) and the fourth node (b). . . . .	99
3.7	A mass-spring model with a unilateral component. . . . .	99
3.8	The displacements of the six nodes for the fourth nonlinear normal mode, the period is $T_{n2} = 4.011$ s and the corresponding frequency is $f_{n2} = 0.249$ Hz. All the components have the same period and they reach their maximum at the same time. 35 steps in $\epsilon$ to reach this nonlinearity, The value of the functional $J_\epsilon$ at the last iteration is $10^{(-6)}$ and the average CPU time is 0.08 s for a calculation of the functional and the gradient, the total CPU time of optimization is 4.65 minutes. . . . .	100
3.9	The configuration and the phase spaces for the fourth nonlinear normal mode for $\epsilon = 0.5$ . The lines in the configuration space are not symmetric as for the linear system's lines. The ellipse in the phase space (solid line) has a small deformation comparing to the ellipse of the linear system (dashed line). . . . .	101

3.10	The displacements of the six nodes for the second nonlinear normal mode, the period is $T_{n2} = 3.97$ s and the corresponding frequency is $f_{n2} = 0.251$ Hz. 55 steps in $\epsilon$ to reach this nonlinearity. The value of the functional $J_\epsilon$ at the last iteration is $10^{(-6)}$ and the average CPU time is 0.09 s for a calculation of the functional and the gradient, the total CPU time of optimization is 8.25 minutes . . . . .	101
3.11	The displacements of the fifth node (a) and the first node (b) of the linear system (dashed line) and of the nonlinear system (solid line) for the second nonlinear normal mode. . . . .	102
3.12	The displacements of the nodes as function of the fifth one, the curve are not a straight line anymore, this shape depends on the form of the nonlinearity. . . . .	102
3.13	The second nonlinear frequency of the system as function of the nonlinearity (a); The FFT of the displacement for an integration time of 50 nonlinear period (b). . . . .	103
3.14	The phase space (solid line) compared to the corresponding linear phase space (dashed line) of the fifth node (a) and the fourth node (b). . . . .	103
3.15	The first nonlinear normal mode of the beam with a unilateral contact (solid line) compared to the linear normal mode (dashed line) for a spring stiffness $k_r = 107000$ N/m and for $\epsilon = 1$ . . . . .	105
3.16	The displacements of six nodes for the first nonlinear normal mode, the period is $T_{n2} = 0.017$ s and the corresponding frequency is $f_{n2} = 57.62$ Hz. 75 steps in $\epsilon$ to reach this nonlinearity, The value of the functional $J_\epsilon$ at the last iteration is $10^{(-5)}$ and the average time computation is 10 seconds for a calculation of the function and the gradient for ten finite elements discretization. The total CPU time is 20 hours. . . . .	105
3.17	The configuration and the phase spaces for the first nonlinear normal mode for $\epsilon = 1$ . The lines in the configuration space are not symmetric as for the linear system's lines. The ellipse in the phase space (solid line) has a small deformation comparing to the ellipse of the linear system (dashed line). . . . .	106
3.18	The second nonlinear normal mode of the beam with a unilateral contact (solid line) compared to the linear normal mode (dashed line) for a spring stiffness $k_r = 107000$ N/m and for $\epsilon = 0.1$ . . . . .	106
3.19	The displacements of six nodes for the second nonlinear normal mode, the period is $T_{n2} = 0.0028$ s and the corresponding frequency is $f_{n2} = 354.91$ Hz. . . . .	107
4.1	The frequency contents of the steady state solution for $\epsilon = 0.1$ , $\xi = 1$ and $\omega = 1.1$ . the frequency axis is normalized by the frequency of excitation, the response contains peaks corresponding to the excitation frequency and to its even harmonic. . . . .	119
4.2	The numerical solution (solid line) and the explicit solution (dashed line) for $\epsilon = 0.1$ , $\xi = 1$ and $\omega = 1.1$ . The two solutions are close but a small difference appear when the displacement is positive. . . . .	119
4.3	The numerical solution (solid line) and the explicit solution (dashed line) for $\epsilon = 0.01$ , $\xi = 1$ and $\omega = 1.1$ . The two solutions feet very well. . . . .	120

4.4	The initial condition vector which ensures the fourth nonlinear normal mode by asymptotic expansion (solid line) and by the numerical algorithm (dashed line) for $\epsilon = 0.02$ . . . . .	130
4.5	The displacement calculated by asymptotic expansion (solid line) and by the numerical algorithm (dashed line) of the first node (a) and the fifth node (b) for $\epsilon = 0.02$ . . . . .	130
4.6	The initial condition vector which ensures the first nonlinear normal mode by asymptotic expansion (solid line) and by the numerical algorithm (dashed line) for $\epsilon = 0.015$ . . . . .	131
4.7	The displacement calculated by asymptotic expansion (solid line) and by the numerical algorithm (dashed line) of the first node (a) and the fifth node (b) for $\epsilon = 0.015$ . . . . .	131
4.8	The first nonlinear normal mode (solid line) compared to the corresponding linear normal mode (dashed line) for $k_r = 107000 \text{ N/m}$ and for $\epsilon = 1$ . The spring is localized at the free end of the beam. . . . .	132
4.9	The second nonlinear normal mode (solid line) compared to the corresponding linear normal mode (dashed line) for $k_r = 107000 \text{ N/m}$ and for $\epsilon = 0.1$ . The spring is localized at the free end of the beam. . . . .	133
4.10	The third nonlinear normal mode (solid line) compared to the corresponding linear normal mode (dashed line) for $k_r = 107000 \text{ N/m}$ and for $\epsilon = 0.1$ . The spring is localized at the free end of the beam. . . . .	133
4.11	The second nonlinear normal mode (solid line) compared to the corresponding linear normal mode (dashed line) for $k_r = 107000 \text{ N/m}$ and for $\epsilon = 1$ . The spring is localized in the middle of the beam. . . . .	134
4.12	The third nonlinear normal mode (solid line) compared to the corresponding linear normal mode (dashed line) for $k_r = 107000 \text{ N/m}$ and for $\epsilon = 1$ . The spring is localized in the middle of the beam. . . . .	134
4.13	The first approximate nonlinear normal mode, the nonlinear frequency is 77.58 Hz for $\epsilon = 5$ and $k_r = 107000 \text{ N/m}$ . . . . .	144
4.14	The first deflexion mode shape for two time points . . . . .	145
4.15	The displacement of the last node for 50 nonlinear periods for an excitation at the first nonlinear mode . . . . .	145
4.16	The second approximate nonlinear normal mode, the nonlinear frequency is 340 Hz for $\epsilon = 5$ and $k_r = 107000 \text{ N/m}$ . . . . .	146
4.17	The second deflexion mode shape for two time points . . . . .	146
4.18	The displacement of the last node for 50 nonlinear periods for an excitation at the second nonlinear mode . . . . .	147

# List of Algorithms

1	Characterization of the rubber . . . . .	31
2	Calculation of the nonlinear normal mode . . . . .	92
3	Energy dependence . . . . .	92



# Introduction

## Motivations

La réduction de la masse des panneaux solaires d'un satellite entraîne une flexibilité qui devient non négligeable. Ces panneaux, soumis à des vibrations de la base durant la phase de lancement, peuvent s'entrechoquer en provoquant un endommagement de la structure. Ainsi, en prévention, des cales sont fixées dans des endroits bien choisis sur la structure; ils jouent le rôle d'un ressort élastique unilatéral. Cependant, cet ajout a une conséquence négative sur la compréhension du phénomène car la dynamique de ces panneaux devient non-linéaire. De nombreux logiciels industriels sont conçus pour traiter des problèmes de vibrations linéaires donc ne peuvent pas prévoir le comportement non-linéaire de la structure. L'objet de cette étude est de fournir un modèle mathématique validé expérimentalement qui pourra traiter le problème de contact entre ces panneaux et les cales unilatérales. On considère alors un problème unidimensionnel de contact élastique. L'analyse modale de ce système apporte une bonne compréhension de la dynamique, d'où la motivation pour l'étude des modes normaux non-linéaires (MNN), une notion introduite par des mécaniciens pour étendre le concept des modes normaux du cas linéaire.

## Problèmes de contact

Si le contact unilatéral dans le cas statique est largement étudié en mathématiques et en mécanique, le cas dynamique est moins étudié. L'existence et l'unicité des solutions dans le cas rigide ont fait l'objet de plusieurs travaux mathématiques dont on cite ici quelques références.

G.Lebeau et M.Schatzman ont montré l'existence et l'unicité pour le problème de propagation d'onde avec une condition unilatérale au bord du domaine [1]; M.Schatzman a aussi montré l'existence d'une solution pour des systèmes unidimensionnels en présence d'un impact [2]. C. Pozzolini et A.Léger ont présenté un résultat de stabilité dans un problème d'obstacle avec une plaque. Ils ont établi un théorème de stabilité qui relie les évolutions de la zone de contact à celles des forces extérieures [3, 4].

## Modes normaux non-linéaires

Les modes normaux non-linéaires sont présentés comme une extension naturelle des modes normaux linéaires. Le calcul de ces modes non-linéaires donne accès à une meilleure com-

préhension de la dynamique des systèmes mécaniques en étudiant l'effet de la non-linéarité sur ses modes propres (linéaires). Un mode normal non-linéaire est défini comme une solution périodique de toutes les composantes du système mécanique de même phase; cette solution peut être trouvée en excitant le système par un vecteur particulier de condition initiale en position et en vitesse; cette condition initiale est à déterminer. Une introduction détaillée est présentée au Chapitre 3.

## Travail présenté dans la thèse

La thèse est composée des deux parties majeures présentées en quatre chapitres. La première partie traite de la modélisation, des simulations et des validations expérimentales d'un modèle de poutre en contact unilatéral avec un ressort unilatéral sous une excitation périodique. Le travail correspondant est présenté aux Chapitres 1 et 2.

La deuxième partie est concentrée sur les modes normaux non-linéaires des systèmes mécaniques. Un algorithme numérique est présenté au Chapitre 3. La méthode des échelles multiples est utilisée dans le Chapitre 4 pour traiter le cas d'un contact unilatéral.

Chaque chapitre commence par une introduction motivant le travail et décrivant le contenu. On ne donnera donc ici qu'une brève description.

Dans le Chapitre 1, on présente un modèle de poutre en contact unilatéral avec un ressort linéaire modélisant respectivement un panneau solaire et une cale élastique. Le système est soumis à une excitation harmonique du support donnée sous forme d'une accélération imposée. Le modèle est validé expérimentalement par des séquences d'essais sur une poutre en aluminium en contact avec une cale en Solithane. Les résultats montrent une cohérence avec les solutions numériques obtenues.

Dans le Chapitre 2, un modèle équivalent à celui du Chapitre 1 est étudié, l'excitation du support est remplacée par une force excitatrice ponctuelle. Une validation expérimentale a été également réalisée et a confirmé le modèle.

Dans le Chapitre 3, une nouvelle formulation est présentée pour trouver ces modes comme zéros d'une application non-linéaire. Un algorithme utilisant des algorithmes existants, basé sur la continuité des solutions périodiques, est développé pour le calcul des modes normaux. Dans le dernier chapitre, on introduit la technique de développement asymptotique par échelles multiples pour le calcul d'une solution analytique approchée d'une équation différentielle avec un terme unilatéral. Le petit paramètre est la rigidité du ressort unilatéral. On utilise ensuite cette technique pour le calcul des modes normaux non-linéaires d'un système autonome à un nombre  $n$  de degrés de liberté avec un contact unilatéral. L'algorithme du Chapitre 3 est ainsi validé pour le cas d'une non-linéarité de type contact. Ceci nous donne un outils mathématiques validé pour le calcul des modes non-linéaires du système traité en Chapitre 1 et 2.

On traite aussi le cas d'un système forcé. Cette démarche abouti à une procédure numérique simple pour le calcul des modes normaux; elle donne aussi une interprétation expérimentale de ce concept.

Cette thèse est financée par Thales Alenia Space, Cannes, France.

# Chapter 1

## Numerical and experimental study for a beam with unilateral elastic contact under a support excitation

### 1.1 Introduction

The mass reduction of satellite solar arrays results in significant panel flexibility. When such structures are launched in a packed configuration there is a possible striking one with another dynamically, leading ultimately to structural damage during the launch stage. To prevent this, rubber snubbers are mounted at well chosen points of the structure and they act as a one sided linear spring. A negative consequence is that the dynamics of these panels becomes nonlinear and it cannot be treated with the classical tools of linear systems. The aim of this study is to provide an efficient numerical model which can predict the nonlinear behaviour produced by the unilateral spring.

#### 1.1.1 State of the problem

A simplified model of the satellite solar arrays with the snubbers will be considered and studied, it can help to understand the effect of the unilateral contact, then one can deduce useful information for the whole structure. In this study a solar array and a snubber are simply modelled as a linear Euler-Bernoulli beam with a one sided linear spring respectively. Rubbers are strongly nonlinear in general with a complicated behaviour law, but it is assumed to behave linearly for small displacement; the results show the relevance of the choice. The whole system is under a support periodic excitation given as an imposed acceleration, the magnitude depends then on the excitation frequency. The modelling does not take in account any friction during the contact between the beam and the spring, moreover the spring is massless and its own dynamics is not taken in account. This is done to simplify the problem since any friction can lead to a non differentiable velocity at the time of impact and then the classical equation of motion does not hold because we cannot calculate the acceleration as a classical derivative of the velocity. Note that the displacement is vertical and the motion takes place in a one dimensional space, it is also assumed that the velocity direction does not change as in shock problems.

### 1.1.2 State of the art

The study of the nonlinear behaviour of structures with a nonlinear contact or support is a relatively new research field of interest for many structural dynamicists. It is a branch of nonlinear dynamics with a special form of nonlinearity: the system has two linear local components and the nonlinearity comes from the interaction between one with the other. A crack in a structure, a fissure or a defect can be modeled as a unilateral linear or cubic spring; this kind of problems can be encountered in the nondestructive testing (NDT) and in wave propagation problems with unilateral constraint.

The effect of a unilateral element to the dynamic of a beam was also studied with an engineering point of view [5–7] where the focus was to study the stability using sweep tests experimentally and comparing numerical simulations, the latter computation uses special packages for nonlinear simulations. Other aspects of the unilateral contact have been studied such as in [8–10]. The vibrations of a beam with a unilateral contact under a force excitation have also been studied in a simple case [11–14]. The interest of the authors was to study the nonlinear systems in both the frequency and the time domains, as well as the internal properties of the systems like nonlinear normal modes (NNM) which is an extension of the well-known linear normal modes (LNM) (see [15–22]).

### 1.1.3 The present contribution

In this study a model of a cantilevered Euler-Bernoulli beam which strikes a one sided linear spring at the free end is presented, the system is under a periodic excitation of the base given as an imposed acceleration. A finite element numerical model was produced and was validated with subsequent experimental tests.

The spring and the beam can be in contact in three configurations: a point one sided contact, a contact with a pre-stress and a contact in the presence of backlash. The model takes in account all these configurations. Both numerical and experimental approaches are studied and completed, the experimental setup and the rig are briefly presented. The numerical results are presented and studied in both the frequency and the time domain. The experimental sequences consisted of exciting the system at different frequencies in an interval which contains the first two natural frequencies of the system, where a significant effect of the unilateral spring is expected to occur. A frequency sweep has also been performed to detect the frequencies of the nonlinear system, it is a classical method for detecting such frequencies. An alternative calculation of these frequencies can be obtained using the concept of the nonlinear normal modes studied in Chapters 3 and 4.

Note that no signal analysis is done by the acquisition system, as the problem is nonlinear and the standard transfer function calculation is only really applicable and useful for linear systems and its use could lose the nonlinearity being investigated. The time signal was acquired and the processing performed using external software (Scilab [23]). The numerical predictions are compared to experimental results and show very good agreement. The study finishes by a general conclusion and perspectives.

## 1.2 Modelling

The present study deals with the behaviour of a beam which strikes a snubber under a periodic excitation. It is a simplified model of a satellite solar array striking a snubber during the launch phase. The vibration of the base is modelled as an imposed harmonic acceleration of the support; the bumper (snubber) is modelled as a unilateral linear spring at the free end of the beam. The contact between the spring and the beam takes three possible positions: a one sided contact, a pre-stressed contact and a contact with a backlash.

The model is presented first, then an equivalent adimensional model is produced to avoid technical problems encountered during the numerical integration of the differential equations obtained after finite element approximation. Finally, a description of the finite elements used for the discretization is discussed as well as the numerical methods used for the computation of periodic solutions.

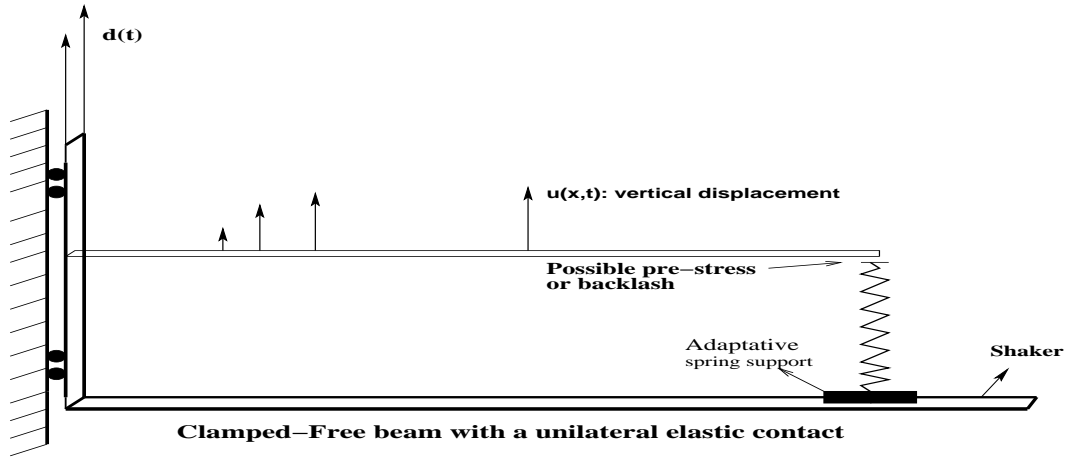


Figure 1.1. Beam system in unilateral contact with a bumper modeled as a linear spring.

### 1.2.1 Partial differential equation of the motion

The equations of motion of an Euler-Bernoulli linear beam in contact with a unilateral spring for the three positions of the spring can be expressed as

$$\rho S \partial_s^2 u(y, s) + \xi \partial_s u(y, s) + EI \partial_y^4 u(y, s) = 0, \quad (1.2.1)$$

where  $s$  is the time,  $\rho$ ,  $S$ ,  $E$ ,  $I$  and  $\xi$  are respectively the beam density, cross-sectional area, Young's modulus of elasticity, second moment of area and the beam structural damping coefficient. Cantilevered beam boundary conditions assume zero slope at the fixed end and zero bending moment at the free end.

The whole system is under a periodic imposed acceleration  $-\frac{a}{\omega^2} d(s)$ ; when the elastic unilateral spring is in contact then a force is present due to the reaction from the spring, it is considered as a boundary force,

$$u(0, s) = d(s) = a \sin(\omega s), \quad \partial_y u(0, s) = 0, \quad EI \partial_y^2 u(L, s) = 0,$$

$$EI\partial_y^3 u(L, s) = [k_r(d(s) - u(L, s) + z)]_+ - \xi_r \left[ \left( \frac{1 - \text{sign}(u(L, s))}{2} \right) \partial_s u(L, s) \right].$$

$z = 0$  for a one sided contact,  $z > 0$  for a pre-stressed contact and  $z < 0$  for a backlash contact.  $k_r$  and  $\xi_r$  are the spring stiffness and damping coefficient respectively. The function  $x_+$  is defined as follows,

$$x_+ = \begin{cases} x & \text{if } x \geq 0 \\ 0 & \text{if } x \leq 0 \end{cases}$$

the spring is assumed to be massless, hence its own dynamics is neglected.

## 1.2.2 Adimensional analysis

The space finite element discretization of equation (1.2.1) yields a mass and a stiffness matrix with high coefficients leading to classical numerical problems. The solution is to find an adimensional equation of motion and then returning to the real physical state after the numerical computation.

The technique consists on changing the time scale and normalizing the displacement by the length of the beam. Consider then the normalized displacement  $v = \frac{u}{L}$ ,  $x = \frac{y}{L}$  and the time  $t = \frac{s}{T}$ , where  $T$  is the new time scale which has to be determined in order to obtain a convenient equation of motion. Let us write equation (1.2.1) using the new variables, to realize this we have to find the time and the space derivatives with respect to the new scales. The time derivative of  $u$  can be expressed as:

$$\partial_s u = \frac{du}{ds} = \frac{d(Lv)}{ds} = L \frac{dv}{dt} \frac{dt}{ds} = \frac{L}{T} \frac{dv}{dt} = \frac{L}{T} \partial_t v,$$

and

$$\partial_s^2 u = \partial_s(\partial_s u) = \frac{d(\frac{L}{T} \partial_t v)}{ds} = \frac{L}{T^2} \partial_t^2 v.$$

On the other hand, the derivative of  $u$  with respect to  $y$  can be expressed as:

$$\partial_y u = \frac{du}{dy} = \frac{d(Lv)}{dy} = L \frac{dv}{dx} \frac{dx}{dy} = \frac{L}{L} \frac{dv}{dx} = \partial_x v.$$

The same procedure is repeated to find the fourth derivative with respect to  $y$ :

$$\partial_y^4 u = \frac{1}{L^3} \frac{d^4 v}{dx^4}.$$

By taking  $\frac{T^2 EI}{L^4 \rho S} = 1$ , the following partial differential equation can be obtained

$$\partial_t^2 v(x, t) + \xi_n \partial_t v(x, t) + \partial_x^4 v(x, t) = 0. \quad (1.2.2)$$

The boundary conditions follow with the change of variables to obtain the updated conditions:

$$v(0, t) = d_1(t) = a_x \sin(\omega_t t), \quad \partial_x v(0, t) = 0, \quad \partial_x^2 v(1, t) = 0,$$

$$\partial_x^3 v(1, t) = [k_{rn}(d_1(t) - v(1, t) + z_x)]_+ - \xi_{rn} \left[ \left( \frac{1 - \text{sign}(v(1, t))}{2} \right) \partial_t v(1, t) \right].$$

$k_{rn}$  and  $\xi_{rn}$  are the spring adimensional stiffness and damping coefficient,  $z_x = \frac{z}{L}$  and  $a_x = \frac{a}{L}$ . Equation (1.2.2) is discretized by finite element to obtain a nonlinear system of differential equations, this is explained in the next section.

### 1.2.3 Finite Element approximations

Many mechanical problems use the finite element approximations to solve the equations governing their dynamics. The basis functions used herein are cubic polynomials of Hermite type, the elementary stiffness and mass matrices of each element are respectively given as follows [24]:

$$K_e = \frac{EI}{l^3} \begin{bmatrix} 12 & 6l & -12 & 6l \\ 6l & 4l^2 & -6l & 2l^2 \\ -12 & -6l & 12 & -6l \\ 6l & 2l^2 & -6l & 4l^2 \end{bmatrix} \text{ and } M_e = \frac{ml}{420} \begin{bmatrix} 156 & 22l & 54 & -13l \\ 22l & 4l^2 & 13l & -3l^2 \\ 54 & 13l & 156 & -22l \\ -13l & -3l^2 & -22l & 4l^2 \end{bmatrix},$$

where  $l$  and  $m$  are the length and the mass of each finite element respectively. A classical assembly process was performed to get the global mass and stiffness matrices of the system. The unilateral spring is incorporated at the node in contact, i.e. in the free end of the beam. Finally, equation (1.2.2) yields the following nonlinear differential system:

$$M\ddot{q} + C\dot{q} + Kq = \left[ k_{rn}(d_1(t) - q_r + z_x)_+ - \xi_{rn} \left( \frac{1 - \text{sign}(q_r)}{2} \right) \dot{q}_r \right] e_r \quad (1.2.3)$$

where  $M$  and  $K$  are respectively the assembled mass and stiffness matrices of size  $n$ ,  $C$  is the damping matrix.  $q$  is the vector of degrees of freedom of the beam,

$$(q_i)_{i=1, \dots, n} = (v_i, \partial_x v_i)_{i=1, \dots, n},$$

$r$  is the index of the node where the spring is in contact with the beam. Numerical time integration was performed using the Scilab routine 'ODE' for 'stiff' problems based on the BDF method (backward differentiation formula) which is a second order scheme for nonlinear systems [23].

### 1.2.4 Existence of the solutions

By applying Theorem 3.4.4, system (1.2.3) has a unique solution since the function  $u_+$  is Lipschitzian.

## 1.3 Experimental validations

In this section, the instrumentation used for the experiment sequences is described and illustrated with schematic and photos. The Solithane rubber used had unknown Young's modulus,

hence a mixture of a numerical and an experimental procedure was performed to characterize it. The natural frequencies of a cantilever beam were tested to ensure the boundary conditions. Finally the damping coefficients of the system and the rubber were identified using the experimental data.

### 1.3.1 Experimental setup and instruments

The instrumentation includes an electromagnetic shaker, an aluminum cantilever beam built in a box-section frame to ensure a perfect clamping, four accelerometers, a sine wave generator and a multi channel acquisition system (see Figures 1.3 and 1.4).

The shaker control system was not able to ensure a perfect sine wave imposed acceleration, the signals contained some noise and, in particular cases, some harmonics. This classical technical problem can be solved by the modelling of the shaker behaviour and incorporating its own dynamic into the numerical model. This problem can also be solved by using the measured acceleration of the base as the input of the numerical model, this technique is well explained in Chapter 2; another problem can be produced in this case because the model becomes weak mathematically and the theoretical investigations meet another kind of difficulties. To conserve a coherent model, the imposed acceleration was always modeled as a sine wave and the shaker motion was not taken in account; the cases where the measured acceleration was not harmonic was processed subsequently in Section 1.5.1

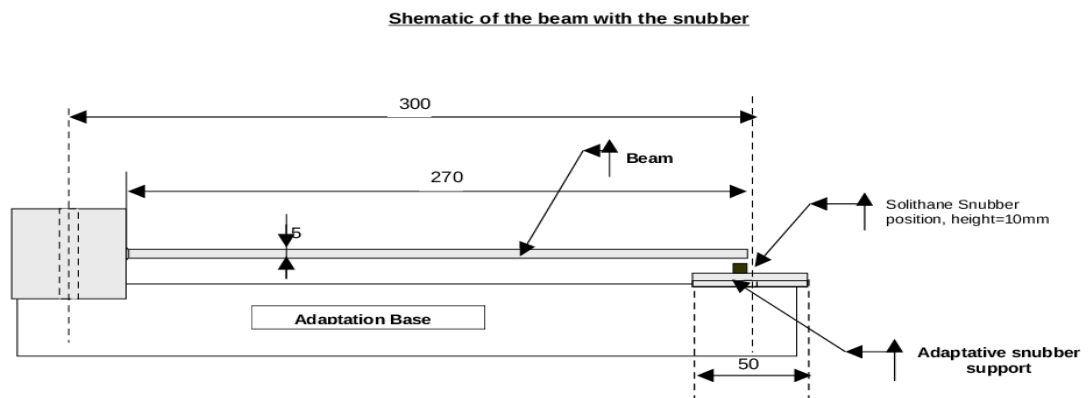


Figure 1.2. Schematic of the cantilever Beam and the unilateral contact, the snubber was modelled as a linear spring.

Beam length	Beam width	Beam thickness	Beam Young's modulus	Beam density	Spring stiffness
0.27m	0.05m	0.005m	$69 \times 10^9 N/m^2$	$2700 kg/m^3$	$559.625 KN/m$

Table 1.1. The physical properties of the beam and the spring. The spring stiffness was evaluated using an algorithm described in Section 1.3.3.

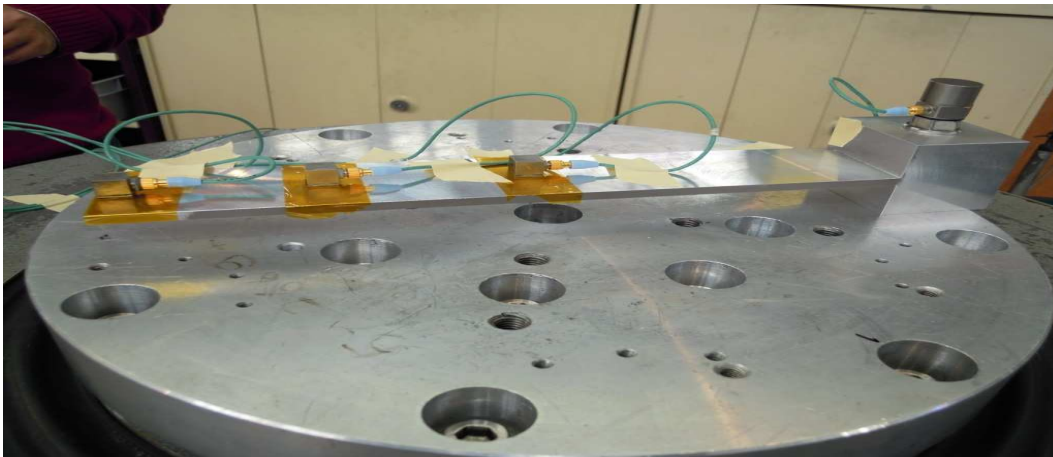


Figure 1.3. Photo of the cantilever aluminum beam on a shaker with four accelerometers.

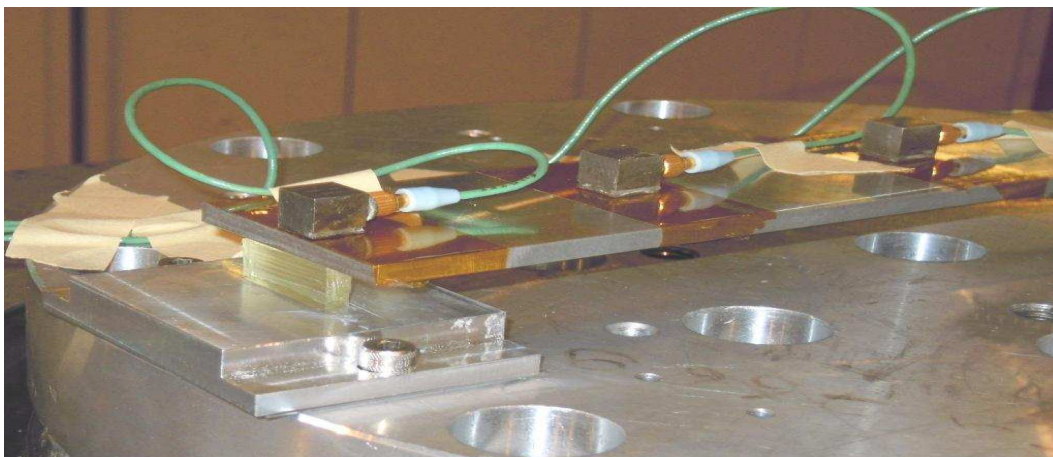


Figure 1.4. The cantilever aluminum beam in contact with the Solithane snubber at the free end. The whole system is based on a shaker which produces a harmonic motion of support given as an imposed acceleration  $a(s) = -\frac{a}{\omega^2}d(s)$ .

### 1.3.2 Highlights on the linear states of the system

The dynamic behaviour of a cantilever beam is well-known, it is presented here to check the boundary conditions of the system and to evaluate the spring stiffness using Algorithm 1. It is also important for the determination of the accelerometers mass effect, this is solved by adding the mass of each accelerometer (45 grams) to the mass matrix of the finite element model. The system has another linear state when the spring is permanently in contact with the beam, the natural frequencies can be found by applying a classical sine sweep or a random noise test. Tables 1.2 and 1.3 show the first three measured and predicted eigenfrequencies of the cantilever beam of the system with bilateral spring; The results show very good agreement.

<b>Natural frequencies</b>	$f_1$	$f_2$	$f_3$
<b>Predicted</b>	52.7 Hz	328.5 Hz	931.3 Hz
<b>Measured</b>	51.9 Hz	329.4 Hz	934.4 Hz
<b>Percentage difference</b>	1.5%	0.2%	0.3%

Table 1.2. The natural frequencies of the clamped-free beam.

<b>Natural frequencies</b>	$F_1$	$F_2$	$F_3$
<b>Predicted</b>	196 Hz	447.1 Hz	966 Hz
<b>Measured</b>	196.5 Hz	448 Hz	969.5 Hz
<b>Percentage difference</b>	0.2%	0.2%	0.3%

Table 1.3. The natural frequencies of the beam with a spring permanently in contact at the free end. The spring stiffness used to compute these frequencies is evaluated using Algorithm 1

### 1.3.3 Characterization of the Solithane snubber

The physical properties of the snubber used for the test sequences were unknown, we present here a mixed method to determine the snubber stiffness. Note that the behaviour of this kind of material depends on the frequency, the temperature and on many other factors. Herein, we assume that for small displacements and for the range of excitation frequencies used, the

material behaves linearly hence it is modelled as a linear spring.

The shift of the frequencies is due to adding a spring to the free end of the beam, this fact can be introduced by adding a coefficient in the stiffness matrix of the finite element model corresponding to the node of contact. Mathematically, the problem is to find, by iterating, a coefficient value  $k_r$  which shifts the first eigenfrequency  $f_1$  of the system without spring to  $F_1$ , the first eigenfrequency of the system with a spring permanently in contact with the beam. Proposition 1.3.1 proves the uniqueness of a such coefficient. Algorithm 1 has been performed to find  $k_r$ , it explains the details of the method.

The spring stiffness obtained by this algorithm is:  $k_r = 559.625 \text{ KN/m}$ , the corresponding

---

**Algorithm 1** Characterization of the rubber

---

**Input:** 1  $f_1$ : The first eigenfrequency of the linear system without spring.

**Input:** 2  $F_1$ : The first eigenfrequency of the linear system with a spring permanently in contact.

**Output:**  $k_r$ : The stiffness of the spring to be determined.

- 1: Initialize  $k = 0.01$
  - 2: Compute the first eigenfrequency  $f$  of the obtained matrices
  - 3: **if**  $|f - F_1| \leq \epsilon$  **then**
  - 4:      $k_r = k$
  - 5: **else**
  - 6:      $k = 1.01 \times k$
  - 7: **end if**
  - 8:  $E_r = \frac{hk_r}{b}$ ,  $h$  is the height of the rubber,  $b$  is the area of the section.
- 

Young's modulus is:  $E_r = 44.77 \times 10^6 \text{ N/m}^2$ .

**Proposition 1.3.1.** *Let  $A$  be a  $n \times n$  real square matrix which has  $n$  eigenvalues  $(\beta_k)_{k=1,\dots,n}$ ,  $(u_k)_{k=1,\dots,n}$  are the corresponding eigenvectors and  $\lambda$  is a mapping from  $[0, \infty[$  in  $\mathbb{R}$*

$$\begin{aligned} [0, \infty[ &\longrightarrow \mathbb{R} \\ \alpha_k &\longrightarrow \lambda(\alpha_k) = \beta_k, \end{aligned} \tag{1.3.1}$$

where  $(\alpha_k)_{k=1,\dots,n}$  are the diagonal coefficient of  $A$  then

$$\lambda(\alpha_k) = \beta_k = {}^t u_k A u_k,$$

and

$$\partial_{\alpha_k} \lambda(\alpha_k) = {}^t u_k \partial_{\alpha_k} (A) u_k = \|u_k\|^2.$$

As results, the mapping  $\lambda$  is one to one from  $[0, \infty[$  in  $\mathbb{R}$ .

In practice, the proposition proves that there exists a unique  $k_r$  which can shift the first eigenfrequency from  $f_1$  to  $F_1$ .

### 1.3.4 Parameters identifications and model adjustments

The data was measured at the middle, the three quarter point and at the free end of the cantilever beam. In this chapter, we take care about the data measured at the free end above the elastic contact where the acceleration is the greatest, hence we do not mention this choice in rest of the text. The Fast Fourier Transform FFT was applied to the measured and to the predicted time signals of this finite element node; the frequency axis was normalized by the excitation frequency. The FFT axis scale was presented in  $dB$  which is  $20 \log_{10}(X)$  where  $X$  is equal to the  $FFT \left( \frac{x(t)}{\max(x(t))} \right)$ ,  $x(t)$  is the considered time signal. The data measured at the other positions showed similar behaviour and it is not presented.

The measured data fits the numerical simulations for a beam structural damping coefficient  $\xi$  equal to 1% and a spring damping coefficient  $\xi_r = 2\%$ . These parameters were fixed for all the subsequent simulations.

## 1.4 Beam in a one sided contact with a spring

We present here an experimental validation of the model in the case of a one sided contact between the spring and the beam at different excitation frequency. As mentioned in previous sections, the data is measured above the contact point, i.e. the free end of the beam. The magnitude of the imposed acceleration was  $a = 2g$  for all the subsequent simulations and experiments. There was no focus for different excitation magnitude in this case since the system is not energy dependent (see Section 2.13 ). The integration time is equal to the measured time data length of  $0.8s$  for the whole cases , it is 5 times greater than the largest period of the linearized system.

### 1.4.1 Comparison in the frequency domain

Figures 1.5, 1.6, 1.7 and 1.8 show the frequency contents of the measured and the predicted accelerations for excitation frequencies at 45 Hz, 65 Hz, 78 Hz, and 160 Hz respectively. The input frequency was split into the odd and the even superharmonics. The results show very good agreement in the peak positions and in their magnitude as well as in the damping effect. Figure 1.8 shows however many subharmonics of the main excitations at 160 Hz, this behaviour is not encountered in the other cases. Remark that there was no signal processing of the measured time signals as the transfer function were no longer valid since the time signals were nonlinear.

### 1.4.2 Comparison in the time domain

The electrodynamic shaker and the instruments used for the experiment sequences were not ideal for a time-data analysis, this will complicate the time comparison of the experiments and the simulations. But the time signal data, which reflect the general dynamic behaviour of the system, can be simulated and compared to the measured. The results were presented in separated figures to avoid the phase difference problems.

Figures 1.9, 1.10, 1.11 and 1.12 show the predicted and the measured accelerations for excitation frequencies at 45 Hz, 65 Hz, 78 Hz, and 160 Hz respectively. For an excitation at 45 Hz, the maximum of the measured and the predicted acceleration was at  $10g$  which is a factor 5 of the input acceleration ( $a = 2g$ ). This maximum rises when approaching the excitation frequency at 78 Hz ( $20g$  for an excitation at  $65Hz$  and  $60g$  for an excitation at  $78Hz$ ). The rise of the magnitude has an important significance here, it provides evidence of a nonlinear mode of the system when approaching 78 Hz. The concept of the nonlinear normal modes and their properties as well as a new numerical method for their computation are the main topics of Chapter 3.

### 1.4.3 Numerical predictions

#### The displacement of the beam free end

After the experimental validation, the model is used to predict the displacements and other useful information to get more insight in the understanding of the system. Figures 1.13 and

1.14 show the numerical displacements of the free end of the beam (above the spring) for an excitation at 45 Hz, 65 Hz, 78 Hz and 160 Hz respectively and for an imposed acceleration magnitude of  $2g$ . At 78 Hz, the displacement is much greater than the other excitation points because it is close to the first nonlinear mode of the system; this case should be carefully taken in account because the structure may be damaged as the elastic applied force is important.

### The contact force

The point applied force at the contact point has an important impact on the beam structure. As the stiffness of the snubber is much greater than the stiffness of the beam in flexure, it can then produce an important damage when the acceleration is high at the free end. This force is produced by the spring and it is computed following the Hooke law of elasticity:

$$f(t) = -k_r[d(t) - q_r(t)]_+,$$

where  $k_r$  is the spring stiffness,  $d(t)$  is the displacement induced from the sine imposed acceleration and  $q_r(t)$  is the displacement of the free end of the beam. Note that the spring is active only when the spring meets the beam; the spring is assumed to be massless so its own dynamics is not taken in account.

Figures 1.15 and 1.16 illustrate the time signal of the point applied force for an excitation at 65 Hz, 45 Hz, 78 Hz and 160 Hz respectively and for an imposed acceleration magnitude of  $2g$ , these signals are continuous, periodic and vanish when the spring leaves the beam.

One of the difficulties encountered when dealing with nonlinear systems is to localize the resonance frequencies as well as their superharmonics and subharmonics. The frequency sweep is very well used to detect such frequencies but it is not enough to study to magnitude dependence and other features; the Non Linear Normal Modes can be an efficient approach to get more insight, it will be the topic of Chapter 4. Finally, to prevent any structural damage, the nonlinear frequencies and their harmonics have to be found and the corresponding forces have to be taken in account.

### 1.4.4 Frequency sweep

Frequency sweep tests have been done to detect the frequencies of the system and to study the effect of the unilateral spring on the natural frequencies. The sweep used is logarithmic with a velocity of 2 octave/min. The frequency interval cover the first two natural frequencies where the impact of the spring is relevant. At each frequency point, the maximum of the displacement of the beam free end, i.e. above the spring support, is saved. Finally these values are plotted against the frequency axis. Figure 1.17 shows the maximum of the displacements of the system with unilateral contact and without spring. The effect of the unilateral contact has shifted the first natural frequency of the system from 52.7 Hz to 82 Hz, the latter is called the nonlinear frequency. There is also a generation of harmonics of the new nonlinear frequency which is a typical feature of nonlinear system. The second linear frequency is shifted from 328 Hz to 352 Hz, there is also a presence of subharmonics of this second nonlinear frequency. Figure 1.18 shows the first nonlinear frequency of the system

with two of its harmonics as well as the first natural frequency. This curve are obtained by a frequency sweep around the nonlinear frequency and its expected harmonics. The curve are normalized by the maximum.

### 1.4.5 Conclusion

The case of a point one sided contact is interesting as the system does not depend on the amplitude of excitation, i.e. when the input excitation magnitude increases linearly then the responses also increases linearly. The model has shown to have a very good agreement with the experiments for different excitation frequencies covering the first and the second natural modes of the system. The effect of the spring contact raises the natural frequency, hence the time responses are important when the excitation is near the new frequency of resonance.

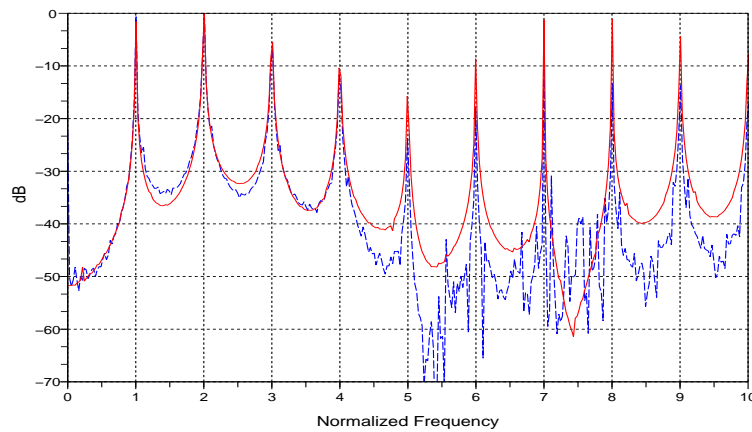


Figure 1.5. The frequency contents of the measured (dashed line) and the predicted (solid line) acceleration for an excitation at 45 Hz and for a magnitude of  $2g$ . The data are measured above the elastic support, the frequency axis is normalized by the excitation frequency.

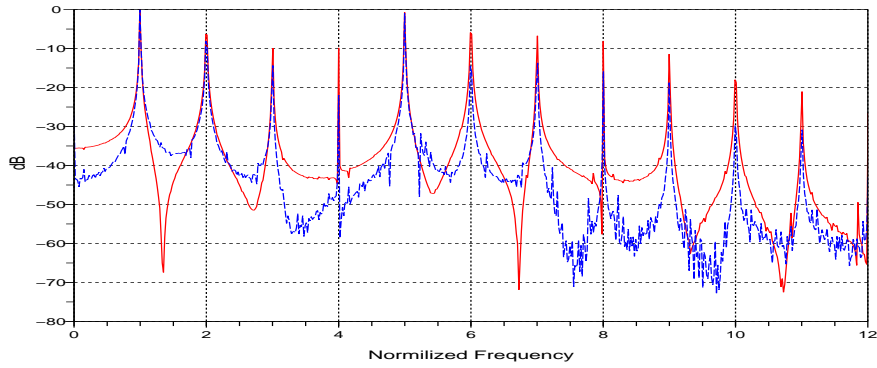


Figure 1.6. The frequency contents of the measured (dashed line) and the predicted (solid line) acceleration for an excitation at 65 Hz and for a magnitude of  $2g$ . The data are measured above the elastic support, the frequency axis is normalized by the excitation frequency.

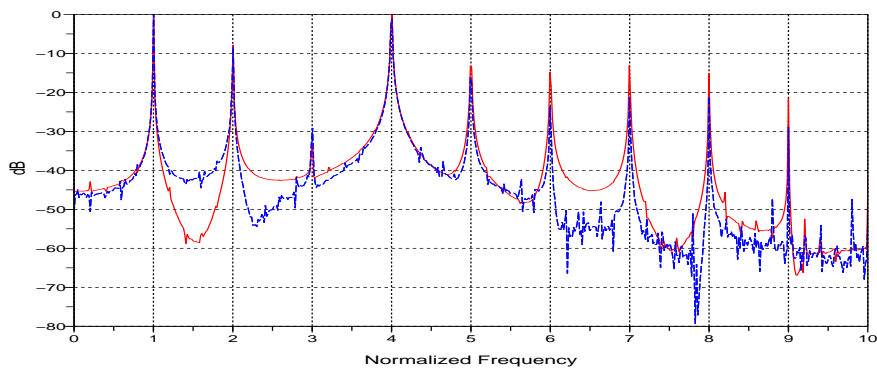


Figure 1.7. The frequency contents of the measured (dashed line) and the predicted (solid line) acceleration for an excitation at 78 Hz and for a magnitude of  $2g$ . The data are measured above the elastic support, the frequency axis is normalized by the excitation frequency.

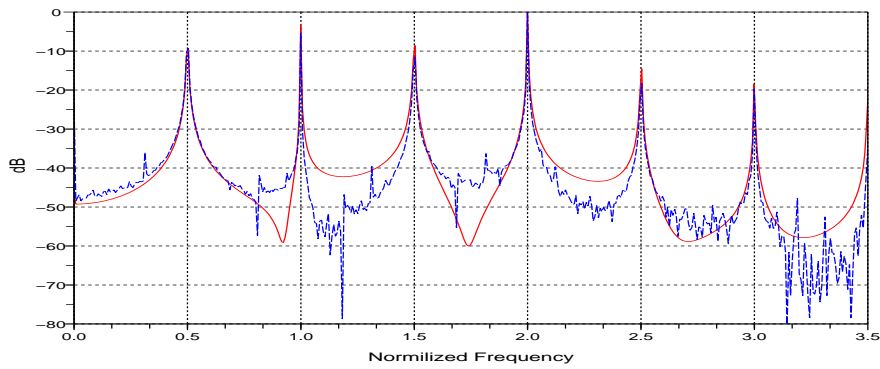


Figure 1.8. The frequency contents of the measured (dashed line) and the predicted (solid line) acceleration for an excitation at 160 Hz and for a magnitude of  $2g$ . The data are measured above the elastic support, the frequency axis is normalized by the excitation frequency.

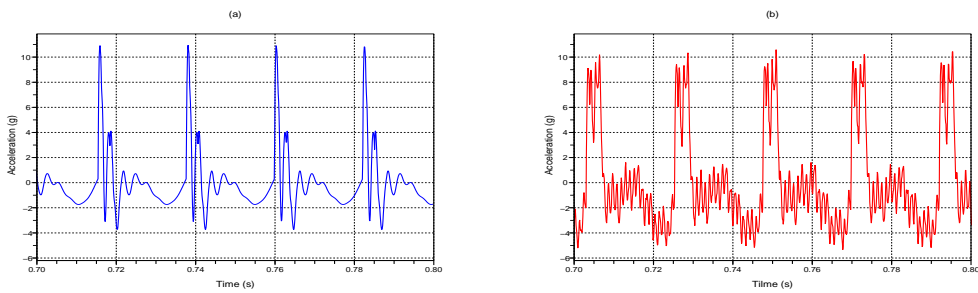


Figure 1.9. the predicted (a) and the measured (b) acceleration for an excitation at 45 Hz and for a magnitude of  $2g$ ; the data are measured above the elastic support

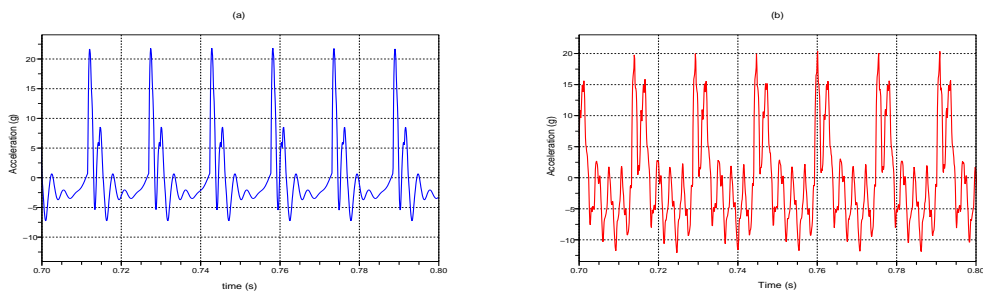


Figure 1.10. the predicted (a) and the measured (b) acceleration for an excitation at 65 Hz and for a magnitude of  $2g$ ; the data are measured above the elastic support

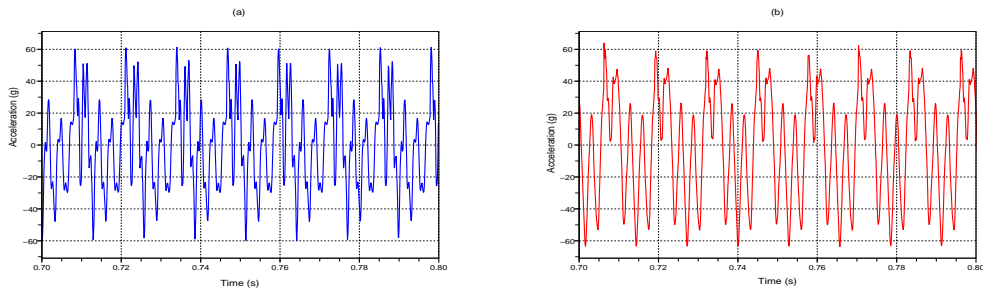


Figure 1.11. the predicted (a) and the measured (b) acceleration for an excitation at 78 Hz and for a magnitude of  $2g$ ; the data are measured above the elastic support

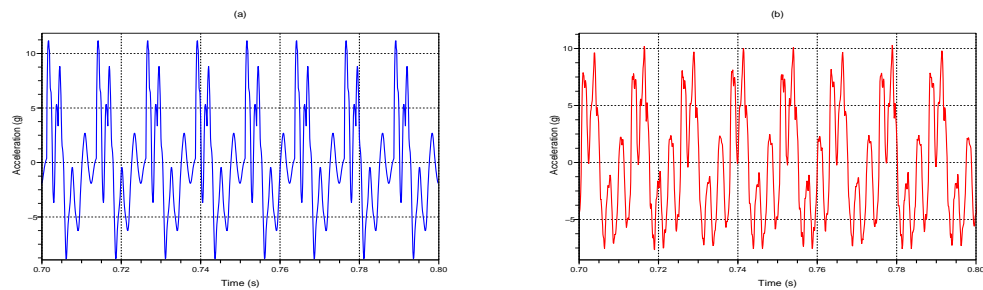


Figure 1.12. the predicted (a) and the measured (b) acceleration for an excitation at 160 Hz for a magnitude of  $2g$ ; the data are measured above the elastic support

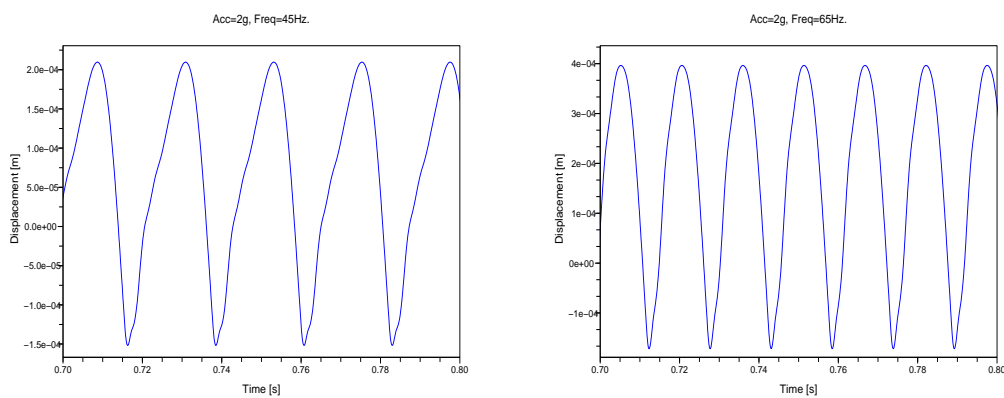


Figure 1.13. The numerical displacement of the free end of the beam for an excitation at 45 Hz and 65 Hz, the magnitude of excitation is  $2g$ .

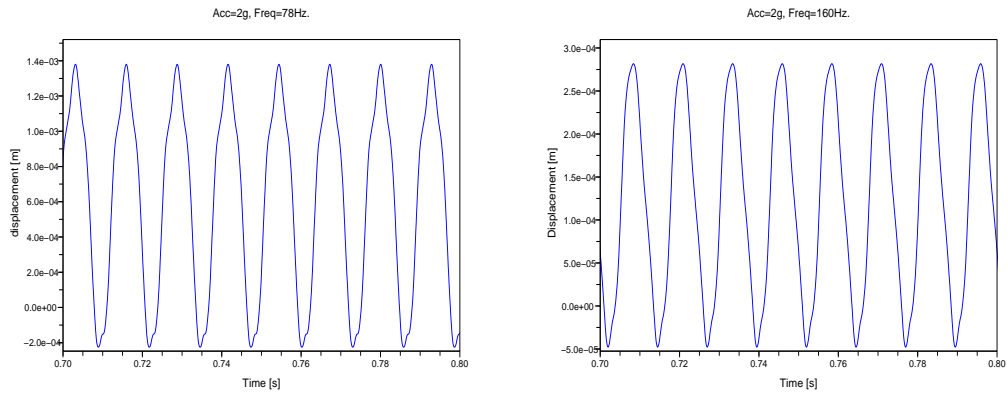


Figure 1.14. The numerical displacement of the free end of the beam for an excitation at 78 Hz and 160 Hz, the magnitude of excitation is  $2g$

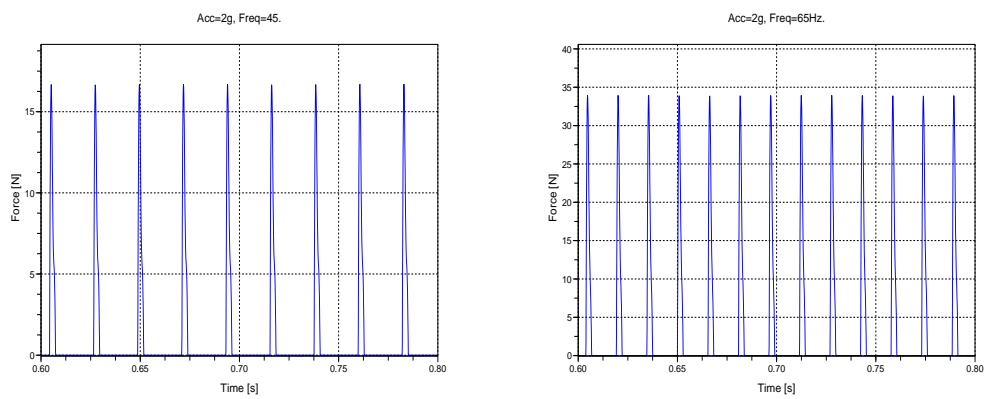


Figure 1.15. The predicted force time signal for an excitation at 45 Hz and 65 Hz, the magnitude of excitation is  $2g$ . The force is induced by the spring contact.

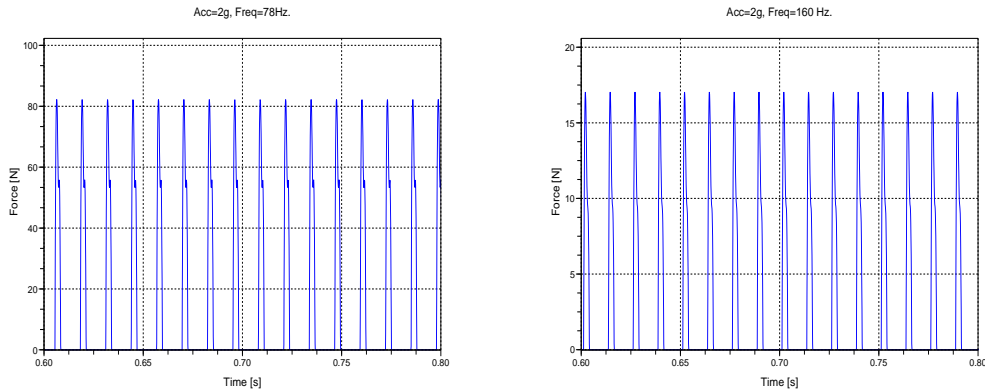


Figure 1.16. The predicted force time signal for an excitation at 78 Hz and 160 Hz, the magnitude of excitation is 2g. The force is induced by the spring contact.

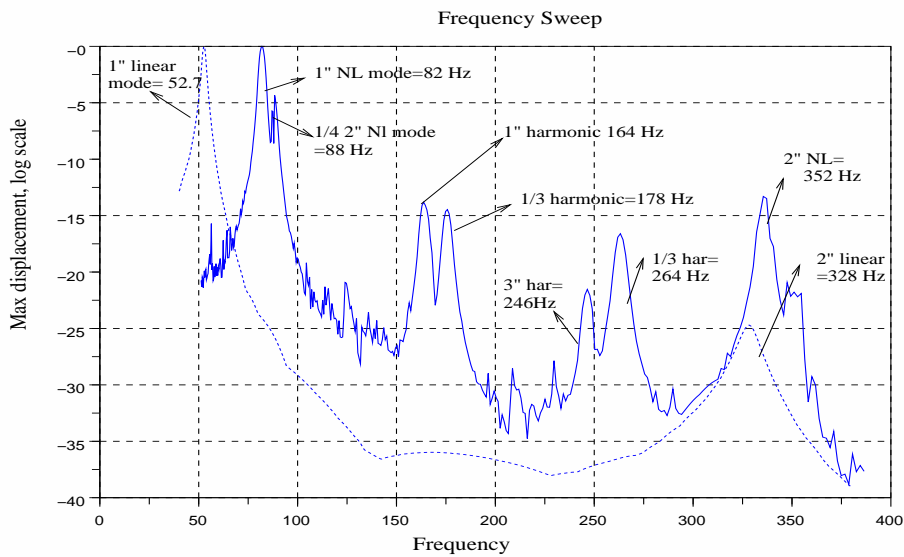


Figure 1.17. Frequency sweep of the system with unilateral contact (solid line) compared to the sweep of the cantilever beam without contact (dashed line). The first natural frequency of the linear system is shifted to the right to become the first nonlinear frequency. The harmonics of this nonlinear frequency also appear as well as the subharmonics of the second nonlinear frequency.

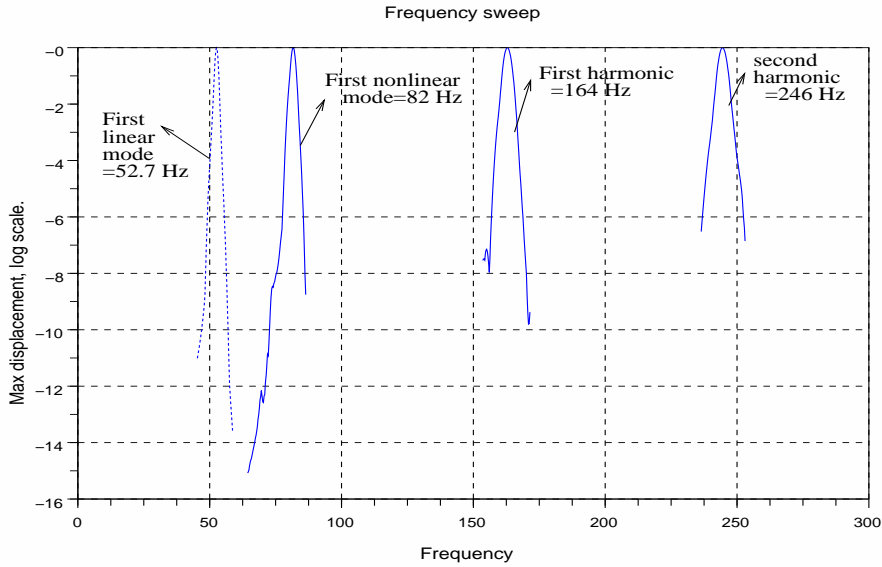


Figure 1.18. Frequency sweep around the position of the first linear normal mode and the corresponding nonlinear normal modes with its harmonics.

## 1.5 Beam in contact with a pre-Stressed spring

The comparison of the measured data with the simulations is discussed in the frequency domain. The harmonic imposed acceleration of the base yields a relative displacement  $d(t)$  which depends on the excitation frequency  $d(t) = \frac{a}{(2\pi f)^2} \sin(2\pi f t)$ . In the case of a pre-stressed spring, the responses depend on the imposed acceleration magnitude and the frequency for a given level of pre-stress  $z$ . The simulations and the experiments showed two general behaviour for a given level of pre-stress and for a given excitation frequency: the responses remain linear for low amplitudes, and behave nonlinearly for high amplitudes. In general, it is difficult to find the excitation amplitude where the system changes its behaviour, however an amplitude sweep can be performed to analyze the system for a given excitation frequency. The same procedure can be performed to find the frequency where the beam remains in contact with the spring, i.e. when it behaves linearly.

### 1.5.1 Comparison in the frequency domain

The results discussed in this section deal with a pre-stress  $z = 5mm$ . The data was measured above the contact point. Different magnitudes of the imposed acceleration was used for the subsequent simulations and experiments. The integration time is equal to the measured time data length of  $0.8s$  for the whole cases, it is 5 times greater than the largest period of the linearized system.

## Linear behaviour

For low amplitudes, the system behaves linearly and the frequency responses contain a single peak corresponding to the excitation frequency. However, the input signal is not a single sine wave as the shaker control is not good enough to reduce the harmonics coming from the shaker. To avoid a modelling of the shaker motion and to keep a sine excitation in the numerical model, the frequency contents of the excitations and the responses are presented to show that the peaks in the responses are coming from the input excitation and not from the system itself. Note that the measured accelerations and input excitations have similar frequency contents. The predicted acceleration contains a single output as the sine excitation; it is a standard feature of linear systems.

Figures 1.19 and 1.21 show the frequency contents of the measured and the predicted accelerations for excitation frequencies at 465 Hz and 90 Hz and for an excitation amplitude of  $1g$  and  $0.5g$  respectively. Figures 1.20 and 1.22 show the frequency contents of the experimental imposed acceleration at 465 Hz and 90 Hz, which shows that the excitation was not a single sine wave. When eliminating the harmonics coming from the shaker, we can see that the predicted response match very well the measured one.

## Nonlinear behaviour

The system had nonlinear behaviour for high amplitude of excitation as the beam could lose contact with the spring; the excitation frequency is split into all superharmonics, the results are very similar to those presented in Section 1.4. Figures 1.24, 1.23, 1.25 and 1.26 show the frequency contents of the measured and the predicted displacement for an excitation frequency at 90 Hz, 160 Hz, 220 Hz and 465 Hz respectively. The results also show very good agreements.

### 1.5.2 Numerical predictions

The main difference between a pre-stressed spring and the other configurations is that the beam is permanently subjected to an static elastic force at the free end, this force depends on the level of the applied pre-stress  $z$ . The displacements and the forces have different shapes from the one sided contact case, they can be differentiable and behave linearly if the spring stays in contact with the beam, they behave nonlinearly when the beam loses the contact with the spring.

#### The displacement of the beam free end

Figures 1.28 and 1.27 show the displacements of the free end of the beam above the spring contact for an excitation frequency/magnitude at (90Hz,  $0.5g$ ) and (465 Hz,  $1g$ ) respectively; The responses are linear as the spring is permanently in contact with the beam and the mean is not zero as the static position is positive. However, for a greater excitation magnitude and for the same excitation frequencies, the displacements behave non-linearly as the beam can lose contact with the spring. Figures 1.29, 1.30 and 1.31 represent the displacements of the free end of the beam for an excitation frequency/magnitude at (45 Hz,  $3g$ ), (90 Hz,  $3g$ ) and (160 Hz,  $5g$ ) respectively. The signals are strictly non linear and periodic, this is due to the

presence of the harmonics generated from the contact. Note that the displacements and the accelerations have the same frequency content.

### The contact force

The elastic forces coming from the reaction of the spring to the beam during the contact take two different shapes depending on the behaviour of the responses. If the system behaves linearly then the forces are also linear with a positive means, however they behave nonlinearly when the responses are nonlinear.

Figures 1.32 and 1.33 show the elastic forces for excitations frequency/magnitude at (90Hz, 0.5g) and (465 Hz, 1g) respectively; the signals are clearly linear with the same period of their corresponding predicted displacements.

Figures 1.34, 1.35 and 1.36 show the elastic force time signals for excitation frequency/magnitude at (45 Hz, 3g), (90 Hz, 3g) and (465 Hz, 15g) respectively. The signals are nonlinear since the beam can loose contact with the spring, and periodic with the same periods as the corresponding predicted accelerations. The forces take similar shapes to those presented in Section 1.4.

### 1.5.3 Conclusion

For this case it is not easy to understand the behaviour of the system, especially because the responses depend on the magnitude of excitation and the level of the pre-stress. The results has shown two major components, a linear behaviour when the beam remains in contact with the spring, i.e. for low amplitude of excitations; it responds nonlinearly for high amplitude and the behaviour is similar to the responses of the one sided contact configuration. The model has also shown its performance for this case.

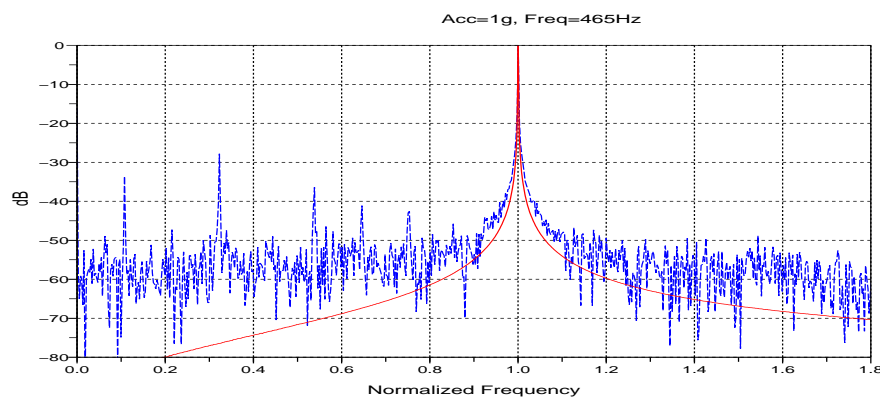


Figure 1.19. The frequency contents of the measured (dashed line) and the predicted (solid line) acceleration for an excitation at 465 Hz and for a magnitude of 1g. The data is measured above the elastic support, the frequency axis is normalized by the excitation frequency. The response contains a single peak which mean that the system responds linearly.

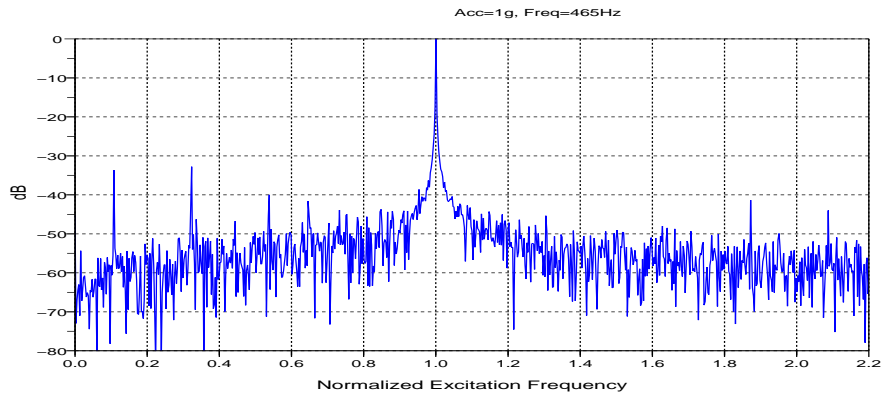


Figure 1.20. The input imposed acceleration frequency contents measured on the shaker for an excitation at 465 Hz and a magnitude of  $1g$ , it is not a single sine wave excitation as there is some noise. The small peaks appears also in the response corresponding to this excitation.

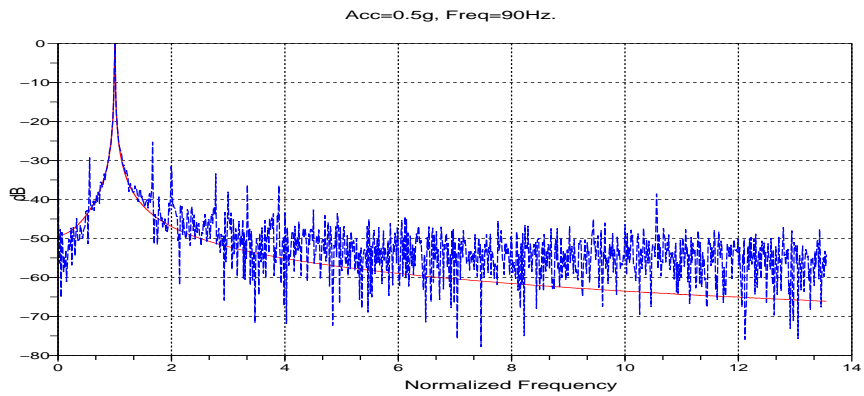


Figure 1.21. The frequency contents of the measured (dashed line) and the predicted (solid line) acceleration for an excitation at 90 Hz and for a magnitude of  $0.5g$ . The data is measured above the elastic support, the frequency axis is normalized by the excitation frequency. The response contains a single peak which mean that the system responds linearly.

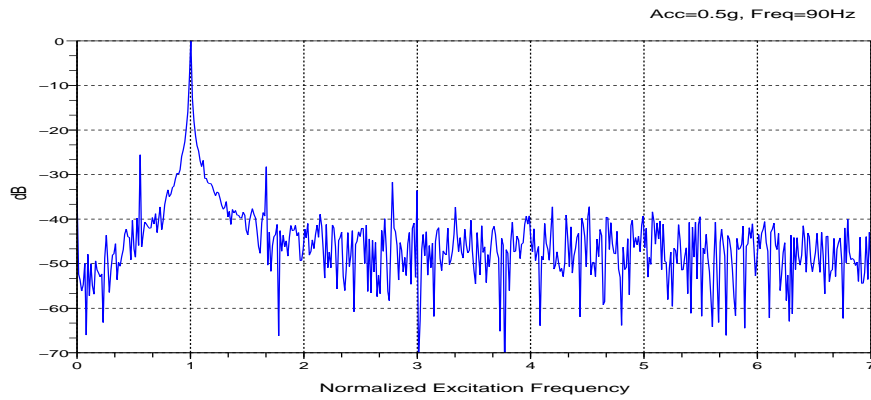


Figure 1.22. The input imposed acceleration frequency contents measured on the shaker for an excitation at 90 Hz and a magnitude of  $0.5g$ , it is not a single sine wave excitation as there is some noise. The small peaks appears also in the response corresponding to this excitation.

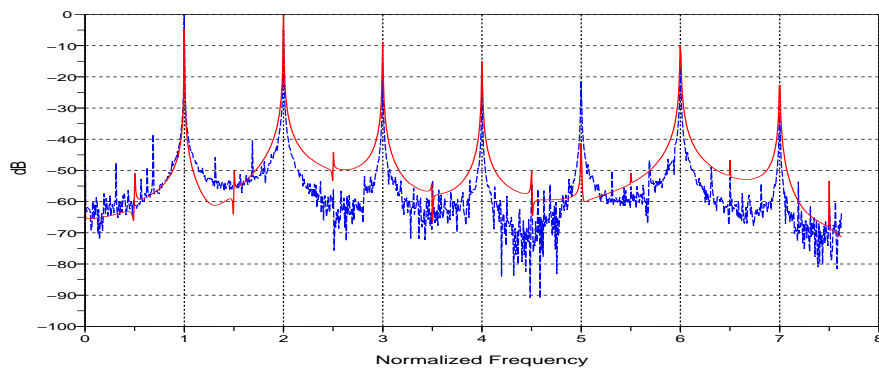


Figure 1.23. The frequency contents of the measured (dashed line) and the predicted (solid line) acceleration for an excitation at 160 Hz and for a magnitude of  $5g$ . The data is measured above the elastic support, the frequency axis is normalized by the excitation frequency. The response contains all the harmonics which means that the system responds nonlinearly.

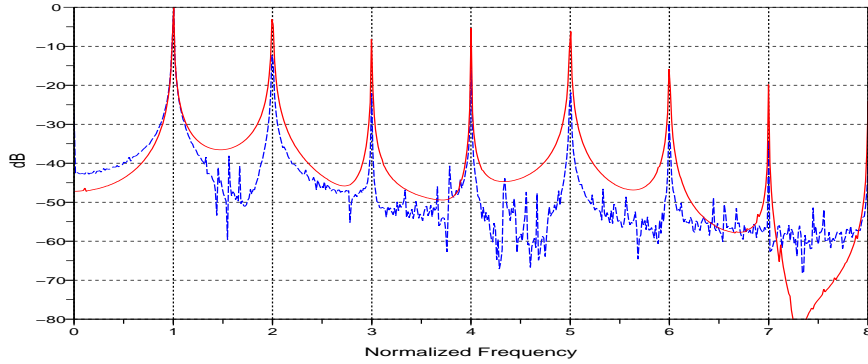


Figure 1.24. The frequency contents of the measured (dashed line) and the predicted (solid line) acceleration for an excitation at 90 Hz and for a magnitude of  $3g$ . The data is measured above the elastic support, the frequency axis is normalized by the excitation frequency. The response contains all the harmonics which means that the system responds nonlinearly.

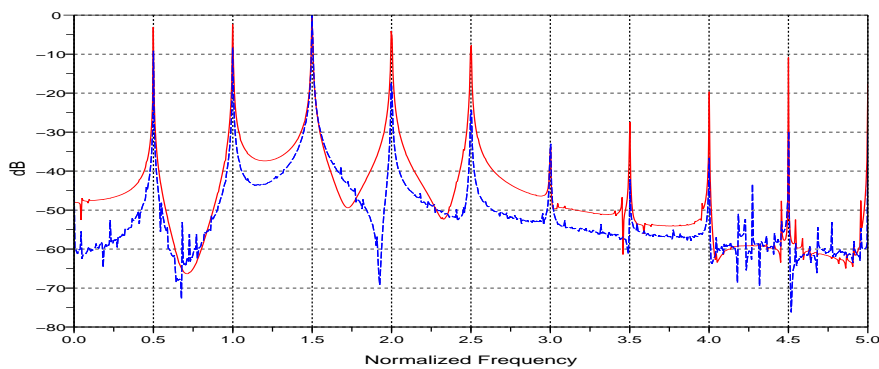


Figure 1.25. The frequency contents of the measured (dashed line) and the predicted (solid line) acceleration for an excitation at 220 Hz and for a magnitude of  $8g$ . The data is measured above the elastic support, the frequency axis is normalized by the excitation frequency. The response contains all the harmonics which means that the system responds nonlinearly.

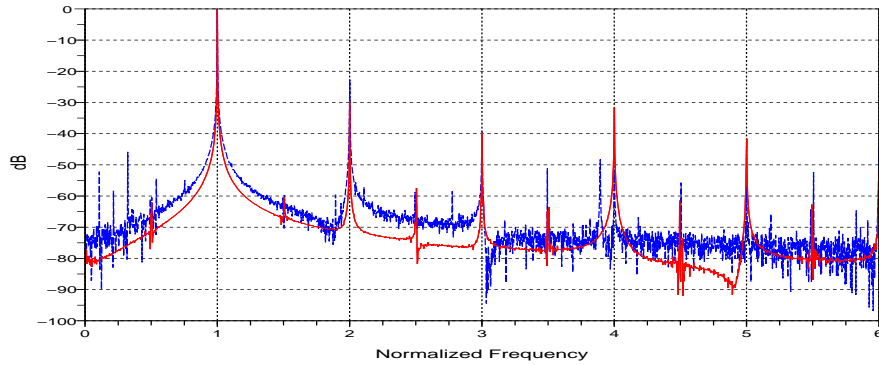


Figure 1.26. The frequency contents of the measured (dashed line) and the predicted (solid line) acceleration for an excitation at 465 Hz and for a magnitude of 15*g*. The data is measured above the elastic support, the frequency axis is normalized by the excitation frequency. The response contains all the harmonics which means that the system responds nonlinearly.

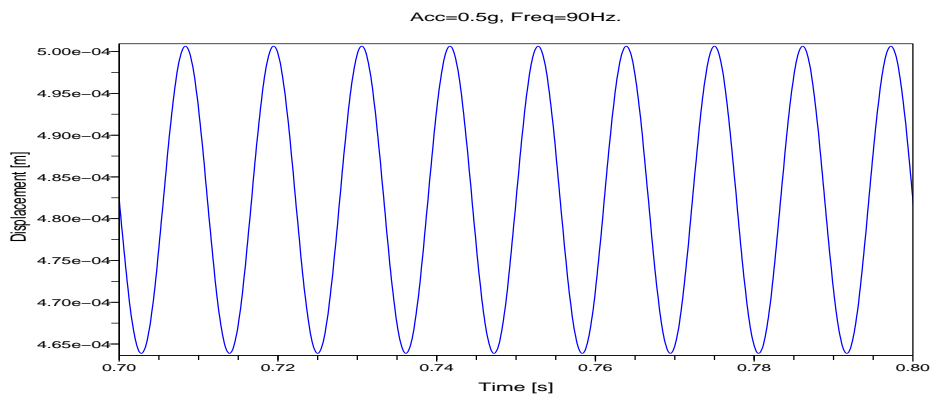


Figure 1.27. The numerical displacement of the free end of the beam for an excitation at 90 Hz, the magnitude of excitation is 0.5*g*. The signal corresponds to a linear system with a positive mean.

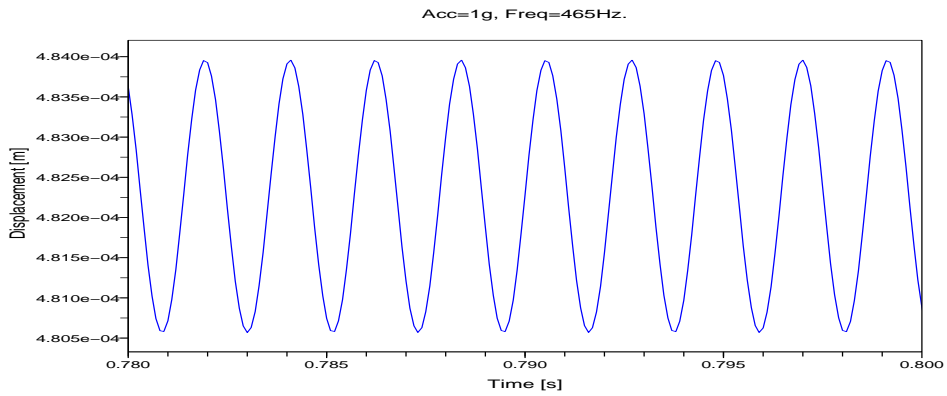


Figure 1.28. The numerical displacement of the free end of the beam for an excitation at 465 Hz, the magnitude of excitation is  $1g$ . The signal corresponds to a linear system with a positive mean.

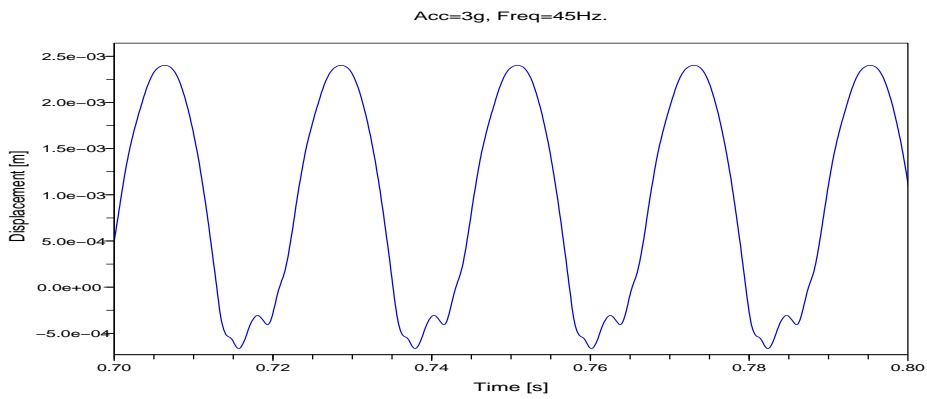


Figure 1.29. The numerical displacement of the free end of the beam for an excitation at 45 Hz, the magnitude of excitation is  $3g$ . The signal corresponds to a nonlinear system with a positive mean.

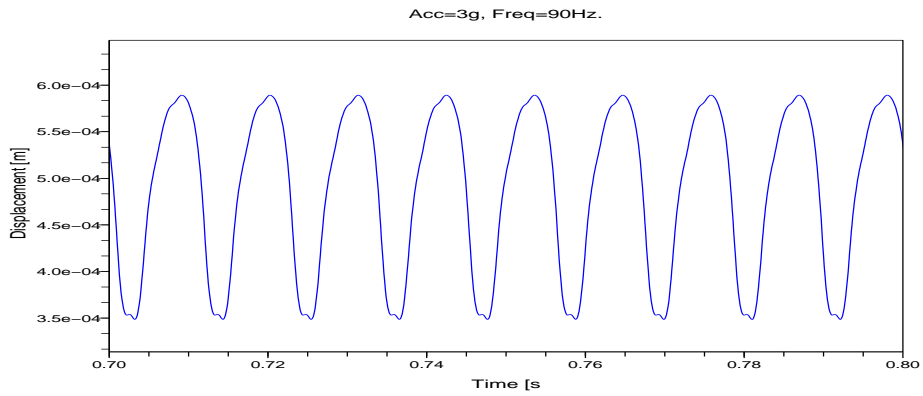


Figure 1.30. The numerical displacement of the free end of the beam for an excitation at 90 Hz, the magnitude of excitation is  $3g$ . The signal corresponds to a nonlinear system with a positive mean.

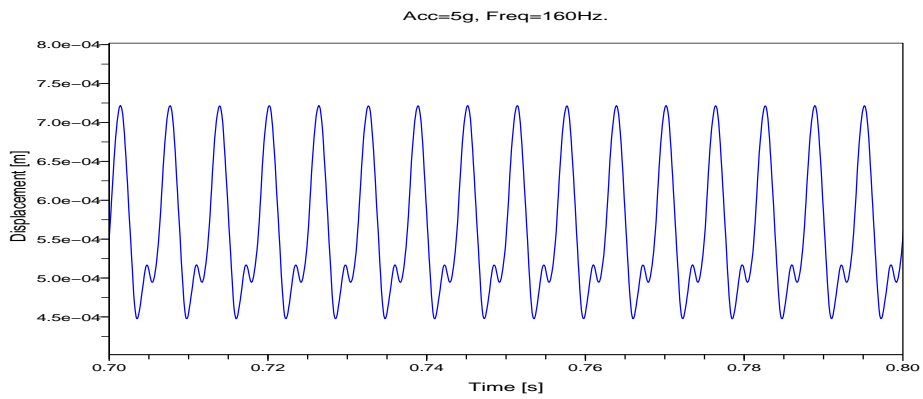


Figure 1.31. The numerical displacement of the free end of the beam for an excitation at 160 Hz, the magnitude of excitation is  $5g$ . The signal corresponds to a nonlinear system with a positive mean.

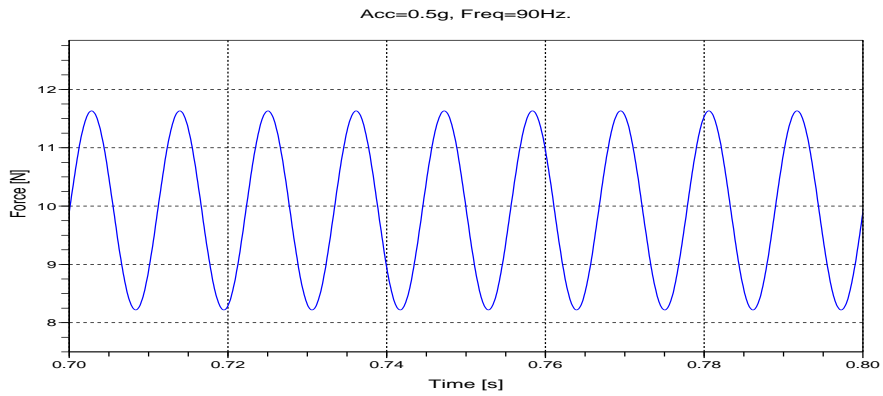


Figure 1.32. The predicted force time signal for an excitation at 90 Hz, the magnitude of excitation is  $0.5g$ . The force is induced by the spring contact, it is linear with the same period as the corresponding acceleration and it is permanently positive.

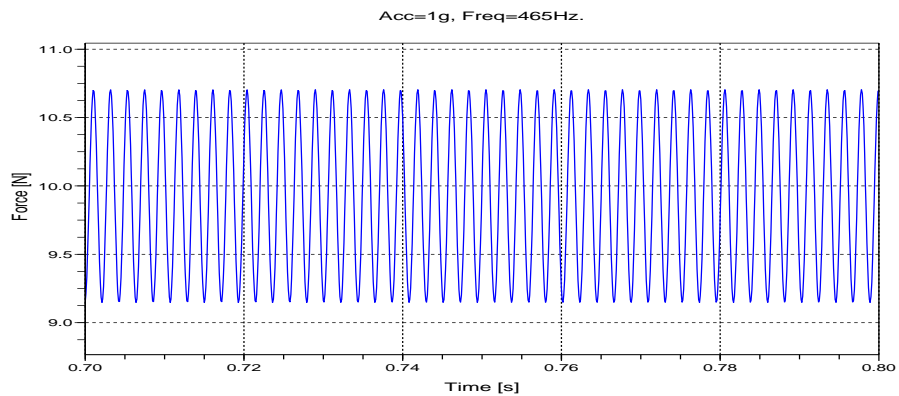


Figure 1.33. The predicted force time signal for an excitation at 465 Hz, the magnitude of excitation is  $1g$ . The force is induced by the spring contact, it is linear with the same period as the corresponding acceleration and it is permanently positive.

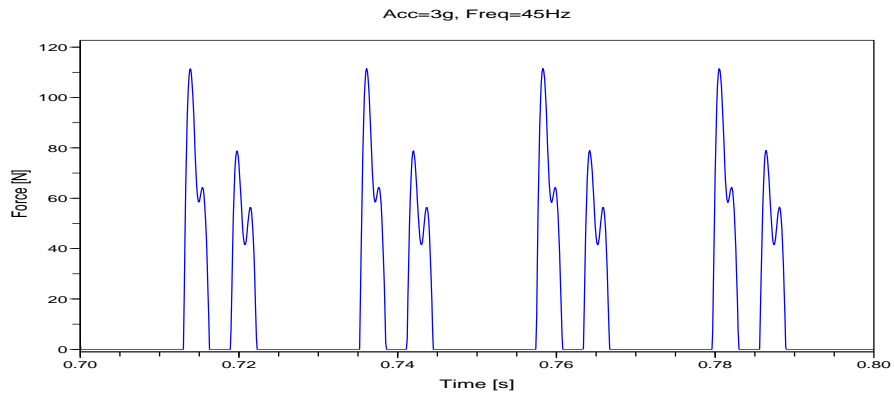


Figure 1.34. The predicted force time signal for an excitation at 45 Hz, the magnitude of excitation is  $3g$ . The force is induced by the spring contact, it is nonlinear with the same period as the corresponding acceleration and it is permanently positive.

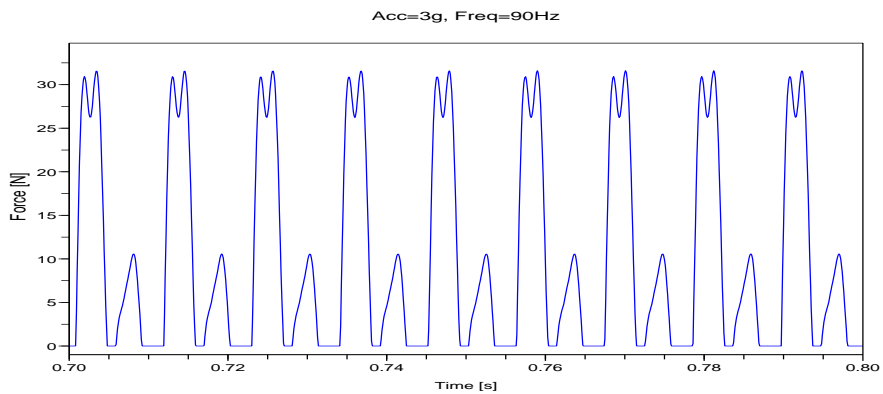


Figure 1.35. The predicted force time signal for an excitation at 90 Hz, the magnitude of excitation is  $3g$ . The force is induced by the spring contact, it is nonlinear with the same period as the corresponding acceleration and it is permanently positive.

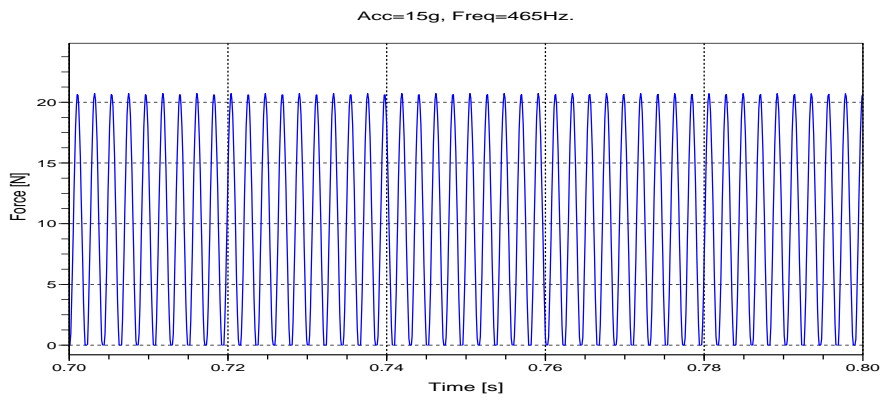


Figure 1.36. The predicted force time signal for an excitation at 465 Hz, the magnitude of excitation is  $15g$ . The force is induced by the spring contact, it is nonlinear with the same period as the corresponding acceleration and it is permanently positive.

## 1.6 Beam in contact with a spring in the presence of backlash

In this section the spring is in a backlash position with the beam, the system has then shown a linear behaviour when the beam does not strike the spring; it behaves nonlinearly when the beam realizes a contact with the spring for a range of excitation magnitudes. Hence, the system has a magnitude dependency. The case where there is not contact between the beam and the spring is reduced to the case of a cantilever beam under periodic excitation which is obvious. The attention is in the case where the beam strikes the spring. The level of the backlash is fixed for all the simulation at  $z = -5mm$ . The data are measured at the free end of the beam.

### 1.6.1 Comparison in the frequency domain

Figures 1.37, 1.38, 1.39 show the FFT of the measured and the predicted accelerations for excitation frequencies/magnitude at (45 Hz, 2g), (65 Hz, 3g) and (110 Hz, 13g) respectively. The main input excitation frequency is split into all the harmonics putting in evidence the impact of the unilateral contact. The results show a similar behaviour to the results presented in Section 1.4.

### 1.6.2 Numerical predictions

Figures 1.40 and 1.41 represent the displacements of the free end of the beam for excitations frequency/magnitude at (65 Hz, 3g) and (110 Hz, 13g) respectively, the signals are nonlinear and similar to the responses in the case of a one sided contact. The corresponding elastic force are illustrated in Figures 1.38 and 1.39.

A frequency sweep test has been done to detect the frequency of the system in presence of the unilateral contact. The sweep procedure is described in Section 1.4.4. Figure 1.44 represents the maximum of the displacement of the beam free end for both linear and nonlinear system (system with unilateral spring). The curve which corresponds to the nonlinear system rises to put in evidence a nonlinear frequency, but at a frequency point the magnitude of the displacement becomes small and the beam loses the contact with the unilateral spring. Then the system behaves as a linear cantilever beam and the curve joins the curve of the maximum displacements of the linear system. This frequency point depends on the magnitude of the excitation.

### 1.6.3 Conclusion

In this case, the system has shown two different behaviours and it depends on the amplitude of excitation. When the amplitude is low the beam cannot reach the spring and the system is similar to a cantilever beam where the dynamics is obvious. For high amplitude, the beam can reach the spring and the responses are similar to the case of a one sided contact. The model is also valid for this configuration.

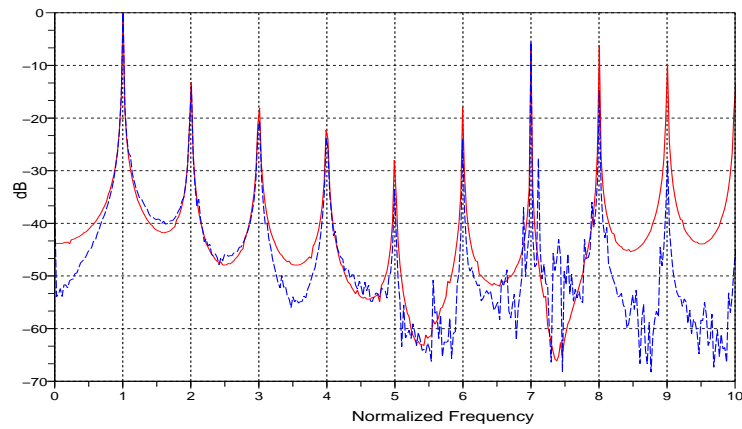


Figure 1.37. The frequency contents of the measured (dashed line) and the predicted (solid line) acceleration for an excitation at 45 Hz and for a magnitude of  $2g$  for  $5mm$  of backlash. The data is measured above the elastic support, the frequency axis is normalized by the excitation frequency. The response contains all the harmonics which means that the system responds nonlinearly.

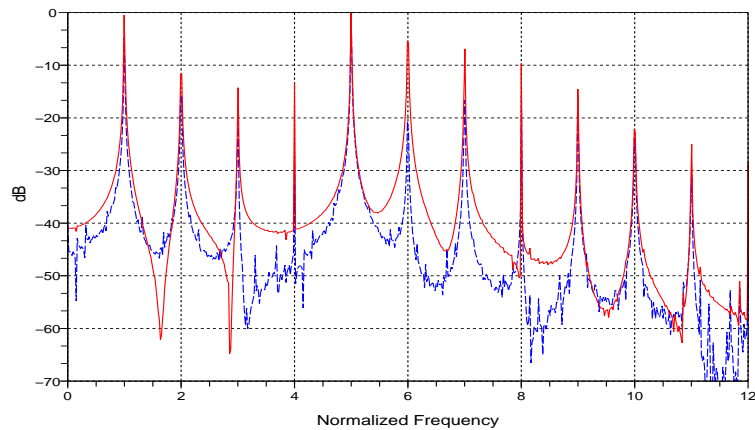


Figure 1.38. The frequency contents of the measured (dashed line) and the predicted (solid line) acceleration for an excitation at 65 Hz and for a magnitude of  $3g$  for  $5mm$  of backlash. The data is measured above the elastic support, the frequency axis is normalized by the excitation frequency. The response contains all the harmonics which means that the system responds nonlinearly.

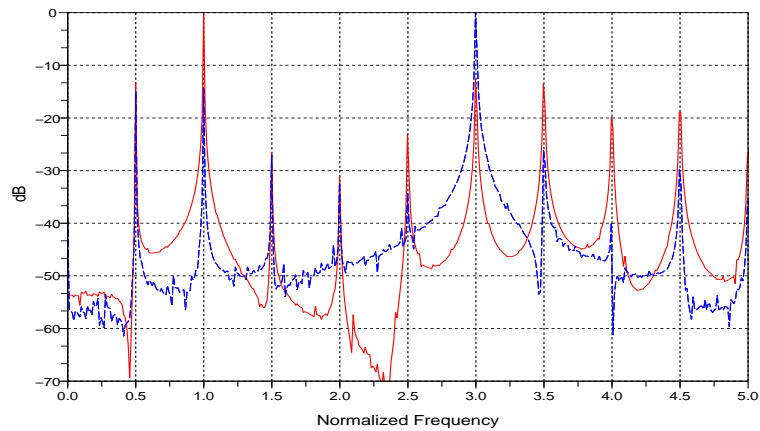


Figure 1.39. The frequency contents of the measured (dashed line) and the predicted (solid line) acceleration for an excitation at 110 Hz and for a magnitude of  $13g$  for  $5mm$  of backlash. The data is measured above the elastic support, the frequency axis is normalized by the excitation frequency. The response contains all the harmonics which means that the system responds nonlinearly.

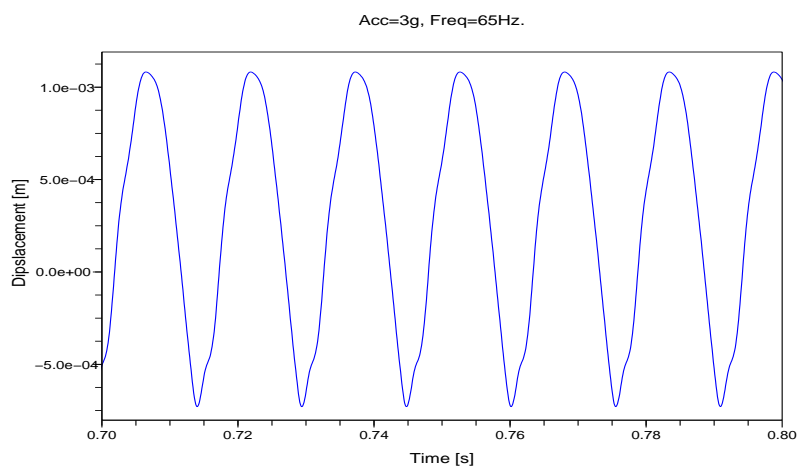


Figure 1.40. The numerical displacement of the free end of the beam for an excitation at 65 Hz, the magnitude of excitation is  $3g$ . The signal corresponds to a nonlinear system.

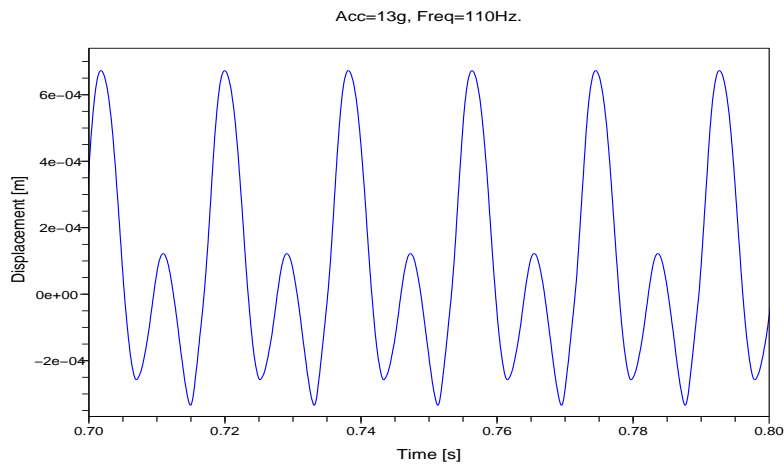


Figure 1.41. The numerical displacement of the free end of the beam for an excitation at 110 Hz, the magnitude of excitation is 13*g*. The signal corresponds to a nonlinear system.

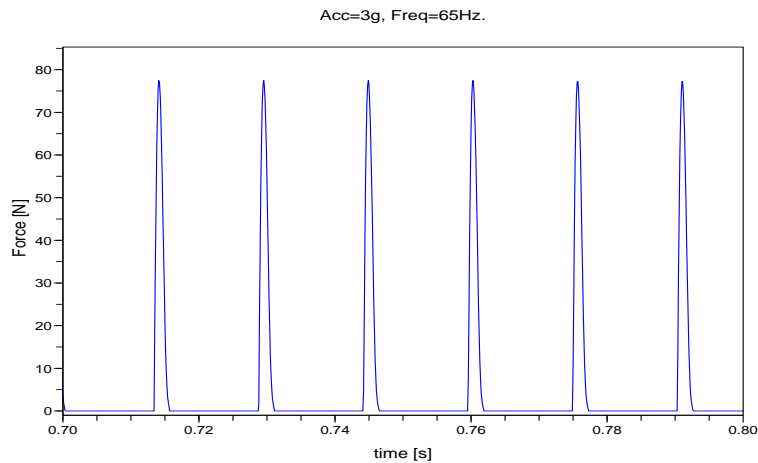


Figure 1.42. The predicted force time signal for an excitation at 65 Hz, the magnitude of excitation is 3*g*. The force is induced by the spring contact.

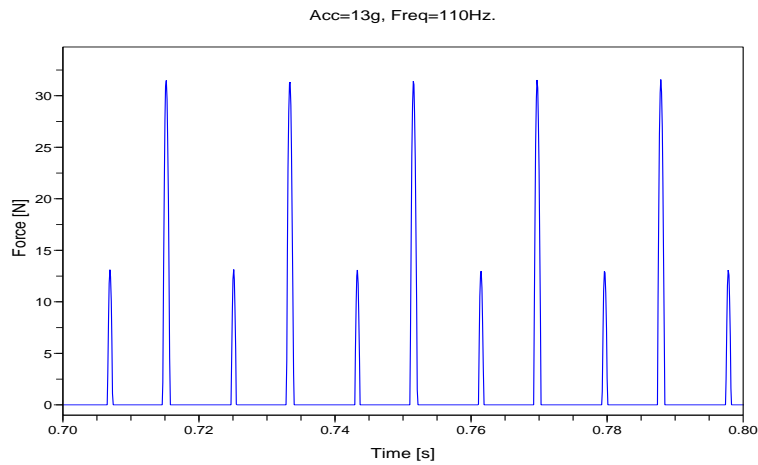


Figure 1.43. The predicted force time signal for an excitation at 110 Hz, the magnitude of excitation is 13g. The force is induced by the spring contact.

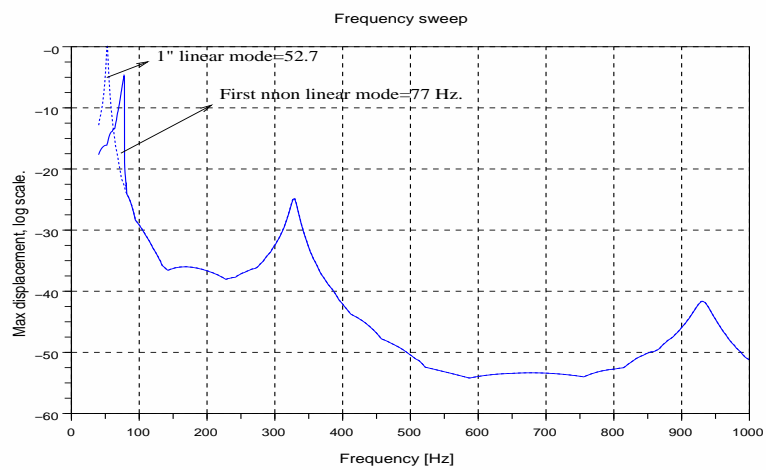


Figure 1.44. Frequency sweep of the system with unilateral spring in a backlash position (solid line) compared to the sweep of the linear free beam (dashed line). Both curves overlay at the frequency where the beam loses contact with the spring. This frequency point depends on the excitation magnitude.

## 1.7 General conclusion and perspectives

A simplified model of satellite solar panels which consists of a linear beam with an elastic support has been performed and validated with experimental sequences. The model has shown very good agreement in all the possible configurations giving a good insight into the system behaviour. The effect of the unilateral contact is to generate all the harmonics of a sine excitation, this can complicate the analysis of these signals because they are nonlinear. The unilateral contact has also an impact on the natural frequencies of the beam, the latter are shifted and generated harmonics which put the structure under a risk of damage when exciting at these frequencies. The solution is then to compute or predict these nonlinear frequencies with its harmonics, this can be done by using a frequency sweep or by using the numerical method for the calculation of the nonlinear normal modes discussed in Chapters 3 and 4.

The responses of the model are in the time domain, this gives an access to the node displacements, the contact force, the accelerations and the energy of the system, the frequency responses are then obtained by the FFT. To avoid a nonlinear response, we can apply a pre-stress between the beam and the spring, this yields a linear behaviour for a range of low amplitudes of excitation. But the spring will put the beam under a continuous stress even in a static position. The spring position can play a role in the beam dynamics, special positions like the nodes of the second or the third linear modes reduces the effect of the unilateral contact on the system when it is excited at frequencies near the corresponding modes. The model can be easily performed to model a plate in contact with unilateral springs or with a two dimensional rubber. This can be done by using a mass and a stiffness matrices which correspond to a plate and by tacking in account the boundary conditions. One can work on the numerical methods used for the integration of the differential equations of the F.E. model. No major difficulties is expected if one wants to use a composite or a carbon beam instead of the aluminum beam used in this work. The Solithane rubber was modeled as a linear spring as the displacement was expected to be small, the model is flexible with another nonlinearity types (quadratic or cubic for example).

## 1.8 Acknowledgment

We gratefully acknowledge Jérôme Buffe and Stéphanie Behar from Thales Alenia Space for their support and for useful discussions. We Thank Dr. Neil Ferguson from the ISVR, Southampton, for the scientific contribution and for helpfull suggestions. We also acknowledge G. Vanderborck and B. Grangier from Thales Underwater system where the experiments were held. Special thanks to Marc Constancio and Roger Thannberger for the technical assistance and for the convivial ambiance.

## **Chapter 2**

# **The vibration of a beam with a local unilateral elastic contact**

---

This chapter is a version of [11] submitted for publication in an international journal. The paper deals with a simple model of a beam with unilateral contact at the free end and excited by a periodic force. This model is similar to that presented in Chapter 1 where the support excitation is replaced by a punctual force but the results have shown similar behaviour. The effect of the spring positions have been studied which can help to localize the perfect position to fixe the rubber on the solar panel.

---

# The vibration of a beam with a local unilateral elastic contact

H.Hazim <sup>a,\*</sup>, N.Ferguson <sup>b</sup>, B.Rousselet <sup>a</sup>

<sup>a</sup>*J.A.D. Laboratory U.M.R. CNRS 6621, University of Nice Sophia-Antipolis, 06108 Valrose, Nice, France.*

<sup>b</sup>*Institute of Sound and Vibration Research, University Road, Highfield, Southampton SO17 1BJ, UK.*

---

## Abstract

The mass reduction of satellite solar arrays results in significant panel flexibility. When such structures are launched in a packed configuration there is a possible striking one with another dynamically, leading ultimately to structural damage during the launch stage. To prevent this, rubber snubbers are mounted at well chosen points of the structure and they act as a one sided linear spring. A negative consequence is that the dynamics of these panels becomes nonlinear. In this paper a solar array and a snubber are simply modelled as a linear Euler-Bernoulli beam with a one sided linear spring respectively.

A numerical and an experimental study of a beam striking a one-sided spring under harmonic excitation is presented. A finite element model representation is used to solve the partial differential equations governing the structural dynamics. The models are subsequently validated and updated with experiments.

*Keywords:* Nonlinear vibrations, unilateral contact, modelling

---

---

\* Corresponding author. tel: +33 04 92076276

*Email address:* hamad.hazim@unice.fr (H.Hazim)

## 2.1 Introduction

The study of the nonlinear behaviour of structures with a nonlinear contact or support is a relatively new research field of interest for many structural dynamicists. It is a branch of nonlinear dynamics with a special form of nonlinearity; the system has two linear local components and the nonlinearity comes from the interaction between one with the other. It is a non differentiable nonlinearity and it could be non continuous if one or two components has a strong damping coefficient. Some papers have been published to study such systems [5–7], where the focus was to study the stability using sweep tests experimentally and comparing numerical simulations, the latter computation using special packages for nonlinear simulations.

In general, non linear dynamics is a very interesting area of modern research for many reasons; the limited application of the linear theory being one of them. The complexity of the systems studied and used in the new generation of space structures and many other mechanical systems, needs a theory which can deal with the nonlinear behaviour encountered. Unfortunately, there is no complete theory for nonlinear systems such as for the linear case, but there exists many studies which could be applied for many particular cases by themselves and from a particular point of view. The interest of the authors was to study the nonlinear systems in both the frequency and the time domains, as well as the internal properties of the systems like nonlinear normal modes (NNM) which is an extension of the well known linear normal modes (LNM) (see [15–19]) .

The objectives of the current study is to simulate the dynamics of a beam under periodic excitation when it strikes a linear spring. A finite element numerical model was produced and was validated with subsequent experimental tests.

The study of the total dynamic behaviour of solar arrays in a folded position with snubbers are so complicated (see Figure 2), that to simplify, a solar array is modeled by a clamped-free Bernoulli beam with a one-sided linear spring. This system is subjected to a periodic excitation force. The real configuration of the problem is similar to a beam with a unilateral contact subjected to a periodic imposed displacement of the base, but the dynamical behaviour of the system does not change significantly if the imposed displacement is replaced by a periodic force excitation. The configuration used was easiest to be realized from a technical point of view as the experimental validation rig is very simple to build.

The experimental setup and the rig are briefly presented. The numerical results are also presented and studied in both the frequency and the time domains. It is expected that some similarities to a linear system behaviour will be observed.

The effect of the spring location has also been studied. It is important to look for particular points to locate the spring, the aim being to reduce the nonlinear effect as much as possible. The spring was introduced at a point corresponding to the node of the second linear beam mode. In this case it is expected that the system will show a linear behaviour for an excitation near the second natural frequency; however a nonlinear behaviour is expected for different excitation frequencies though. Note that no signal analysis is done by the acquisition system, as the problem is nonlinear and the standard transfer function calculation is only really applicable and useful for linear systems. The time signal was acquired and the processing

performed using external software (Scilab [23]). The numerical predictions are compared to experimental results and show very good agreement.

## 2.2 Numerical modelling

The present study simulated the behaviour of a beam which strikes a snubber under a periodic excitation. As the frequency range of interest was to consider the first three linear eigen frequencies, the beam was modelled using ten linear Euler Bernoulli beam finite elements. The numerical simulations are presented and compared in the frequency domain. The Fast Fourier Transform was applied to the predicted and the experimental displacements at the free end, i.e. corresponding to the last node of the beam finite element model. The mass effect of the force transducer used for experimental validation was also taken into account in the finite element model.

The beam equation of motion with an elastic snubber can be expressed as:

$$\rho S \ddot{u}(x, t) + EI u^{(iv)}(x, t) = F(t) \delta_{x_0} - (k_r u(x_1, t))_- \delta_{x_1} \quad (2.2.1)$$

where  $\rho$ ,  $S$ ,  $E$ ,  $I$ ,  $F$  and  $k_r$  are respectively the beam density, cross-sectional area, Young's modulus of elasticity, second moment of area, point applied harmonic force at position  $x_0$  and an elastic spring attached at position  $x_1$ .

Cantilevered beam boundary conditions assume zero displacement and slope at the fixed end and zero bending moment at the free end. When the elastic unilateral spring is in contact then a shear force is present due to the reaction from the spring,

$$u(0, t) = 0, \quad \partial_x u(0, t) = 0; \quad u(x, 0) = 0, \quad \partial_t u(x, 0) = 0, \quad \partial_x^2 u(l, t) = 0.$$

The compression of the spring is given by

$$u(x, t)_- = \begin{cases} u(x, t) & \text{if } u \leq 0 \\ 0 & \text{if } u > 0 \end{cases} \quad (2.2.2)$$

The classical Hermite cubic finite element approximation was used to solve the PDE (see [24]), it yields an ordinary nonlinear differential system in the form:

$$M \ddot{q} + K q = -[k_r (q_{n_1})_-] e_{n_1} + F(t) e_{n_2} \quad (2.2.3)$$

where  $M$  and  $K$  are respectively the assembled mass and stiffness matrices,  $q$  is the vector of degrees of freedom of the beam,  $q_i = (u_i, \partial_x u_i)$ ,  $i = 1, \dots, n$ , where  $n$  is the size of  $M$ ,  $n_1$  and  $n_2$  are the indices of the nodes where the spring and the excitation force are applied to the beam respectively. Numerical time integration was performed using an ODE numerical integration for 'stiff' problems, the package ODEPACK was used based on the BDF method (backward differentiation formula, see [23]). Small damping was introduced in the spring, there is no damping assumed in the beam structure.

## 2.3 Experimental validation

In this section, the experimental setup is briefly presented. The instrumentation used for the measurement exercises are not cited in detail as they are standard. The principal instruments used are shown in Figures 2.3 and 2.19 and include accelerometers on the beam, an electrodynamic shaker driving the beam through a force transducer and a multichannel signal analyser (Data Physics).

The physical rig consists of a cantilevered aluminum beam in contact with an elastic rubber at the free end. The beam was excited at one point with an applied periodic excitation. The beam properties and the rubber stiffness are given in Table 2.1.

In practice, the use of a small electrodynamic shaker yields a technical problem due to the reaction of the beam. It is difficult to realize an input force  $F(t)$  which is a simple sine wave unless the impedance of the shaker is significantly higher than the beam impedance. To deal with this problem, a force transducer was fixed between the shaker and the beam to measure the actual supplied excitation force to the beam. The numerical simulations use the actual measured force signal coming from the acquisition system which was periodic. This method is an alternative to modelling the electrodynamic shaker motion. Figure 2.8 shows typical examples of the input force signals with the corresponding spectral content.

From a simulation and comparison shown later, using the actual measured force is appropriate given the simplified excitation system without any feedback control which would be necessary to produce a strict harmonic signal.

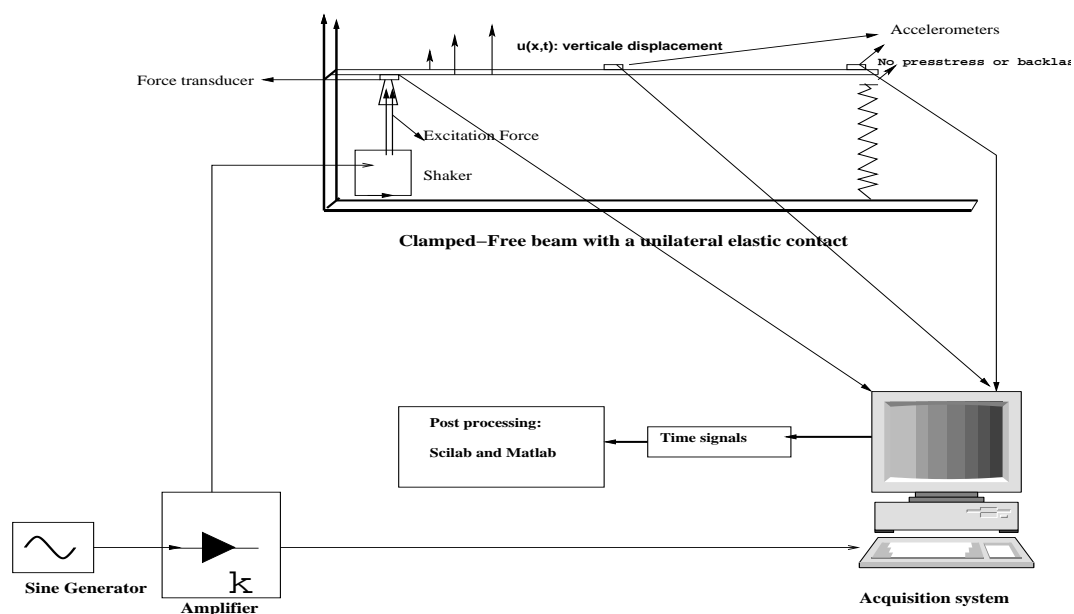


Figure 2.1. A schematic of the experimental setup.

## 2.4 Beam piecewise linear system dynamics

The system has two linear configurations or states. The first consists of the beam without the spring in contact and the second when the beam is permanently in contact with the elastic support, which is modeled as a linear spring. The advantage of these two states is to give an idea on the effect of the spring on the overall system dynamics.

Usually, adding a spring to a simple beam model at one point raises the eigen frequency sequence for the system; this shift is realized numerically by adding the spring stiffness to the coefficient corresponding to the contact point in the stiffness matrix of the system. The spring is massless, so the mass matrix of the F.E. model is intact.

Some experimental problems were encountered; one of these problems is to implement a perfect clamping for the beam, which is impossible in practice but can be reasonably assumed. Another issue is that the Young's modulus of the rubber spring used for the experiments was unknown. An algorithm was developed to determine the stiffness of the rubber for small displacements. This was subsequently used in the numerical simulations performed for comparison with experiments.

### 2.4.1 The two linear states

Firstly, predictions of the forced response of the cantilever beam without a point elastic support were produced and compared with the experiments. Good agreement showed that the model reasonably accurately represents the cantilever beam and its boundary conditions. The results for the natural frequencies are shown in Table 2.2. On the other hand, predictions of the cantilever beam with a spring permanently in contact at the free end were produced and compared with the experiments, good agreement was found (see Table 2.3). The last state was used to determine the stiffness of the spring using an algorithm described in the next subsection.

### 2.4.2 Characterization of the spring support stiffness

After initially finding the natural frequencies of the system for the two states of linearity mentioned in the pervious subsection, an algorithm was developed to find a suitable spring stiffness by iteration.

The shift of the frequencies due to adding a spring at the free end of the beam were recorded.

Beam length	Beam width	Beam thickness	Beam Young's modulus	Beam density	Spring stiffness
0.35m	0.0385m	0.003m	$69 \times 10^9 N/m^2$	$2700 kg/m^3$	57.14 KN/m

Table 2.1. The physical properties of the beam and the spring. The spring stiffness was evaluated using an algorithm described in (2.4.2).

The stiffness matrix of the finite element model incorporated a point spring at the node in contact. Mathematically, the problem is to find a coefficient value  $k_r$  which shifts the first eigen frequency  $f_0$  of the system without spring to  $f_1$ , the first eigen frequency of the same system with a spring permanently in contact. The method is based on the uniqueness of the sequence of the generalized eigen frequencies of the stiffness and mass matrices.

The subsequent value obtained for the point stiffness by this algorithm was  $k_r$  equal to  $57.14KN/m$ . The corresponding Young's modulus  $E_r$ , assumes the stiffness  $k_r$  equals to the product of the Young's modulus with the spring area divided by the spring length. The estimated Young's modulus for the rubber spring being  $4 \times 10^6 N/m^2$ .

## 2.5 Comparison of simulations with experiments

In this section the simulations are compared to the measured data in the frequency domain; the acquisition system provides just the time signals of the accelerations and the input force. The processing of these signals and the numerical results were done using external software (Scilab [23]).

The total length of data predicted corresponds to an integration time which is fixed at  $t$  equal to  $1s$  for all of the simulations and the acquired experiment of samples. It is five times the fundamental (lowest) period of the system. The data are measured immediately above the support and the frequency axis is normalized by the excitation frequency

For the industrial application it was necessary to consider the response in the first three

	1 <sup>th</sup> natural freq	2 <sup>th</sup> natural freq	3 <sup>th</sup> natural freq
Predicted	19.97 Hz	122.2 Hz	318.8Hz
Measured	19.38 Hz	118.6 Hz	314.47 Hz
Percentage difference	3%	3%	1.4%

Table 2.2. The natural frequencies of the clamped-free beam

	1 <sup>th</sup> natural freq	2 <sup>th</sup> natural freq	3 <sup>th</sup> natural freq
Predicted	84.57 Hz	246.14 Hz	443.53Hz
Measured	84.47 Hz	243.5 Hz	440 Hz
Percentage difference	0.1%	1%	0.7%

Table 2.3. The natural frequencies of the clamped beam with a permanently attached spring

modes, hence the beam was modelled using ten equal length finite elements. In principle, the model is able to be applied to higher frequency excitations but typically any fatigue or damage in practice is likely to occur in the lower order modes.

### 2.5.1 Comparison in the frequency domain

The effect of the unilateral contact is clear, the input frequency is split into its all harmonics. From an energetic point of view, the input energy is split, each subharmonic of the main excitation takes its part thus the contribution of each harmonic is evident.

Figures 2.5, 2.6 and 2.7 show the FFT of the numerical and the experimental displacements for an excitation signal at 32 Hz, 124 Hz and 100 Hz respectively. The height of the peaks are normalized by the maximum. The predicted frequencies found are exactly the same as measured for a large number of harmonics. However, a small shift in the height of these peaks appears for the fifth harmonic; the peak in Figure 2.5 appears at a multiple of 5 times the original main excitation frequency, i.e. at approximately 160Hz in the acceleration response. At this frequency there is no guarantee that the actual support of the beam and the spring is itself rigid, as it might have its own dynamics as would the bench that supports the rig, so there might be some influence of that on the response. Other tests with random excitations have shown good agreement. Figures 2.8 and 2.9 show the input excitation force and the measured acceleration at 32 Hz and 124 Hz respectively. It is clear from the time signal and from the frequency content that the forces are not pure harmonic single frequency sine waves, but they are periodic.

Figures 2.10, 2.11 and 2.12 show the predicted displacement for an excitation at 32 Hz, 124 Hz and 100 Hz respectively. The displacements are almost always positive so they have positive means. This is due to the high stiffness of the spring, but the time response is still periodic.

### 2.5.2 Magnitude-Energy dependence

The magnitude-energy dependence is a typical dynamical feature of nonlinear systems under excitation; the maximum of the solution plotted against the input energy can take different shapes depending on the form of the nonlinearity. For linear systems under periodic excitation, the maximum of the solution is proportional to the input energy. The model studied in this paper is a piecewise linear system, the numerical and the experimental results is expected to exhibit a linear behaviour for different levels of input energy.

The magnitude-energy dependence can be represented by different ways. Herein, a mathematical and an experimental proof are presented to demonstrate the magnitude-energy independence. From a mathematical point of view, the level of excitation energy depends on the magnitude of the excitation force  $F(t)$ . The idea here is to examine the variations of the solution in the time domain as the amplitude of the excitation force  $F(t)$  changes linearly. Consider then equation (2.2.1) and multiply both sides by a constant  $\lambda \geq 0$  the equation becomes:

$$\lambda[\rho S\ddot{u}(x, t) + EIu^{(iv)}(x, t)] = \lambda[F(t)\delta_{x_0} - (k_r u(x_1, t)_-)\delta_{x_1}] \quad (2.5.1)$$

In general, the only problem to substitute the parameter  $\lambda$  in the equation is the nonlinear term; in this case,  $\lambda[k_r u(x_1, t)_-] = k_r[\lambda u(x_1, t)]_-$  (see definition of  $u_-$ ). Equation (2.5.1) can then be written as follow:

$$\rho S \ddot{v}(x, t) + EI v^{(iv)}(x, t) = \lambda[F(t)\delta_{x_0}] - k_r(v(x_1, t)_-)\delta_{x_1} \quad (2.5.2)$$

such that  $v = \lambda u$ . In conclusion, the solution  $v$  of the PDE governing the motion is proportional to the excitation force  $F(t)$ .

Note that this substitution for the parameter  $\lambda$  is not generally possible, e.g. if a prestress is applied between the spring and the beam; it is the case for many other nonlinearities too ( $\lambda x^3 \neq (\lambda x)^3$ ).

Experimentally, the mean square responses of each harmonic is plotted against the power spectral density  $G_{xx}$  of the input force for three levels of excitation. The mean square response of the mode is calculated approximately by using the Mean Square Bandwidth  $\pi\zeta\omega_n$ . The experimental estimate of the equivalent viscous damping ratio is  $\zeta = \frac{\omega_2 - \omega_1}{2\omega_n}$ , where  $\omega_n$  is the resonance frequency,  $\omega_1$  and  $\omega_2$  are the frequencies corresponding to the half-power points (-3dB below the maximum peak response).

Usually, this method is used to approximate the mean square response at the natural frequency of a linear system. Herein, it is used at the first resonance frequency of the nonlinear system (32 Hz) which can be calculated as the inverse of the mean of the linear periods of the two piecewise linear systems; it is also applied to its harmonics. Figure 2.13 shows the mean square responses for the fundamental mode and for the first two harmonics normalized by the excitation mean square level, against three different input levels. As the excitation level increases the response at the excitation frequency and its harmonics increases proportionally, the relationship between the fundamental mode and its harmonics is linear; this linear behaviour is due to the linearity of the spring and the beam.

## 2.6 Numerical simulations

In this section, some further numerical simulations are presented in order to investigate and understand better the system behaviour. Figures 2.14 and 2.15 show the displacement for a sine excitation at 32 Hz and 124 Hz respectively; Figure 2.16 shows the frequency content of the displacement for a sine excitation at 32 Hz; the results cannot be compared to the experiments as it is not easy to realize a simple sine excitation. The dynamic behaviour of the system is similar to those presented in the previous section. The main response is split into all the subharmonics of the excitation frequency.

The elastic force from the spring is applied to the free end of the beam and should be taken in account as it can damage the structure; this force is non differentiable as the spring is only on contact when the beam has a negative displacement and its magnitude is proportional to the spring compression. Figure 2.17 and 2.18 show the predicted time signal of the force applied to the beam for a sine excitation at 32 Hz and 124 Hz respectively. Note that in case of a bilateral spring (spring attached to the beam), the time signal should be differentiable and periodic with a zero mean.

## 2.7 The effect of the unilateral spring position

An aim of this work is to provide a model which can predict the dynamic behaviour of a beam striking an elastic support. It is also necessary to choose the preferable points of the structure to position the support. In this section, the spring is moved to the node of the second linear beam mode which corresponds to a particular node of the F.E. model (see Figure 2.19). The subsequent numerical results show a linear behaviour of the system for an excitation near the second eigen frequency. They show a nonlinear behaviour as in the previous case for any other frequency of excitation. The results are presented in the frequency domain as before taking in account the new spring's position. Figure 2.20 shows the FFT of the numerical and the experimental displacements for an excitation at 122 Hz, very close to the second eigen frequency of the linearized system (see Table 2.2). It is clear that the response primarily has a single frequency content as the input signal (Figure 2.21), which is a fundamental property of a linear system.

Figure 2.22 shows the FFT of the experimental and the numerical displacements for an excitation of 32 Hz. The input frequency is split into all subharmonics, the behaviour of the beam is the same as described in the previous section, as the system is no longer linear.

## Conclusions

A numerical and experimental study of a beam with a unilateral elastic contact has been presented, the model used for the predictions having been validated by experiments. The comparison was performed in the frequency domain for different excitation frequencies; the results showed a very good agreement.

The comparison in the time domain needs a sophisticated processing of the time domain signals to eliminate or reduce the contribution from higher order frequencies not involved in the motion; this aspect will be in the scope of the future.

The results showed the effect of the spring position on the dynamic behaviour; other positions could be of interest if the system is subjected to high frequency excitation as the number of nodes increase with respect to the excited modes. Some experimental results for a prestressed contact is currently under investigation, this will be reported in the future. Also, future work will consider other types of excitation such as broadband random base excitation which might be present for the practical application of launching stacked solar array panels.

## Acknowledgements

This work was conducted for a PhD project of the first author with a scholarship from Thales Alenia Space, France. The authors also gratefully acknowledge the financial support of the "Conseil Générale des Alpes Maritimes" to realize this project.

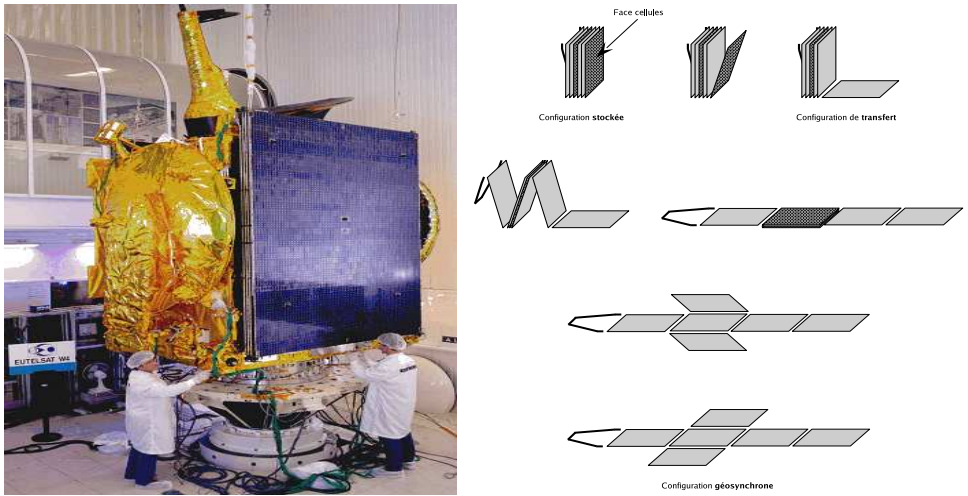


Figure 2.2. Left: Solar array of a satellite under a test on a shaker. Right: A solar array from the folded to the final position

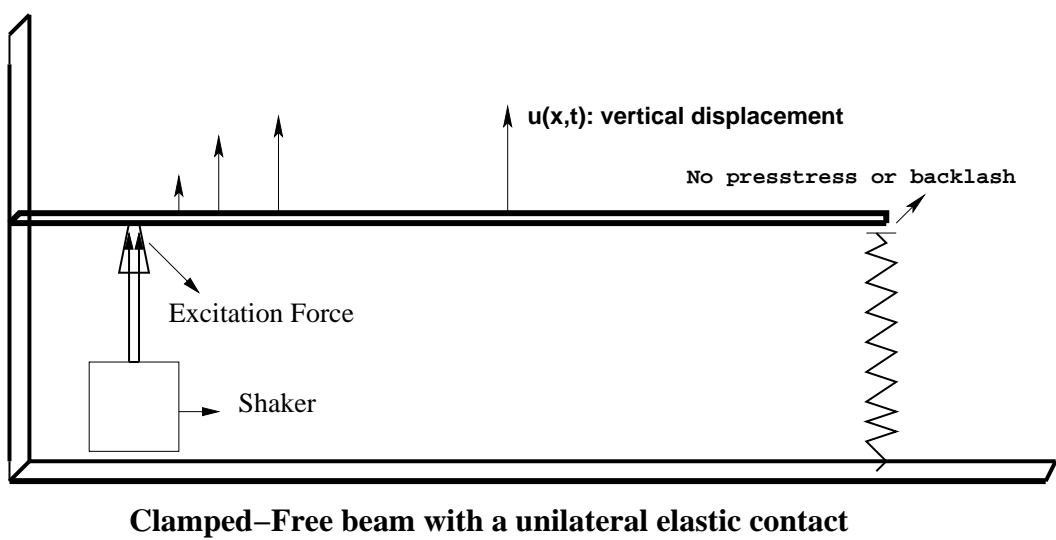


Figure 2.3. beam system with an unilateral spring under a periodic excitation

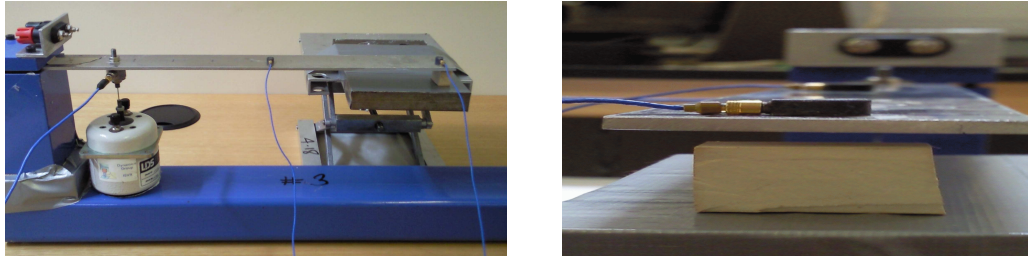


Figure 2.4. The rig used for the experiments: a linear clamped-free beam in contact with a rubber support (enlarged photograph on the right).

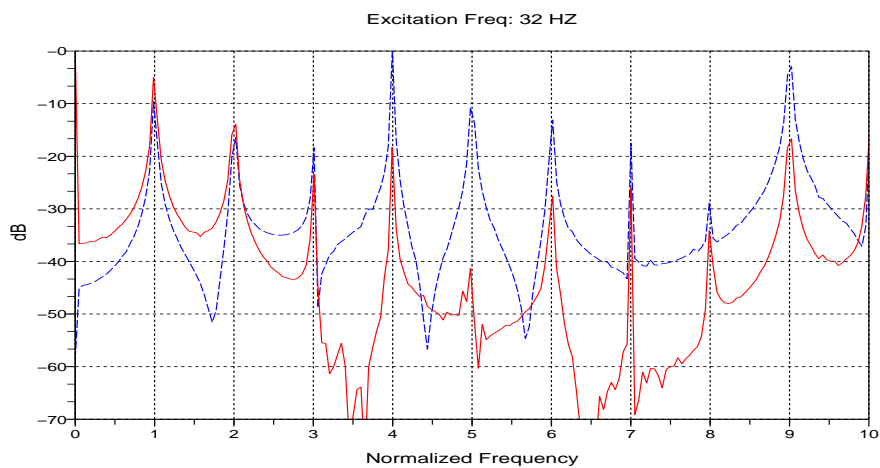


Figure 2.5. Predicted (solid) and measured displacements (dashed) (dB) for an excitation at 32 Hz applied to the beam with unilateral support stiffness. The displacement is normalized by the peak value and is measured immediately above the support and the frequency axis is normalized by the excitation frequency.

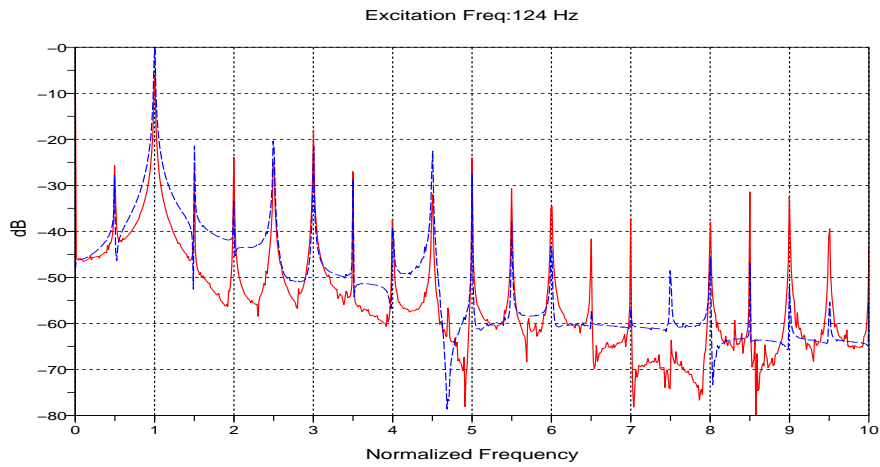


Figure 2.6. Predicted (solid) and measured displacements (dashed) (dB) for an excitation at 124 Hz applied to the beam with unilateral support stiffness. The displacement is normalized by the peak value and is measured immediately above the support and the frequency axis is normalized by the excitation frequency.

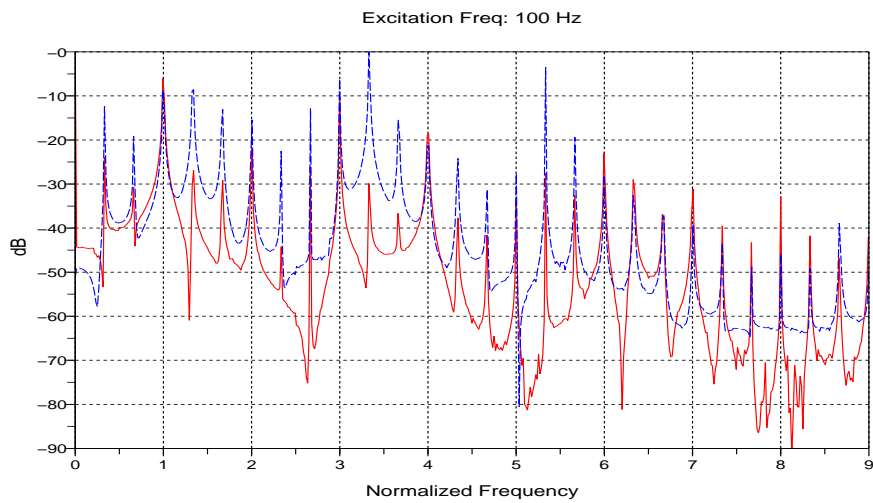


Figure 2.7. Predicted (solid) and measured displacements (dashed) (dB) for an excitation at 100 Hz applied to the beam with unilateral support stiffness. The displacement is normalized by the peak value and is measured immediately above the support and the frequency axis is normalized by the excitation frequency.

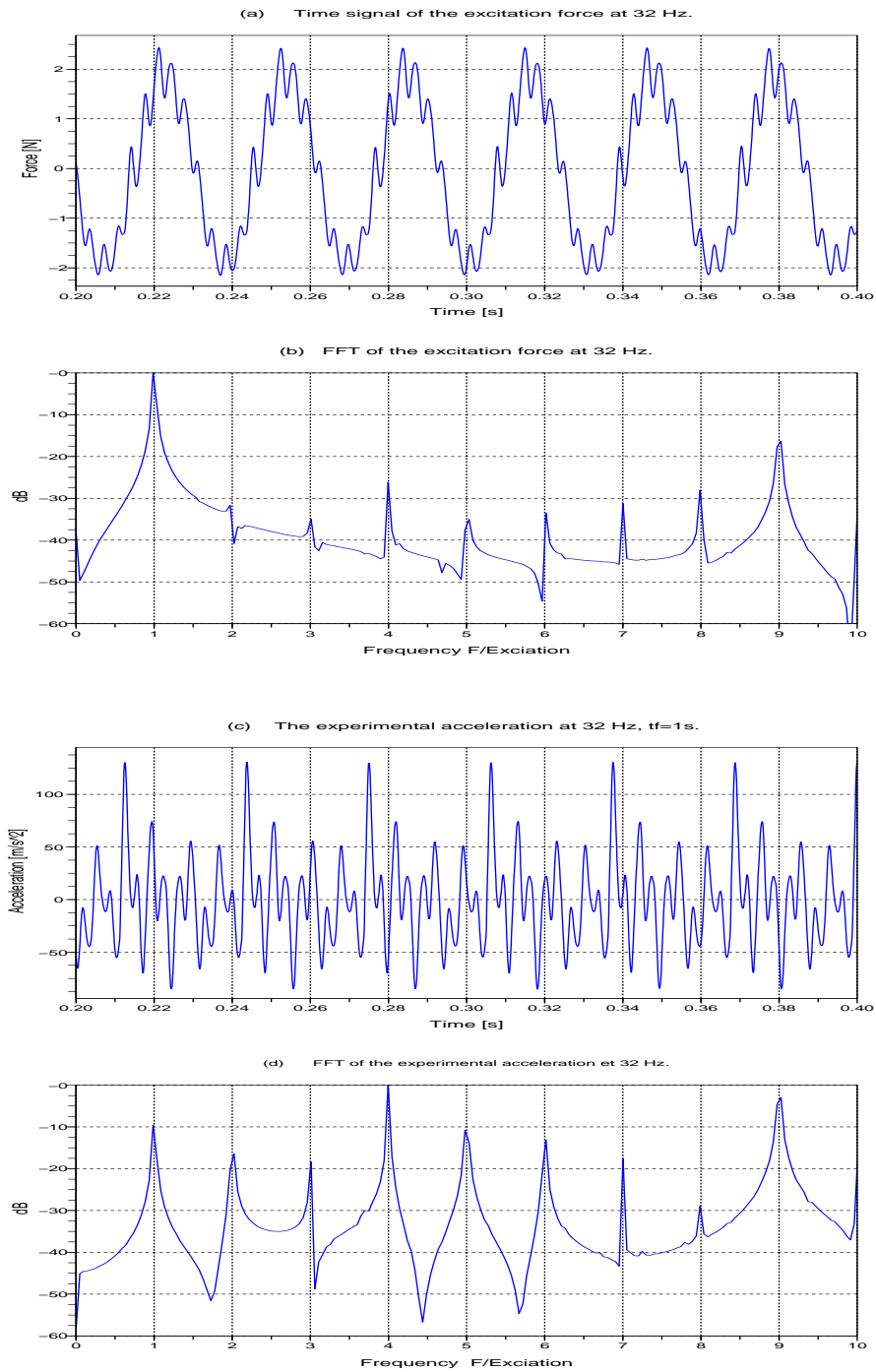


Figure 2.8. Measured excitation force (a) and its frequency contents (b), measured acceleration response (c) and its frequency content (d) for an excitation at 32 Hz. Strictly the force is not harmonic.

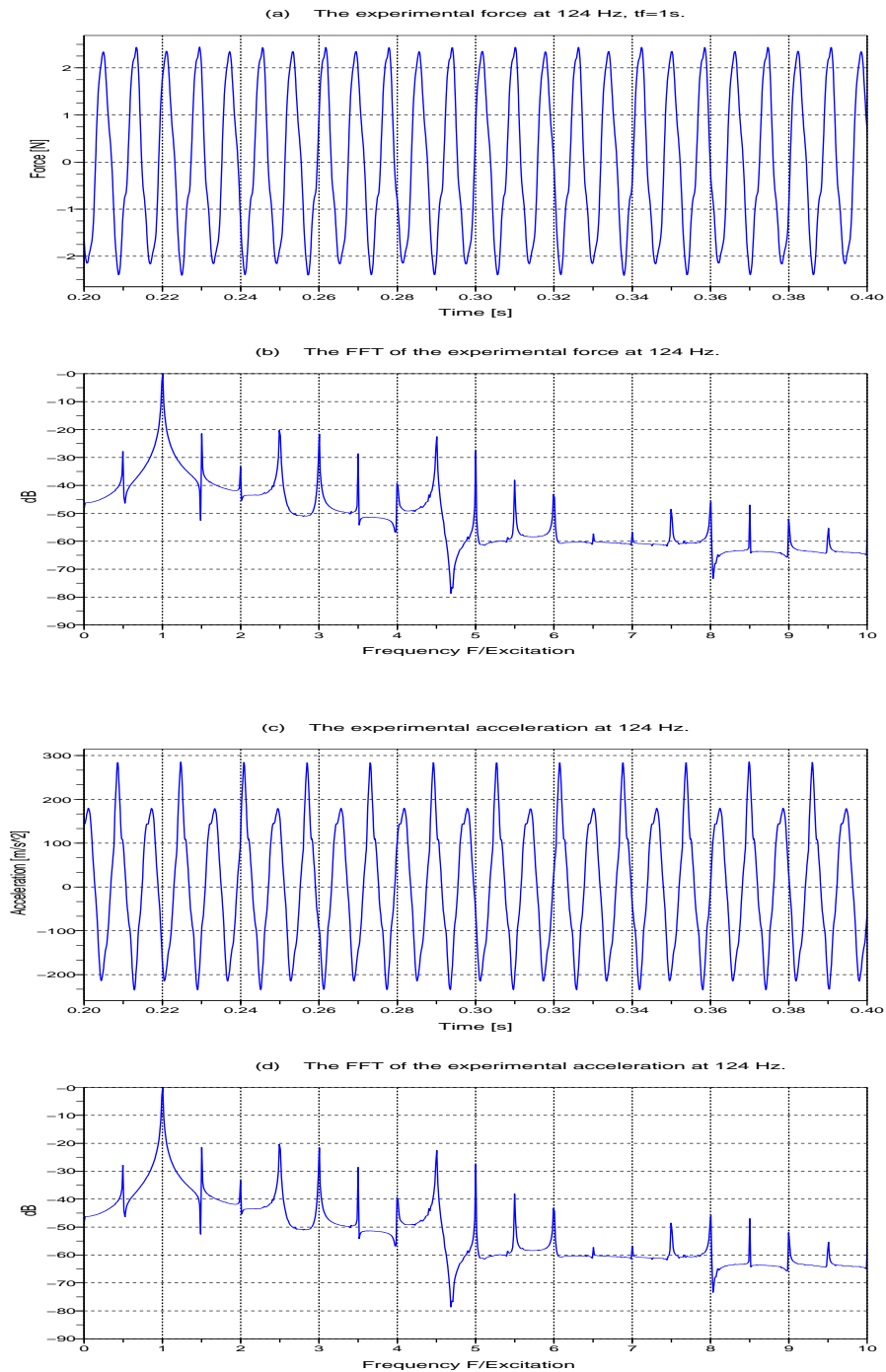


Figure 2.9. Measured excitation force (a) and its frequency contents (b), the measured acceleration response (c) and its frequency content (d) for an excitation at 124 Hz. Strictly the force is not harmonic.

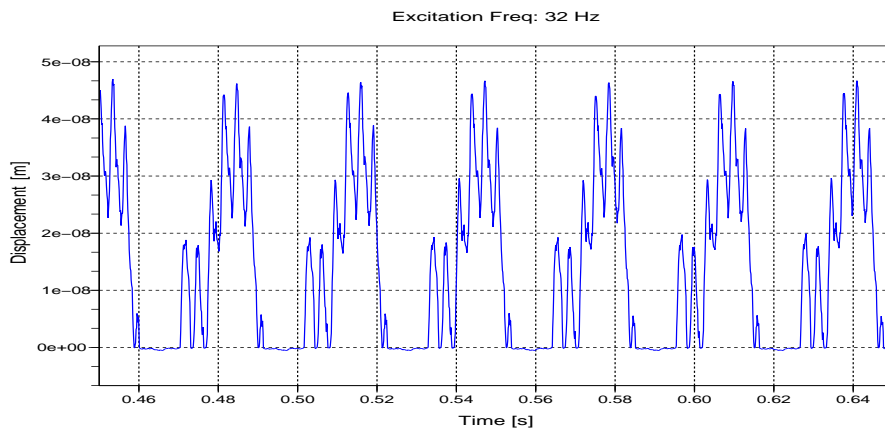


Figure 2.10. The predicted displacements for an excitation at 32 Hz; the displacement is measured immediately above the support. The high unilateral stiffness yields almost a positive displacement.

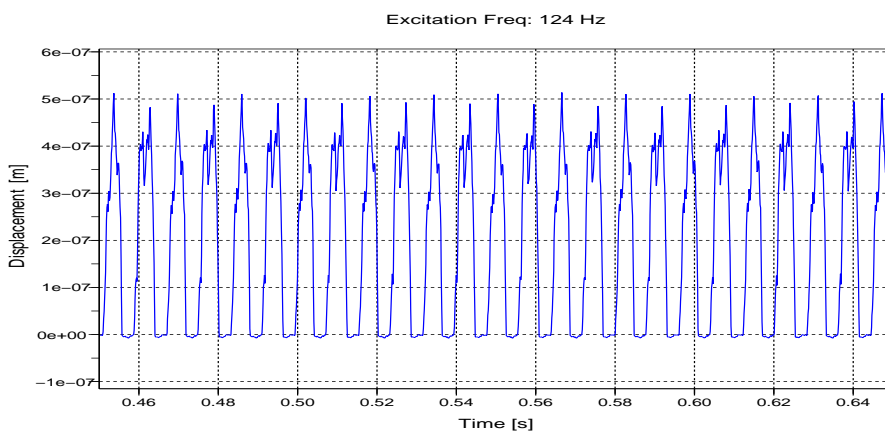


Figure 2.11. The predicted displacements for an excitation at 124 Hz, the displacement is measured immediately above the support.

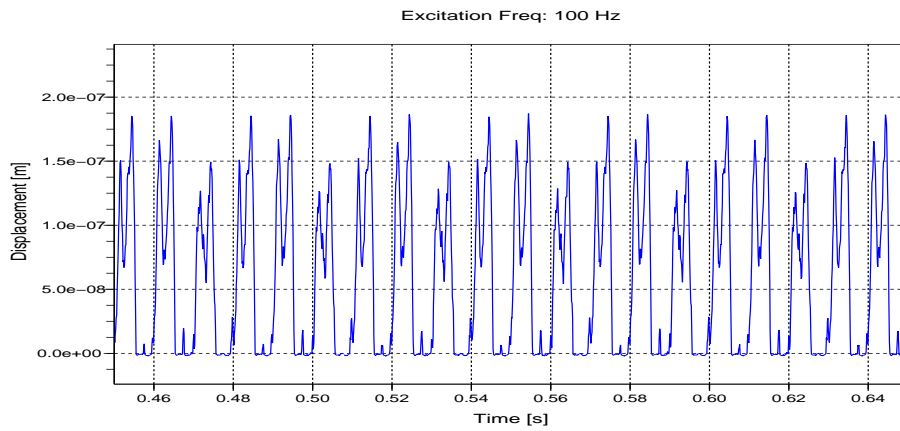


Figure 2.12. The predicted displacements for an excitation at 100 Hz, the displacement is measured immediately above the support.

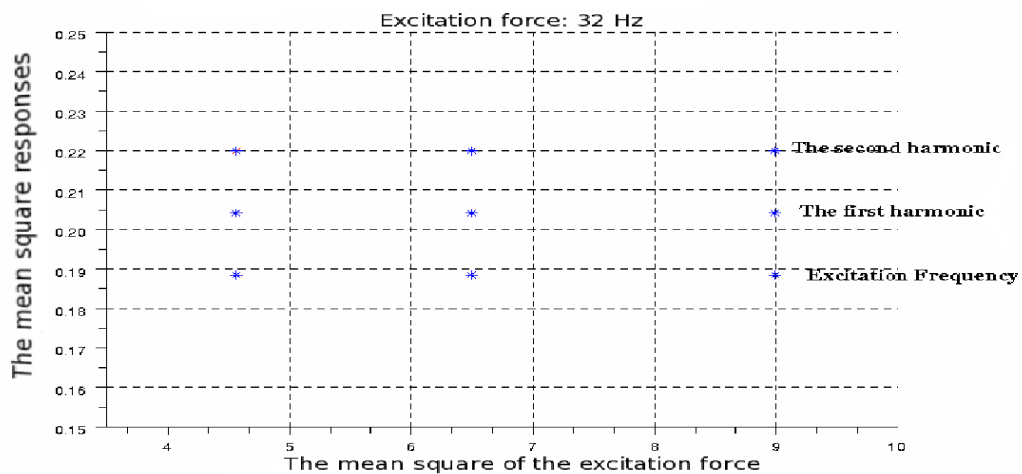


Figure 2.13. The normalized mean square responses (mean square displacement divided by the mean square excitation force) in each harmonic for inputs at three different mean square force levels. The excitation frequency is 32 Hz, the acceleration is measured immediately above the support.

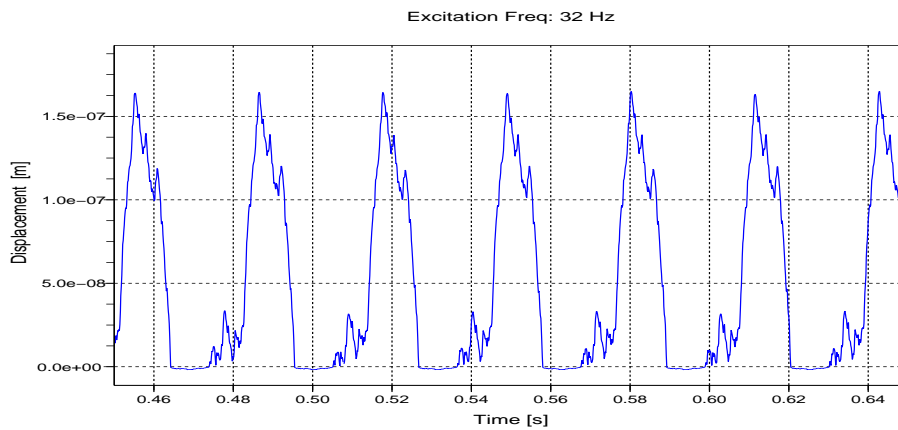


Figure 2.14. The predicted displacements for a sine excitation at 32 Hz, The acceleration magnitude is  $a = 1 \text{ m/s}^2$ . The displacement is measured immediately above the support.

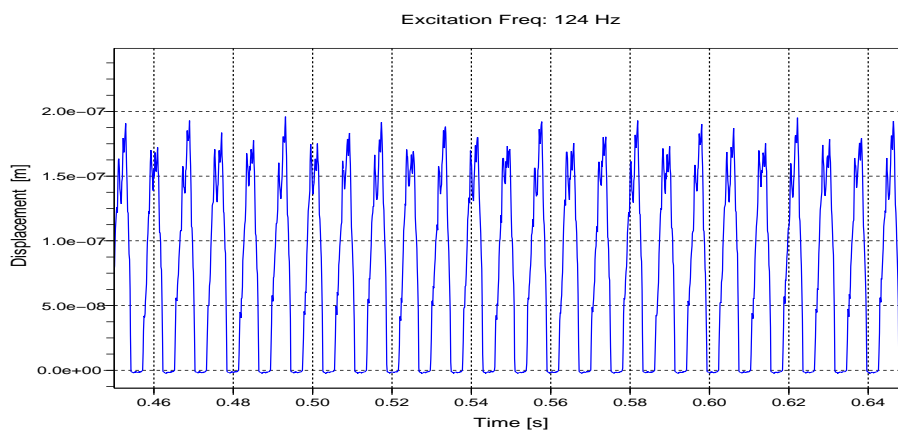


Figure 2.15. The predicted displacements for a sine excitation at 124 Hz. The acceleration magnitude is  $a = 1 \text{ m/s}^2$ . The displacement is measured immediately above the support.

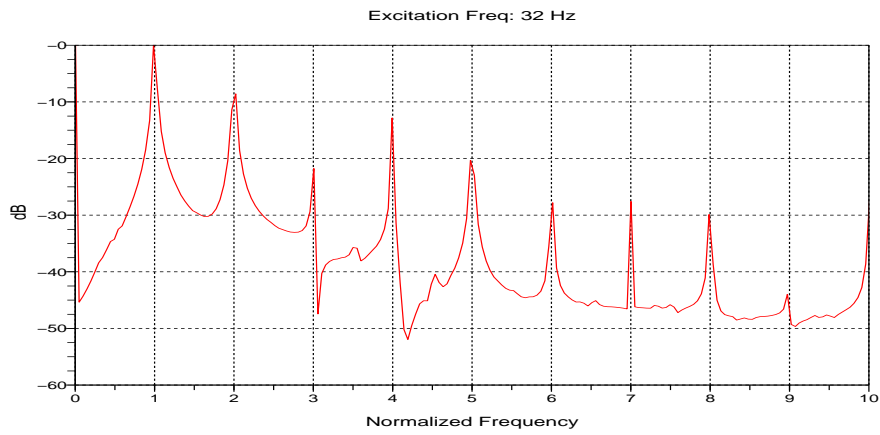


Figure 2.16. The frequency content of the predicted numerical displacement for sine excitation at 32 Hz, the displacement is measured immediately above the support. The excitation frequency is split into all its harmonics.

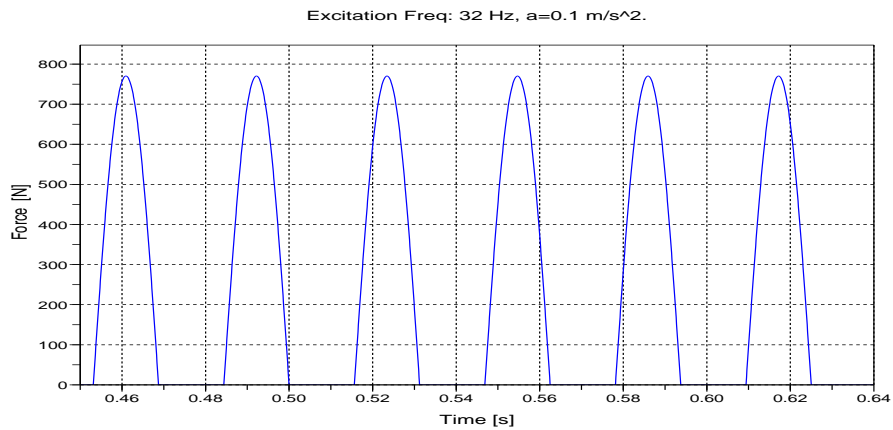


Figure 2.17. The predicted elastic force of the spring support for an excitation at 32 Hz. The acceleration magnitude is  $a = 0.1m/s^2$  and the spring is only in contact at times where the beam displacement is negative.

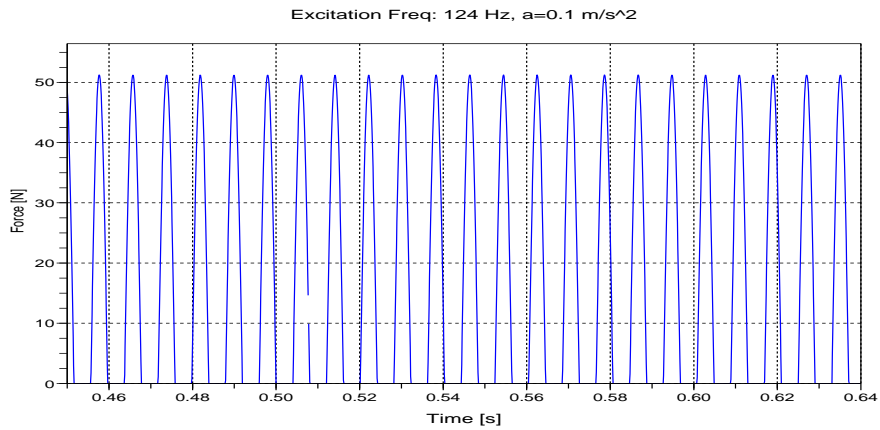


Figure 2.18. The predicted elastic force of the spring support for an excitation at 124 Hz. The acceleration magnitude is  $a = 0.1m/s^2$  and the spring is only in contact at times where the beam displacement is negative.

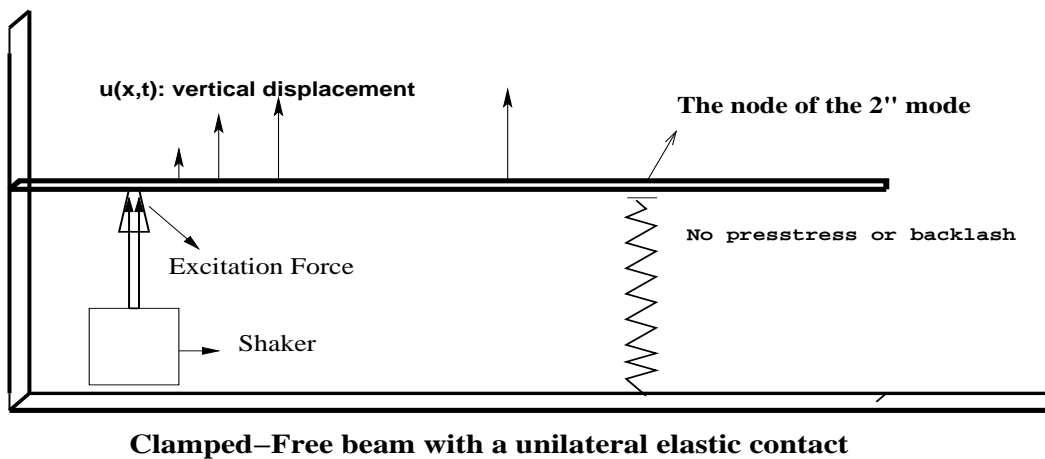


Figure 2.19. beam system with an unilateral spring under a periodic excitation

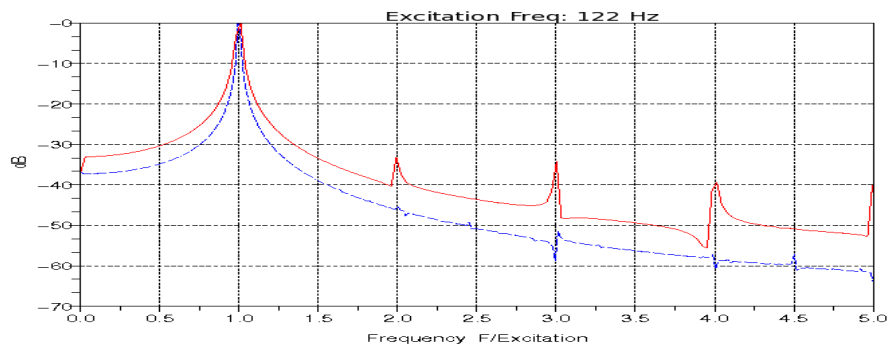


Figure 2.20. Predicted (solid) and measured displacements (dB) for an excitation at 122 Hz applied to the beam with unilateral support stiffness. The displacement is measured immediately above the support and the frequency axis is normalized by the excitation frequency.

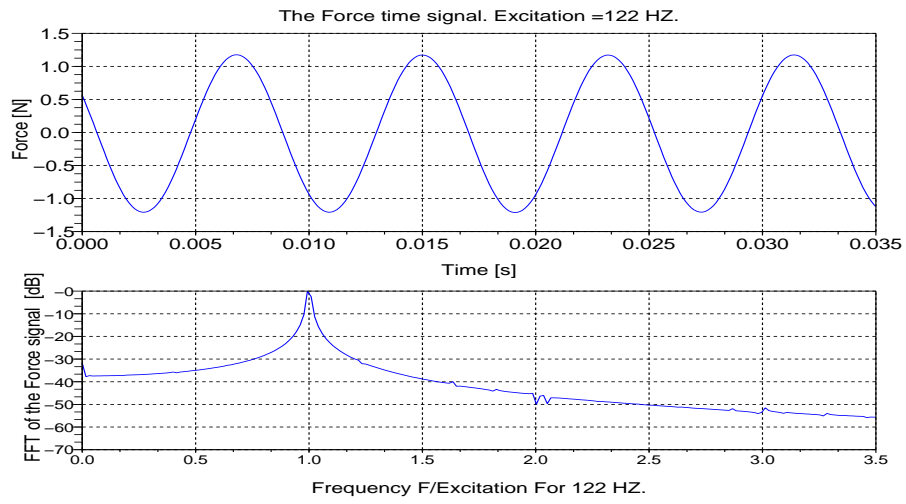


Figure 2.21. The time signal and its FFT of the input force for an excitation at 122 Hz.

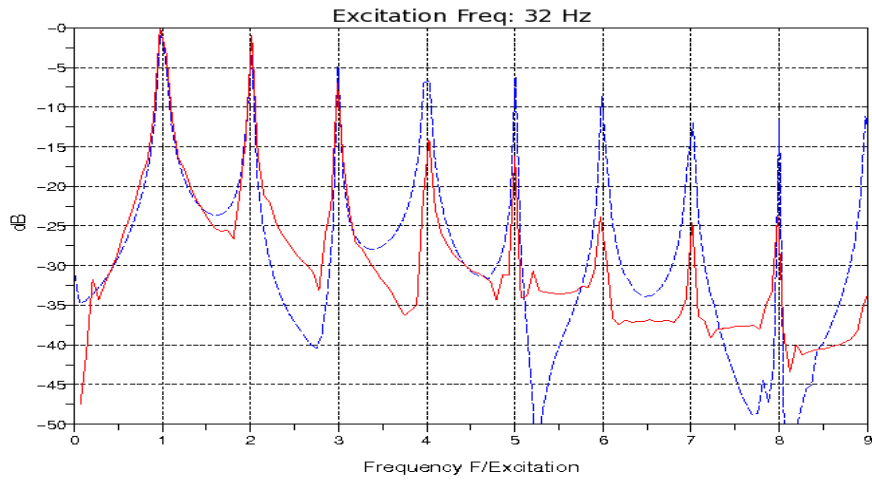


Figure 2.22. Predicted (solid) and measured displacements (dB) for an excitation at 32 Hz applied to the beam with unilateral support stiffness. The displacement is measured immediately above the support and the frequency axis is normalized by the excitation frequency.



## Chapter 3

# A numerical method to compute nonlinear normal modes of mechanical systems

---

The concept of nonlinear normal modes is discussed in this paper. A new formulation is given to find these modes as a zero of a nonlinear mapping. An algorithm based on the continuation of periodic solution is performed using optimization methods. Finally, numerical results are presented for a mass-spring model with a cubic nonlinearity. The algorithm is also used for the calculation of the nonlinear normal modes of the mechanical system of Chapter 1 without proof, but an asymptotic approach is studied in Chapter 4 to validate the numerical results via multiple scales method.

---

# Nonlinear normal modes of mechanical systems: Existence - Numerical method

H.Hazim <sup>a,\*</sup> , B.Rousselet <sup>a</sup>

<sup>a</sup>*J.A.D. Laboratory U.M.R. CNRS 6621, University of Nice Sophia-Antipolis, 06108 Valrose, Nice, France.*

---

## **Abstract**

A new mathematical formulation is given to find the nonlinear normal modes as a zero of a nonlinear mapping. A numerical algorithm based on the continuation of periodic solutions is performed using optimization methods. Numerical results for models with cubic nonlinearity and for unilateral contact are also presented.

*Keywords:* Nonlinear vibrations, Nonlinear normal modes (NNM), Modelling.

---

---

\* Corresponding author. tel: +33 04 92076276

*Email address:* hamad.hazim@unice.fr (H.Hazim)

## 3.1 Introduction

The concept of nonlinear normal modes has been the main topic of many structural dynamists during the last twenty years. These modes are presented to be a natural extension of the well-known linear normal modes of linear mechanical systems. The linear theory has shown its limits especially because nonlinearities are encountered in most of mechanical systems and structures with different types. Any sophisticated modelling of a real situation cannot be done without incorporating the nonlinearity coming from the compartment law of the structure or from an interaction between its components and etc... The linear theory cannot predict bifurcations, instabilities, harmonics, jumps and many other features of nonlinear systems. However there is not a complete theory to deal with all this phenomena such as the linear one, therefore the need of new theoretical tools able to clarify the nonlinear behavior of systems which cannot be treated and analyzed with linear tools. The nonlinear normal modes can clarify and get more insight in the understanding of nonlinear behaviour of a wide range of mechanical systems.

A linear normal mode is defined to be a periodic solution of all the components of the system with the same phase. This normal mode can be obtained by providing an eigenvector as initial condition to the system and the solution will remain in the subspace which corresponds to this eigenvector with the corresponding period. It is easy to prove this fact since a linear system can be decoupled in the eigenvector basis. The second main property of a linear system is the superposition of solutions: the solution of a system excited by an initial condition which is a linear combination of many eigenvectors can be written as a linear combination of the solutions given by each eigenvector. The superposition of the solutions does not hold for a nonlinear system, in contrast a periodic solution can be found, this is proved in this paper for smooth nonlinearities.

### 3.1.1 State of the Art

The nonlinear normal mode of a nonlinear undamped autonomous system was first defined by Rosenberg as a motion in unison of the system in early sixties [25,26]. Rand also studied the nonlinear normal modes for a two-degree-of-freedom oscillator [27]. In the nineties an important progress was recorded thanks to the work of Vakakis and Pierre and Shaw. The Ph.D. dissertation of the first was focused on the analysis and identifications of linear and nonlinear normal modes in vibrating systems, he also published other papers on the NNM [28]. Pierre and Shaw defined the nonlinear normal mode as a motion which takes place on a two-dimensional invariant manifold in the system's phase space [18,29]. G.Iooss and E. Lombardi published a recent paper on the normal forms and the invariant manifold, the paper deals with general nonlinear differential systems with a rigorous proof [30]. S.Junca and B.Rousselet submitted a paper on the nonlinear normal modes using asymptotic expansion [31], it is a fundamental reference for Chapter 4. Nayfeh et al also worked on the calculation of the nonlinear normal modes via asymptotic approach by treating the partial differential equation governing the dynamic of the continuous system [32,33]. Asymptotic expansion has been used to evaluate nonlinear normal modes for a piece wise linear two d-o-f system [34]. Bellizzi et al worked on the normal modes and provided different methods [35–38]. In 2009, G.Kerschen et al published a two parts paper on the nonlinear normal mode, they

presented an overview about the previous works and about the use of these modes in the modern mechanical engineering. They also presented a numerical methods to compute the nonlinear normal modes using a shooting and continuous methods [17, 39]. The authors recommend these papers and its citations for more insight and for a general state of the art.

### **3.1.2 In this paper**

We present an algorithm for the computation of the nonlinear normal modes using existing numerical methods. The method presented here is based on the fact that the nonlinear normal modes are a natural extension of the linear normal modes. The paper is structured as following, a new definition and formulation of the nonlinear normal modes are presented, then an algorithm for the calculation of these modes are presented with some applications. An interest of the authors is the study of nonlinearities of contact type, the algorithm is then used to calculate the nonlinear normal modes of discrete systems with a unilateral contact; the proof of existence in this non smooth case is in progress. Alternatively a multiple scales method is improved to compute the response of a system with a unilateral contact for autonomous and for forced systems, see Chapter 4.

## 3.2 Mechanical system and normal modes

Consider the non linear undamped autonomous differential system

$$M\ddot{X} + KX + G(X) = 0 \quad G(0) = 0, \quad G'(0) = 0, \quad (3.2.1)$$

where  $X \in \mathbb{R}$ ,  $K$  and  $M$  are two  $m \times m$  symmetric and positive definite matrices,  $G(X) \in \mathbb{R}^m$  is a nonlinear term which depends only on  $X$ . We denote by  $(\omega_i^2)_{i=1,\dots,m}$  and  $(v_i)_{i=1,\dots,m}$  the generalized eigenvalues and the generalized eigenvectors of  $M$  and  $K$  respectively

$$Kv_i = \omega_i^2 Mv_i.$$

In general, this system does not have an explicit solution for any given  $G$ . The goal of this study is to calculate a periodic solution of the system based on the non linear normal modes (NNM) concept which is an extension of the normal modes of the linear system.

### 3.2.1 Normal Modes of the linearized system

The linearized system of (3.2.1) can be written as

$$M\ddot{X} + KX = 0. \quad (3.2.2)$$

If the system is excited by an eigenvector as initial condition with a zero velocity, then the solution will be periodic with a period which corresponds to the considered eigenvalue. If  $v_i$  is a generalized eigenvector of  $M$  and  $K$ ,  $T_i = \frac{2\pi}{\omega_i}$  the corresponding linear period, then we have a solution of the system given by

$$X_i = v_i \cos(\omega_i t), \quad (3.2.3)$$

$X_i(0) = v_i$  and

$$X_i(T_i) = v_i \cos(\omega_i T_i) = v_i \cos(\omega_i \frac{2\pi}{\omega_i}) = v_i, \quad \dot{X}_i(T_i) = 0.$$

The couple  $[v_i, T_i]$  is a linear normal mode of system (3.2.1). The solution can also be found by writing the system in the eigenvector basis and solving it component by component. This technique does not hold for nonlinear systems as nonlinear terms will be present in all components.

### 3.2.2 Nonlinear Normal Modes (NNM) of the nonlinear system

We cite the two main definitions of the nonlinear normal modes. The definition given in the next section is inspired from the Rosenberg's definition.

**Definition 3.2.1.** [Rosenberg's definition] During the normal mode motion of a linear conservative system, each component moves with the same frequency and with a fixed ratio amongst the displacement of the components. An NNM is a vibration in unison of the system. This definition require that all material points of the system reach their extreme values and pass through zero simultaneously and allow all displacements to be expressed in terms of a single reference displacement.

**Definition 3.2.2.** [Pierre and Shaw definition] A normal mode of motion for a non-linear, autonomous and undamped system is a motion which takes place on a two-dimensional invariant manifold in the system's phase space. This manifold has the following properties: it passes through the stable equilibrium point  $(x, y) = (0, 0)$  of the system and at this point, it is tangent to a plane which is an eigenspace of the system linearized about  $(x, y) = (0, 0)$ .

### 3.3 Nonlinear normal modes: mathematical formulation

We present in this section the mathematical formulation used to calculate the nonlinear normal modes.

#### 3.3.1 Nonlinear differential system

We consider the parametric differential system associated to system (3.2.1) and written in the eigenvector basis,

$$\ddot{X} + \Omega^2 X + \epsilon F(X) = 0 \quad F(0) = 0, \quad F'(0) = 0, \quad (3.3.1)$$

where  $\epsilon$  is a continuation parameter,  $\Omega^2 = \text{diag}(\omega_1, \dots, \omega_n)$  and  $F(X)$  is a non linear term depending only on  $X$ . The idea is to find, corresponding to the linear normal mode  $(v_i, \frac{2\pi}{\omega_i})$ , initial condition vectors in position  $(X_0^i)$  and in velocity  $(X_1^i)$  which yield a periodic solution  $(X^i(t))$  of system (3.3.1) of a period  $T_i$  to be determined,  $\forall i \in \{1, \dots, m\}$ .

**Definition 3.3.1.**  $\forall i \in \{1, \dots, m\}$ ,  $(X_0^i, X_1^i, T_i)$  is the nonlinear normal mode of system (3.3.1) corresponding to the linear normal mode such as

1.  $X_0^i \rightarrow v_i$  and  $T_i \rightarrow \frac{2\pi}{\omega_i}$  when  $\epsilon \rightarrow 0$ ,
2.  $X^i(T_i) = X_0^i$ ,
3.  $\dot{X}^i(T_i) = X_1^i$ .

For convenience, system (3.3.1) is written as a first order differential system in  $Z$ ,

$$\dot{Z} = AZ + \epsilon f(Z) \quad (3.3.2)$$

with  $Z = [X, \dot{X}]$ ,  $A = \begin{pmatrix} 0 & I_n \\ -\Omega^2 & 0 \end{pmatrix}$  and  $f(Z) = [0, F(X)]$ .

We denote by  $[Z_0, T]$  the nonlinear normal mode for  $i=1$  and by  $Y_0 = [Z_{T_0}, T_0] = [[v_1, 0], \frac{2\pi}{\omega_1}]$  the corresponding linear normal mode, there is no restriction to deal with the other nonlinear modes.

*Remark 3.3.2.* The nonlinear normal mode is defined with a vector and an associated period which ensure a periodic solution of all the degree of freedom of a nonlinear system with no phase delay. This is in agreement with the Rosenberg's definition.

### 3.3.2 Formulation

We will present an algorithm to calculate then nonlinear normal mode  $(Z_0, T)$ , the same technique can be used to calculate the other modes. The continuation of periodic solutions will play an important part in this approach because the algorithms may not converge for a large  $\epsilon$ . Two major difficulties are encountered to solve our problem, the first is to prove the existence of a periodic solution and the second is to perform a robust numerical method to calculate this nonlinear mode. In both cases, a convenient mathematical formulation should be in place to allow the use of existent theorems and algorithms. The unknowns  $Z_0$  and  $T$  are then considered as the zeros of a mapping  $\Phi$  defined as following

#### Definition 3.3.3.

$$\begin{aligned} \Phi : \quad \mathbb{R} \times \mathbb{R}^n \times \mathbb{R} &\longrightarrow \mathbb{R}^{n+1} \\ (\epsilon, Z_0, T) &\longrightarrow \Phi(\epsilon, Z_0, T) = \begin{pmatrix} Z(T, Z_0, \epsilon) - Z_0 \\ E(Z_0) - c \end{pmatrix}, \end{aligned} \quad (3.3.3)$$

where

1.  $Z(T, Z_0, \epsilon)$  is the solution of system (3.3.2) integrated numerically on  $[0, T]$  with  $Z_0$  as initial condition and evaluated at  $T$ , it depends on  $\epsilon$  implicitly by the nonlinear term,
2.  $E$  is the total energy of the initial condition,  $E = {}^t Z_0 N Z_0$ , where  $N = \begin{pmatrix} \Omega^2 & 0 \\ 0 & I_n \end{pmatrix}$ ,
3.  $c$  is a level of energy.

To find the nonlinear normal mode  $(Z_0, T)$  the following nonlinear system of equations has to be solved

$$\begin{cases} Z(T, Z_0, \epsilon) - Z_0 = 0, \\ E(Z_0) - c = 0. \end{cases} \quad (3.3.4)$$

## 3.4 Theoretical investigation in the smooth case

### 3.4.1 Useful theorems

In this section, we will cite some useful theorems for the existence and the uniqueness of solutions of ordinary differential systems and for nonlinear systems of equations without proof. Let  $E$  be a Banach space,  $I$  an open set in the field  $\mathbb{R}$ ,  $H$  an open subset of  $E$ ,  $f$  a continuously differentiable mapping of  $I \times H$  into  $E$ . A differentiable mapping  $u$  of an open ball  $J \subset I$  into  $H$  is called a solution of the differential equation

$$x' = f(t, x) \quad (3.4.1)$$

if, for any  $t \in J$ , we have

$$u'(t) = f(t, u(t)). \quad (3.4.2)$$

It follows at once from (3.4.2) that  $u$  is then continuously differentiable in  $J$ .

**Proposition 3.4.1.** *In order that, in the ball  $J \subset I$  of center  $t_0$ , the mapping  $u$  of  $J$  into  $H$  be a solution of (3.4.1) such that  $u(t_0) = x_0 \in H$ , it is necessary and sufficient that  $u$  be continuous in  $J$  and such that*

$$u(t) = x_0 + \int_{t_0}^t f(s, u(s)) ds$$

*This follows from the definition of a primitive.*

**Theorem 3.4.2.** *[Cauchy's existence theorem]*

*If  $f$  is continuously differentiable in  $I \times H$ , for any  $t_0 \in I$  and any  $x_0 \in H$  there exists an open ball  $J \subset I$  of center  $t_0$  such that there is in  $J$  one and only one solution  $u$  of equation (3.4.1) such that  $u(t_0) = x_0$ .*

**Definition 3.4.3.**

A mapping  $f(t, x)$  satisfies a Lipschitz condition in a  $I \times H$ , when, for some constant  $L$  (Lipschitz constant), it satisfies the inequality

$$\|f(t, x) - f(t, y)\| \leq L\|x - y\| \quad (3.4.3)$$

for all point-pairs  $(t, x)$  and  $(t, y)$  in  $I \times H$ .

**Theorem 3.4.4.** *[Uniqueness theorem] [40]*

*If  $f$  satisfies a Lipschitz condition in a domain  $H$ , then there is at most one solution  $u(t)$  of equation (3.4.1) such that  $u(t_0) = x_0$  in  $H$ .*

**Theorem 3.4.5.** *[Dependence of the solution on initial conditions]*

*Let  $f$  be locally Lipschitzian in  $I \times H$ . Then for any point  $(a, b) \in I \times H$ :*

1. *There exists an open ball  $J \subset I$  of center  $a$  and an open ball  $V \subset H$  of center  $b$  such that, for every point  $(t_0, x_0) \in J \times V$ , there exists a unique solution  $t \rightarrow u(t, t_0, x_0)$  of (3.4.1) defined in  $J$ , taking its values in  $H$  and such that  $u(t_0, t_0, x_0) = x_0$ .*
2. *The mapping  $(t, t_0, x_0) \rightarrow u(t, t_0, x_0)$  is uniformly continuous in  $J \times J \times V$*
3. *There is an open ball  $W \subset V$  of center  $b$  such that, for any point  $(t, t_0, x_0) \in J \times J \times W$ , the equation  $x_0 = u(t_0, t, x)$  has a unique solution  $x = u(t, t_0, x_0)$  in  $V$ .*

**Theorem 3.4.6.** *With the notation of Theorem 3.4.5, suppose that  $f$  is continuously differentiable (resp.  $p$  times continuously differentiable) in  $I \times H$ . Then it is possible to take  $J$  and  $V$  such that the function  $(t, t_0, x_0) \rightarrow u(t, t_0, x_0)$  is continuously differentiable (resp.  $p$  times continuously differentiable) in  $J \times J \times V$ .*

**Theorem 3.4.7.** *[The implicit function theorem]*

*Let  $E, F, G$  be three Banach spaces,  $f$  a continuously mapping of an open subset  $A$  of  $E \times F$  into  $G$ , Let  $(x_0, y_0)$  be a point of  $A$  such that  $f(x_0, y_0) = 0$  and that the partial derivative  $D_2 f(x_0, y_0)$  be a linear homeomorphism of  $F$  into  $G$ . Then, there is an open neighborhood  $U_0$  of  $x_0$  in  $E$  such that, for every open connected neighborhood  $U$  of  $x_0$ , contained in  $U_0$ , there is a unique continuous mapping  $u$  of  $U$  into  $F$  such that  $u(x_0) = y_0$ ,  $(x, u(x)) \in A$  and  $f(x, u(x)) = 0$  for any  $x \in U$ . Furthermore,  $u$  is continuously differentiable in  $U$ , and its derivative is given by  $u'(x) = -(D_2 f(x, u(x)))^{-1} \circ (D_1 f(x, u(x)))$ .*

A classical optimization routine will be used to minimize  $J$  but the method may not converge directly for strong nonlinearities. An algorithm based on the continuation of periodic solutions is then proposed.

## 3.5 An algorithm to compute the nonlinear normal modes

In this section, we will recall an algorithm to compute the nonlinear normal modes introduced in [31] based on the formulation already studied in the previous section. In practice, we will solve the problem by the least square method to allow the use of optimization methods and to benefit of the large number of existing algorithms. In this case, the classical challenge is to find an accurate gradient of the function being optimized. Herein, two semi-analytical methods for the calculation of the gradient were developed [41, 42].

### 3.5.1 A relaxed problem

We use the notation of Section 3.3.2. System (3.3.4) is solved by the least square method. Consider then the following function to be minimized

$$J_\epsilon(Z_0, T) = \|Z_\epsilon(T) - Z_0\|^2 + \|E - c\|^2. \quad (3.5.1)$$

### 3.5.2 The algorithm

The main idea of the algorithm is to minimize  $J$  for small  $\epsilon$  and for a given level of energy  $c$  with the linear normal mode  $Y_0$  as initial guess. The solution found will then be used as an initial guess point of the optimization algorithm after a small increase of  $\epsilon$  and so on. If the algorithm does not converge for the updated  $\epsilon$  then we go back and we choose again a smaller  $\epsilon$ . We repeat the procedure until reaching a needed level of nonlinearity. Algorithm 2 illustrates the steps.

### 3.5.3 Energy dependence

The energy dependence is an important feature of nonlinear mechanical systems. The nonlinear normal mode can take different shapes when increasing the level of energy of the system. This form depends on the nonlinearity, it is then useful to study its effect to get more insight in the understanding of the dynamic behaviour. The algorithm used to calculate the nonlinear normal mode allows easily the calculation of the mode for different levels of energy. The idea is to recalculate  $Z_0$  and  $T$  by increasing the energy level  $c$  after the calculation of the nonlinear mode for a given level of nonlinearity  $\epsilon_{max}$ . Algorithm 3 illustrates the steps.

---

**Algorithm 2** Calculation of the nonlinear normal mode

---

**Input:**  $f(Z)$ , the nonlinear term.

**Input:**  $\epsilon$ , a small parameter in the neighborhood of 0.

**Input:**  $Y_0$ , the first guess point and  $c = {}^t Z_{T_0} N Z_{T_0}$ .

**Input:**  $\delta\epsilon$  the increment step.

**Output:**  $(Z_0, T)$ , the **nonlinear normal mode**.

- 1: **while**  $\epsilon \leq \epsilon_{max}$  **do**
- 2:   Solve  $\dot{Z} = AZ + \epsilon f(Z)$  with  $Z_0$  as initial condition on  $[0, T]$ .
- 3:   Compute  $E = {}^t Z_0 N Z_0$ .
- 4:   Calculate the gradient of  $J_\epsilon$  (see the method later).
- 5:   Minimize  $J_\epsilon(Z_0, T) = \|Z_\epsilon(T) - Z_0\|^2 + \|E - c\|^2$  using a conjugate gradient algorithm with the guess point  $Y_0 = (Z_{T_0}, T_0)$ .
- 6:   Update  $Y_0 = (Z_0, T)$
- 7:   **if** The optimization converge **then**
- 8:     Update  $\epsilon$ :  $\epsilon = \epsilon + \delta\epsilon$ .
- 9:   **else**
- 10:      $\epsilon = \epsilon - \frac{\delta\epsilon}{2}$ .
- 11:   **end if**
- 12: **end while**

---

---

**Algorithm 3** Energy dependence

---

**Input:**  $(Z_0, T)$  the nonlinear normal mode already computed using Algorithm 2.

**Input:**  $c$  the energy of the linear part of the system.

**Input:**  $\delta c$  the increment step.

**Output:**  $(Z_c, T_c)$ , the **nonlinear normal mode for different levels of energy**.

- 1: **while**  $c \leq c_{max}$  **do**
- 2:   Solve  $\dot{Z} = AZ + \epsilon f(Z)$  with  $Z_0$  as initial condition numerically on  $[0, T]$ .
- 3:   Compute  $E = {}^t Z_0 N Z_0$ .
- 4:   Calculate the gradient of  $J_\epsilon$  (see the method later).
- 5:   Minimize  $J_\epsilon(Z_0, T) = \|Z_\epsilon(T) - Z_0\|^2 + \|E - c\|^2$  with the guess point  $Y_0 = (Z_0, T_0)$ .
- 6:   Update  $Y_0 = (Z_0, T)$ .
- 7:   **if** The optimization converge **then**
- 8:     Update  $c$ :  $c = c + \delta c$ .
- 9:   **else**
- 10:      $c = c - \frac{\delta c}{2}$ .
- 11:   **end if**
- 12: **end while**

---

### 3.5.4 Calculation of the gradient in the smooth case

As mentioned before, one major challenge in optimization problems is to provide a precise gradient of the function being optimized. This gradient has to be computed fast as it will be called at each iteration of the optimization algorithm. We provide herein a direct semi-analytical calculation of the gradient of the function  $J_\epsilon$  in the smooth case. It requires the integration of  $n$  differential systems which takes a long time for the computation. In turn, we calculate the gradient with the adjoint state of the problem which is much faster as it requires the integration of just one differential system. Both methods are performed and compared to the numerical calculation of the gradient based on the finite difference methods.

**Proposition 3.5.1.** *Let  $\nabla J_\epsilon$  be the gradient of  $J_\epsilon$  computed directly,  $N$  as in Definition 3.3.3 and  $h = (\varphi, 1)$  a vector of  $\mathbb{R}^{n+1}$  then,*

$$\begin{aligned} \langle \nabla J_\epsilon, h \rangle &= \sum_j \left\langle \frac{\partial J}{\partial Z_{0j}}, \varphi_j \right\rangle + \left\langle \frac{\partial J}{\partial T}, 1 \right\rangle \\ &= \sum_j 2^t (Z(T) - Z_0) \left( \frac{\partial Z(T)}{\partial Z_{0j}} \varphi_j - \varphi_j \right) + 4(E - c) ({}^t Z_0 N \varphi_j) \\ &\quad + {}^t (Z(T) - Z_0) \left( \frac{\partial Z(T)}{\partial T} \right). \end{aligned} \quad (3.5.2)$$

*Proof.*

Let us begin with the derivative of  $J_\epsilon$  with respect to  $Z_{0j}$ ,  $\forall j \in \{1, \dots, n\}$ :

$$\begin{aligned} \left\langle \frac{\partial J_\epsilon}{\partial Z_{0j}}, \varphi_j \right\rangle &= \left\langle 2^t (Z(T) - Z_0) \left( \frac{\partial Z(T)}{\partial Z_{0j}} - \frac{\partial Z_0}{\partial Z_{0j}} \right) + 2(E - c) \left( \frac{\partial E}{\partial Z_{0j}} \right), \varphi_j \right\rangle \\ &= 2^t (Z(T) - Z_0) \left( \frac{\partial Z(T)}{\partial Z_{0j}} \varphi_j - \varphi_j \right) + 4(E - c) ({}^t Z_0 N \varphi_j). \end{aligned} \quad (3.5.3)$$

as  $\frac{\partial E}{\partial Z_{0j}} = \frac{\partial ({}^t Z_0 N Z_0)}{\partial Z_{0j}} = 2^t Z_0 N \varphi_j$ .

The derivation with respect to  $T$  is given as:

$$\begin{aligned} \left\langle \frac{\partial J}{\partial T}, 1 \right\rangle &= 2^t (Z(T) - Z_0) \left( \frac{\partial Z(T)}{\partial T} - \frac{\partial Z_0}{\partial T} \right) + 2^t (E - c) \left( \frac{\partial E}{\partial T} \right) \\ &= 2^t (Z(T) - Z_0) \left( \frac{\partial Z(T)}{\partial T} \right), \end{aligned}$$

since  $E$  depends only on  $Z_0$  which does not depend on  $T$ . □

Finally, to achieve the computation of  $\nabla J_\epsilon$ , we need to compute  $\frac{\partial Z(T)}{\partial Z_{0j}}$ . The last term to compute is  $\frac{\partial Z(T)}{\partial T}$  which can be found easily as it is equal to  $(AZ + \epsilon f(Z))_{t=T}$ .

**Proposition 3.5.2.** *[Gradient with the adjoint state]*

*The derivative of  $J_\epsilon$  with respect to  $Z_{0j}$ ,  $\forall j \in \{1, \dots, n\}$ , can be expressed as*

$$\left\langle \frac{\partial J_\epsilon}{\partial Z_{0j}}, \varphi_j \right\rangle = -2(Z(T) - Z_0) (\varphi_j) + 4(E - c) ({}^t Z_0 N \varphi_j) - {}^t p_j(0) \varphi_j, \quad (3.5.4)$$

$\varphi \in \mathbb{R}^n$ ,  ${}^t p$  is the adjoint state and it is solution of the following differential system

$${}^t \dot{p} + {}^t p A + \epsilon {}^t p \frac{\partial f(Z)}{\partial Z} = 0, \quad {}^t p(T) = -2(Z(T) - Z_0). \quad (3.5.5)$$

*Proof.* We consider again the following equation by taking in account  $\frac{\partial f(Z)}{\partial Z_{0j}} = \frac{\partial f(Z)}{\partial Z} \frac{\partial Z}{\partial Z_{0j}}$ , we have

$$\frac{d}{dt} \left[ \frac{\partial Z}{\partial Z_{0j}} \right] = A \left[ \frac{\partial Z}{\partial Z_{0j}} \right] + \epsilon \frac{\partial f(Z)}{\partial Z} \left[ \frac{\partial Z}{\partial Z_{0j}} \right], \quad \frac{\partial Z}{\partial Z_{0j}}(0) = e_j, \quad (3.5.6)$$

we take its inner product with a function  ${}^t p$  to be determined later and we integrate by parts between zero and  $T$ , we get:

$${}^t p(T) \frac{\partial Z(T)}{\partial Z_{0j}} \varphi_j - {}^t p(0) \frac{\partial Z(0)}{\partial Z_{0j}} \varphi_j - \int_0^T \left[ {}^t \dot{p} + {}^t p A + \epsilon {}^t p \frac{\partial f(Z)}{\partial Z} \right] \frac{\partial Z}{\partial Z_{0j}} \varphi_j dt = 0. \quad (3.5.7)$$

Assume that  ${}^t p$  verifies the following differential equation with the final condition

$$\begin{aligned} {}^t \dot{p} + {}^t p A + \epsilon {}^t p \frac{\partial f(Z)}{\partial Z} &= 0, \\ {}^t p(T) &= -2^t(Z(T) - Z_0). \end{aligned} \quad (3.5.8)$$

Then  ${}^t p_j(0) \varphi_j = -2(Z(T) - Z_0) \frac{\partial Z(T)}{\partial Z_{0j}} \varphi_j$ . Finally, we replace in equation (3.5.3), we get directly the proof of the proposition. □

**Corollary 3.5.3.** *The gradient of  $J_\epsilon$  is given as*

$$\begin{aligned} \langle \nabla J_\epsilon, h \rangle &= -2(Z(T) - Z_0) \varphi + 4(E - c) ({}^t Z_0 N \varphi) - {}^t p(0) \varphi \\ &\quad + 2(Z(T) - Z_0) \left( \frac{\partial Z(T)}{\partial T} \right). \end{aligned} \quad (3.5.9)$$

$h$  is like in proposition 3.5.1. This can provide a gradient of  $J_\epsilon$  by solving two differential systems instead of  $n$  differential systems involved in a direct calculation.

## 3.6 Numerical results

We present numerical results obtained by the use of Algorithm 2. A mass-spring model with a cubic or a unilateral spring is presented as it is important from an engineering point of view. A beam with a unilateral spring at the free end is also studied. Note that, in the unilateral case, there is no proof of the existence of the nonlinear normal modes, moreover the calculation of the gradient uses a nonclassical derivation of the nonlinear term. But multiple scales method is presented in Chapter 4 where a comparison between the numerical and the analytical solutions has shown a good agreement.

In each case, the algorithm used for the integration of the differential equation as well as the algorithm used for the optimization are described with all the parameters. All the computations are performed using Scilab [23].

### 3.6.1 Mass-spring model with a cubic spring

Consider a discrete model of six mass-spring with only a cubic component (see Figure 3.1). The equation of motion can be written as

$$\ddot{X} + KX + \epsilon F(X) = 0, \quad (3.6.1)$$

where  $\epsilon$  is a positive number,  $X = [X_1, \dots, X_6]$ ,  $K = \text{tridiag}(-1, 2, -1)$  of size  $6 \times 6$  and  $(F(X))_i = X_5^3 \delta_{5i}$ .

The natural frequencies and their corresponding periods are given in Table 3.1. For this classical model, we will show the fourth nonlinear normal mode for a large  $\epsilon$  in the time and in the frequency domain, we will also show the solution in the phase and the configuration spaces to compare with the linear one. Finally the frequencies will be plotted against the nonlinearity level.

The differential equations are solved using a Runge-Kutta 4<sup>th</sup> order method with 20 points in the time interval for the first optimization iterations and then 1000 points for the last iterations.  $d\epsilon$  of Algorithm 2 is equal to 0.1 with  $\epsilon_0 = 0.1$ . The optimization uses a conjugate gradient algorithm as the nonlinearity is differentiable.

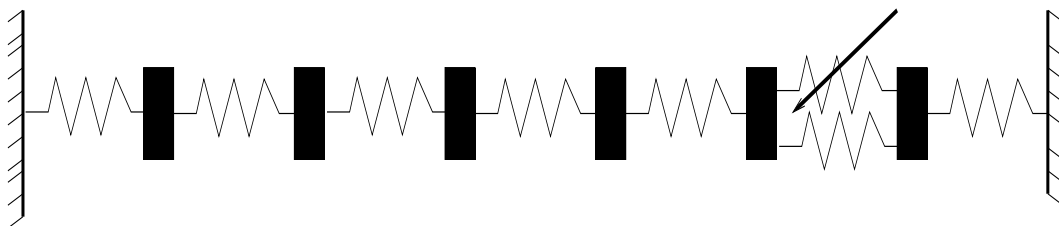


Figure 3.1. A mass-spring model with a cubic component.

The fourth linear period decreases from  $T_2 = 4.03$  s to the fourth nonlinear period  $T_{n2} = 3.93$  s. The corresponding frequency rises from  $f_2 = 0.248$  Hz to  $f_{n2} = 0.254$  Hz.

Figure 3.2 represents the displacements of all nodes for the fourth nonlinear mode for  $\epsilon = 50$ . All the components reach their maximum at the same time and they have the same period. These results are obtained by the integration of system (3.6.1) using an initial conditions vector and a period provided by Algorithm 2. Figure 3.3 shows the displacements of the first and the fifth nodes of the system compared to the linear one without a nonlinear spring. This can put in evidence the impact of the nonlinearity on the time solutions.

Figure 3.4 shows the periodic solutions in the configuration space, the components are plotted against the fifth node. These curves are straight lines for the linear system, their shapes depend on the nonlinearity form, they are symmetric and have a unique intersection point.

Figure 3.5 shows the frequency of the system as function of the nonlinearity level. Note that for  $\epsilon = 0$  this frequency is equal to the linear eigenfrequency  $f_4$ ; it also shows the frequency contents of the time solution for an integration time of 50 nonlinear periods. The spectrum content shows the even harmonics which is a typical feature of cubic nonlinearity. Figure 3.6 shows periodic solutions in the phase space for the fifth and the fourth nodes compared to the corresponding linear phase space solutions.

The fifth nonlinear periodic solution has an important deformation, this is due to the high stiffness of the cubic spring which is connected to this node. The curves are symmetric and have the same center, this is not always true for other forms of nonlinearities.

<b>Frequencies <math>f_i</math></b>	0.07 Hz	0.138 Hz	0.198 Hz	0.248 Hz	0.286 Hz	0.31 Hz
<b>Periods <math>T_i</math></b>	14.11s	7.24s	5.03 s	4.03 s	3.48s	3.22 s

Table 3.1. The natural frequencies of the linearized system with their corresponding periods.

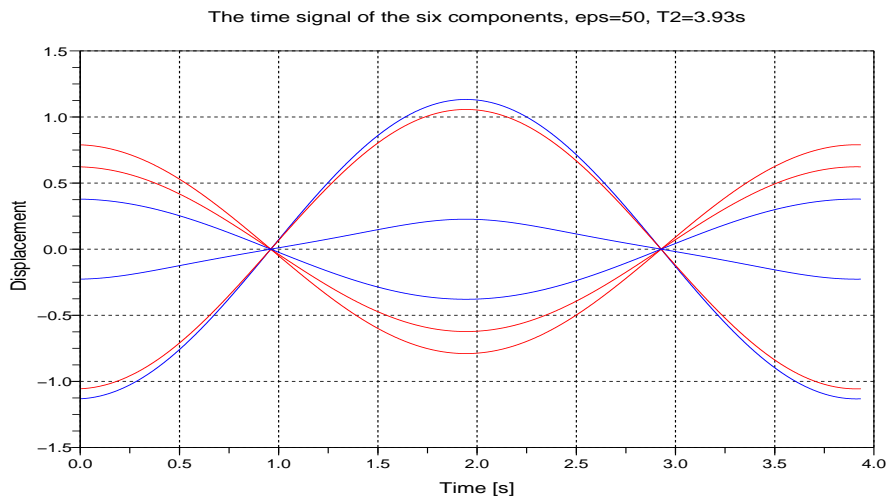


Figure 3.2. The displacements of the six nodes for the fourth nonlinear normal mode, the period is  $T_{n2} = 3.93$  s and the corresponding frequency is  $f_{n2} = 0.254$  Hz. All the components have the same period and they reach their maximum at the same time. 66 steps in  $\epsilon$  to reach this nonlinearity, The value of the functional  $J_\epsilon$  at the last iteration is  $10^{(-6)}$  and the average CPU time is 0.06 s for a calculation of the function and the gradient. The total CPU time is 6.6 minutes.

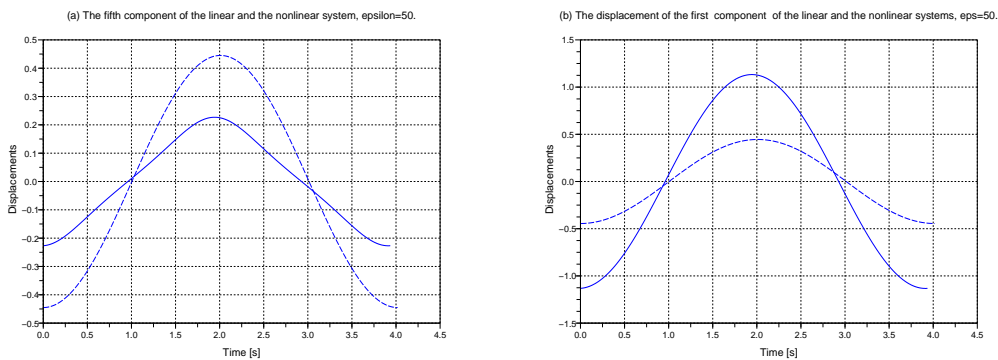


Figure 3.3. The displacements of the fifth node (a) and the first node (b) of the linear system (dashed line) and of the nonlinear system (solid line) for the second nonlinear normal mode.

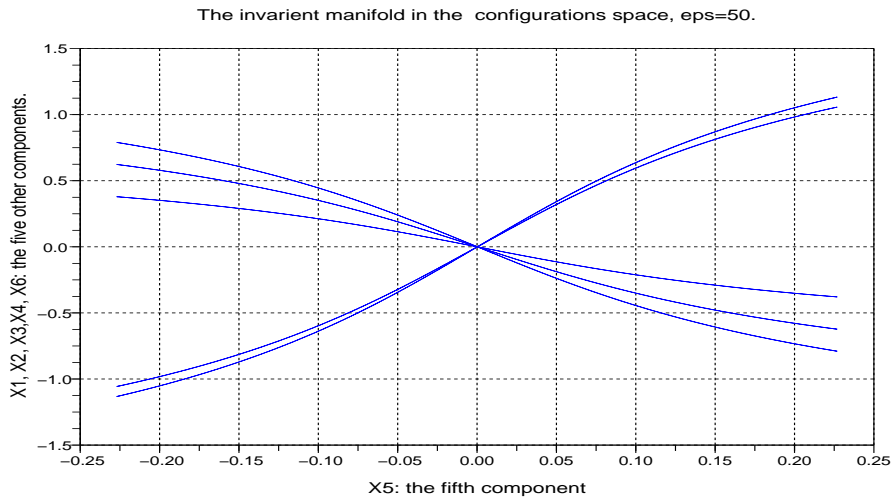


Figure 3.4. The displacements of all nodes as function of the fifth one, the curves are not straight lines and their shapes depend on the form of the nonlinearity.

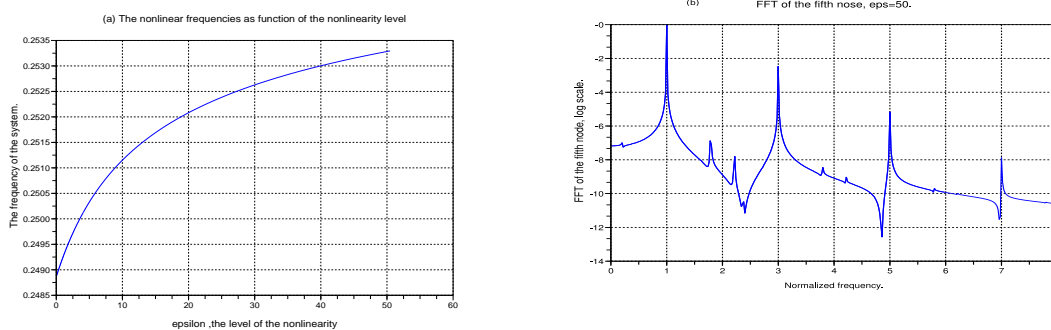


Figure 3.5. The second nonlinear frequency of the system as function of the nonlinearity (a), the FFT of the displacement for an integration time of 50 nonlinear period (b).

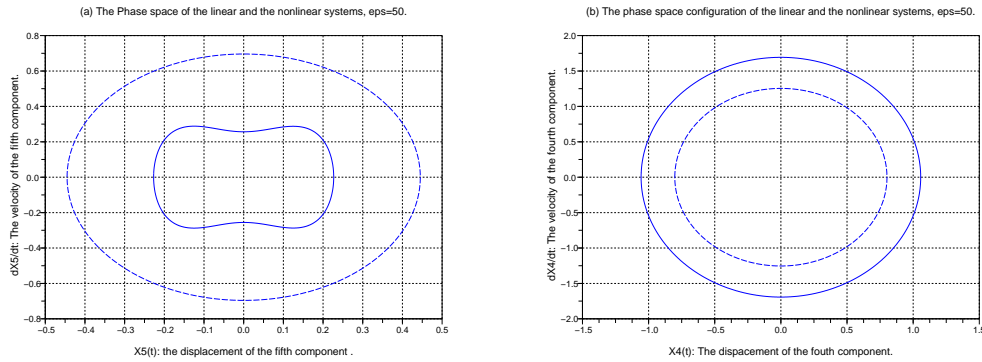


Figure 3.6. The phase space (solid line) compared to the corresponding linear phase space (dashed line) of the fifth node (a) and the fourth node (b).

### 3.6.2 Mass-spring model with a unilateral spring

The same model as in Section 3.6.1 is considered but the cubic spring is replaced by a unilateral one (see Figure 3.7). The equation of motion is the same as equation (3.6.1) but with different nonlinear term  $F(X)$  which is given as following

$$(F(X))_i = (X_5)_+ \delta_{5i}.$$

The linear periods and eigenfrequencies are given in Table 3.1. The differential equations are solved using the BDF method (backward differentiation formula) which is a second order scheme for nonlinear systems and appropriate for stiff problems with 20 points in the time interval for the first iterations and then 1000 points for the lasts.  $d\epsilon$  of Algorithm 2 is equal to 0.1 with  $\epsilon_0 = 0.1$ , the optimization uses an algorithm for non differentiable optimization. The simulations showed that for a small  $\epsilon$  we can find periodic solutions where all the solutions pass through zero at the same time. For large  $\epsilon$  we can find periodic solutions but the solutions does not pass through zero at the same time. This problem can be of interest as the solutions are not in phase even if the initial conditions in velocity is zero. We will present results for both cases.

We deal with the fourth nonlinear mode. Figure 3.8 shows the periodic solutions for all

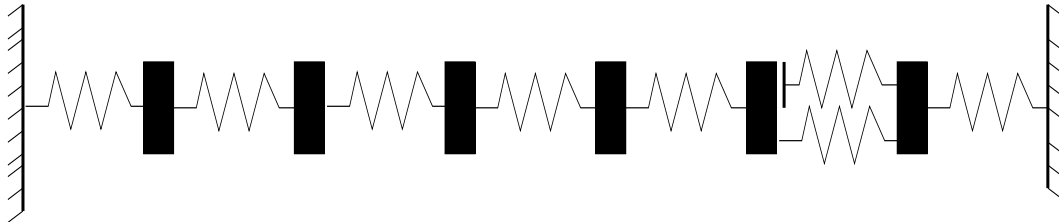


Figure 3.7. A mass-spring model with a unilateral component.

the components for  $\epsilon = 0.5$ . The solutions in the configuration and the phase spaces are presented in Figure 3.9.

For  $\epsilon = 18$ , the fourth nonlinear frequency and nonlinear period are respectively  $f_{n2} = 0.251$  Hz and  $T_{n2} = 3.97$  s

Figure 3.10 represents the displacements of all nodes for the fourth nonlinear mode for  $\epsilon = 18$ . All the components reach their maximum at the same time and they have the same period. These results are obtained by the integration of the equation of motion using an initial condition vector and a period provided by Algorithm 2.

Figure 3.11 shows the displacements of the first and the fifth nodes of the system compared to the linear one without a unilateral spring, this can put in evidence the impact of the unilateral contact to the time solutions. Figure 3.12 shows the periodic solutions in the configuration space, the components are plotted against the fifth node. The curve shapes depend on the nonlinearity form, they are not symmetric and they do not have a unique intersection point, this is due to the asymmetry of the system in presence of the unilateral spring.

Figure 3.13 shows the frequency of the system as function of the nonlinearity level. It also shows the frequency contents of the time solution for an integration time of 50 nonlinear periods. The spectrum content shows the subharmonics and the superharmonics. Figure 3.14 shows periodic solutions in the phase space for the fifth and the fourth nodes compared to the corresponding linear phase space solutions. The effect of the unilateral contact on the fifth nonlinear periodic solution is important as the stiffness of the spring which is in contact with this node is high. The curves are non symmetric but still periodic.

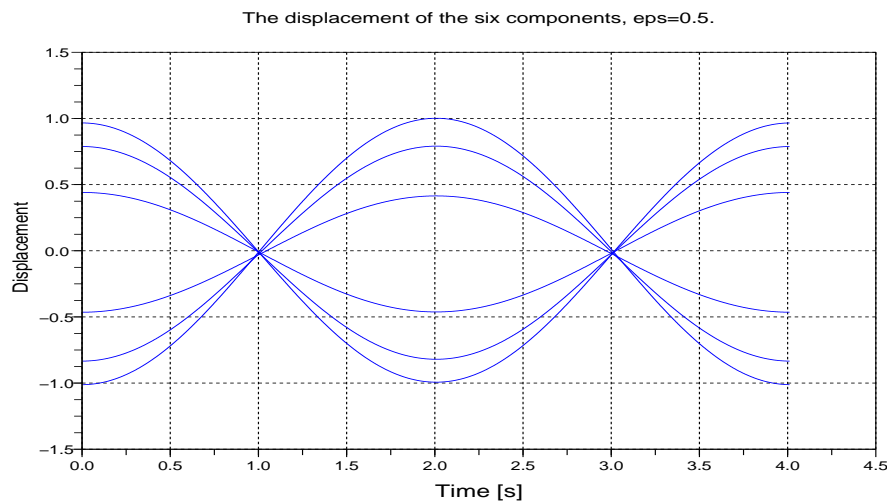


Figure 3.8. The displacements of the six nodes for the fourth nonlinear normal mode, the period is  $T_{n2} = 4.011$  s and the corresponding frequency is  $f_{n2} = 0.249$  Hz. All the components have the same period and they reach their maximum at the same time. 35 steps in  $\epsilon$  to reach this nonlinearity, The value of the functional  $J_\epsilon$  at the last iteration is  $10^{(-6)}$  and the average CPU time is 0.08 s for a calculation of the functional and the gradient, the total CPU time of optimization is 4.65 minutes.

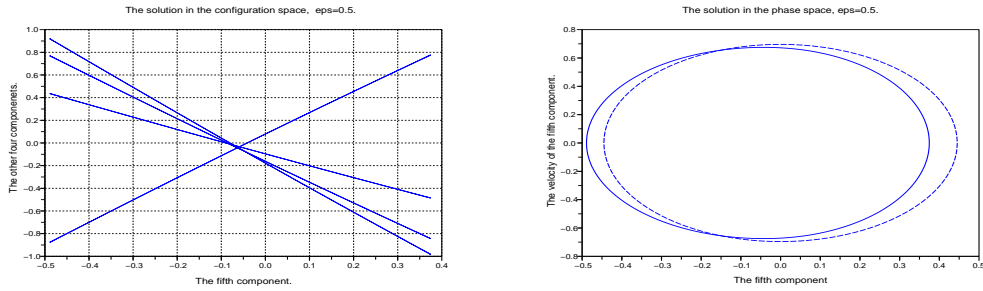


Figure 3.9. The configuration and the phase spaces for the fourth nonlinear normal mode for  $\epsilon = 0.5$ . The lines in the configuration space are not symmetric as for the linear system's lines. The ellipse in the phase space (solid line) has a small deformation comparing to the ellipse of the linear system (dashed line).

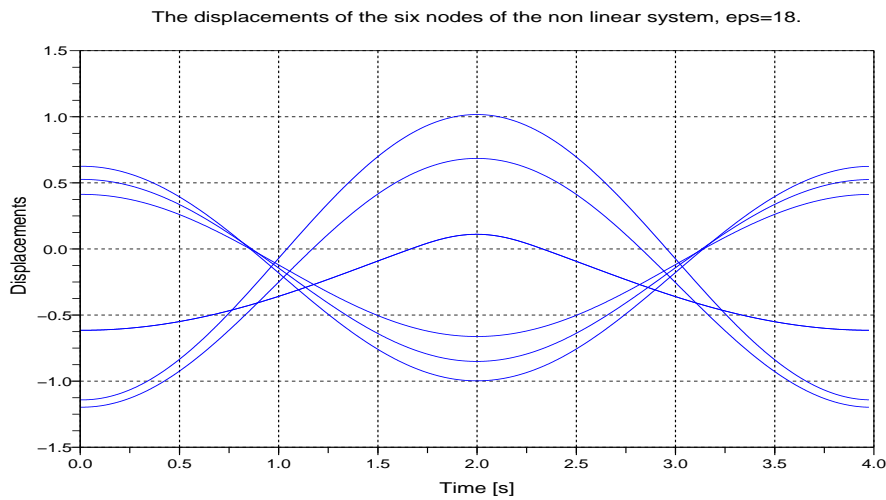


Figure 3.10. The displacements of the six nodes for the second nonlinear normal mode, the period is  $T_{n2} = 3.97$  s and the corresponding frequency is  $f_{n2} = 0.251$  Hz. 55 steps in  $\epsilon$  to reach this nonlinearity. The value of the functional  $J_\epsilon$  at the last iteration is  $10^{(-6)}$  and the average CPU time is 0.09 s for a calculation of the functional and the gradient, the total CPU time of optimization is 8.25 minutes

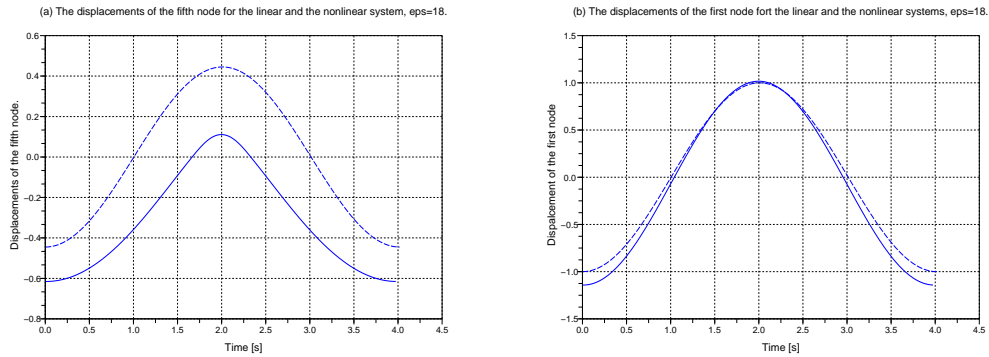


Figure 3.11. The displacements of the fifth node (a) and the first node (b) of the linear system (dashed line) and of the nonlinear system (solid line) for the second nonlinear normal mode.

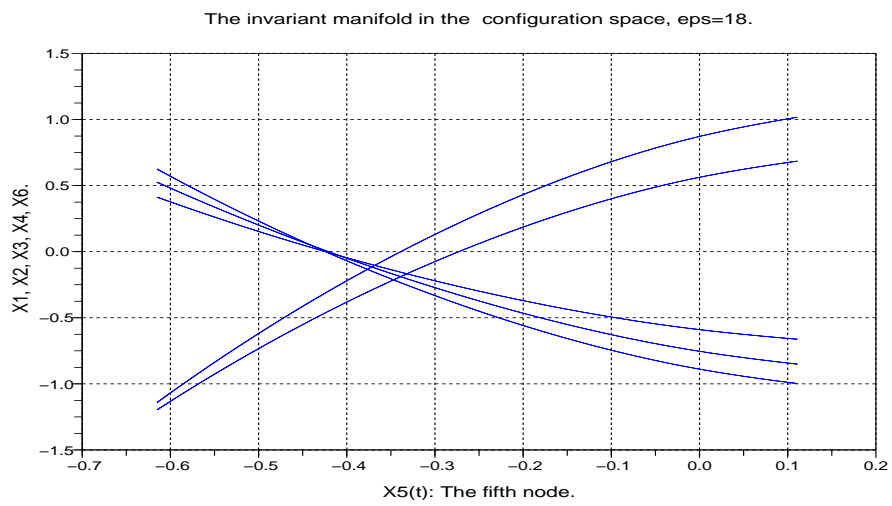


Figure 3.12. The displacements of the nodes as function of the fifth one, the curves are not straight lines anymore, this shape depends on the form of the nonlinearity.

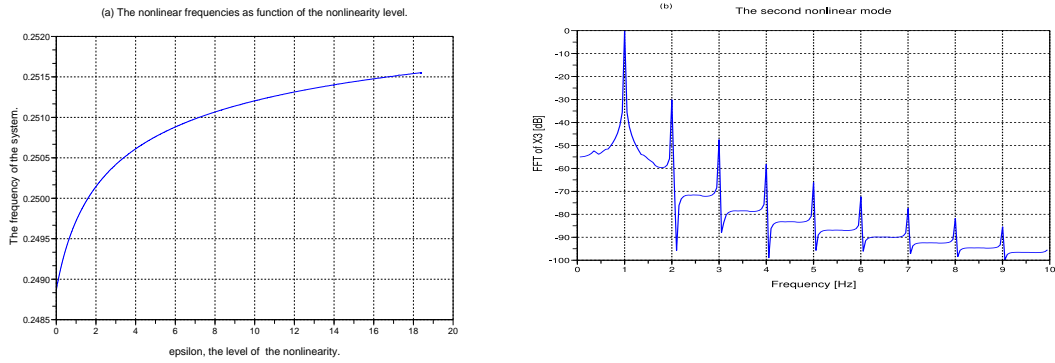


Figure 3.13. The second nonlinear frequency of the system as function of the nonlinearity (a); The FFT of the displacement for an integration time of 50 nonlinear period (b).

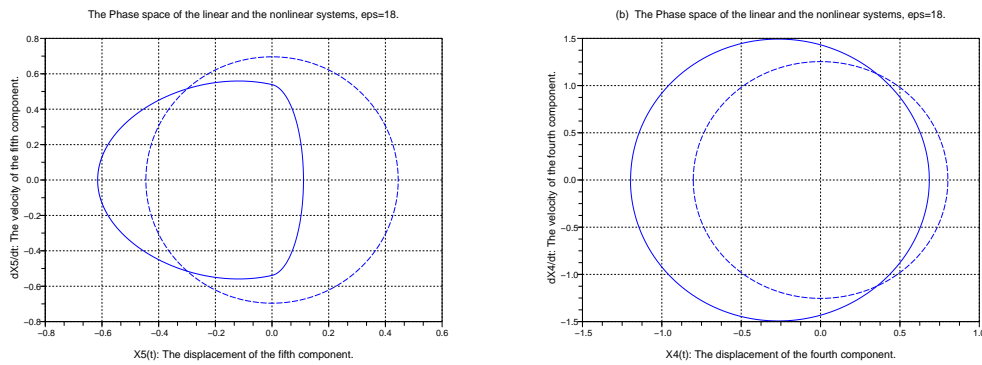


Figure 3.14. The phase space (solid line) compared to the corresponding linear phase space (dashed line) of the fifth node (a) and the fourth node (b).

### 3.6.3 Cantilever beam with a unilateral spring

Consider a cantilever beam with a unilateral elastic contact; we calculate its nonlinear normal modes. The equation of motion can be written as

$$M\ddot{q} + Kq + \epsilon k_r(q_r)_+ e_r = 0 \quad (3.6.2)$$

where  $K_r$  is the stiffness of the unilateral spring,  $r$  is the index of the node where the spring is incorporated,  $M$  and  $K$  are the mass and the stiffness matrices respectively. The physical properties are given in Table 3.2. This beam was used for experimental validations of a numerical model studied in Chapter 1. The first three linear frequencies of the beam are given in Table 3.3. The numerical methods for the integration and for the optimization are the same as for the mass-spring model with a unilateral contact.

70 points are used in the time interval for the first iterations and then 1000 points for the last iterations.  $d\epsilon$  of Algorithm 2 is equal to 0.1 with  $\epsilon_0 = 0.1$ , the optimization uses an algorithm for non differentiable optimization.

Figure 3.15 shows the first nonlinear normal mode of the beam for  $\epsilon = 1$  corresponding to the linear normal mode. Figure 3.16 shows the nonlinear normal mode in the time domain, i.e. a periodic solution for all the components of the discretized system. The nonlinear frequency of this nonlinear mode is 57.62 Hz instead of 52.7 Hz. These results are obtained by the use of Algorithm 2. Figure 3.17 shows the periodic solution in the configuration and the phase spaces, the nonlinearity effect has curved the straight lines of the linear system. The ellipse in the phase space is also deformed comparing to the linear system one. Finally, Figures 3.18 and 3.19 show the second nonlinear normal mode of the beam for  $\epsilon = 0.1$  in the space and the time domains respectively. The nonlinear frequency of this nonlinear mode is 354.91 Hz instead of 328.5 Hz. The modes of the beam computed with the algorithm are also found by asymptotic expansion in section 4.4.6 of Chapter 4. This gives a validation of the algorithm in the unilateral case.

Beam length	Beam width	Beam thickness	Beam Young's modulus	Beam density	Spring stiffness
0.27m	0.05m	0.005m	$69 \times 10^9 N/m^2$	$2700 kg/m^3$	107KN/m

Table 3.2. The physical properties of the beam and the spring.

Natural frequencies	$f_1$	$f_2$	$f_3$
Predicted	52.7 Hz	328.5 Hz	931.3 Hz

Table 3.3. The natural frequencies of the clamped-free beam.

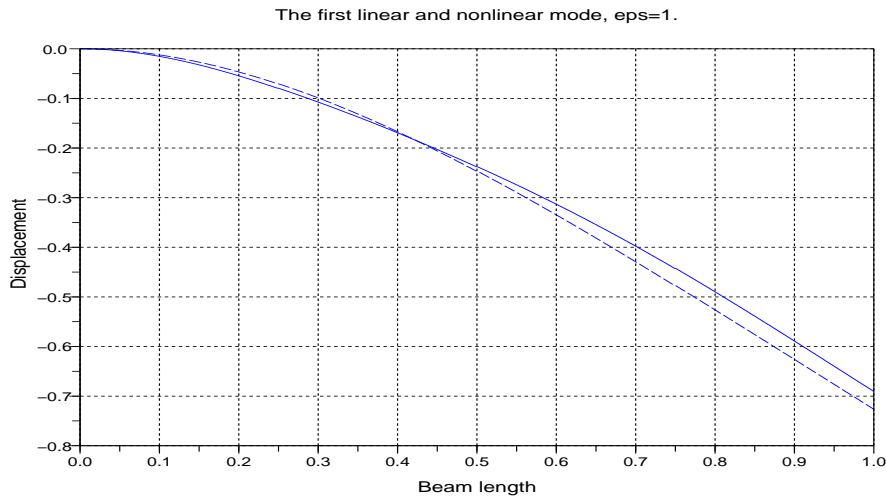


Figure 3.15. The first nonlinear normal mode of the beam with a unilateral contact (solid line) compared to the linear normal mode (dashed line) for a spring stiffness  $k_r = 107000$  N/m and for  $\epsilon = 1$ .

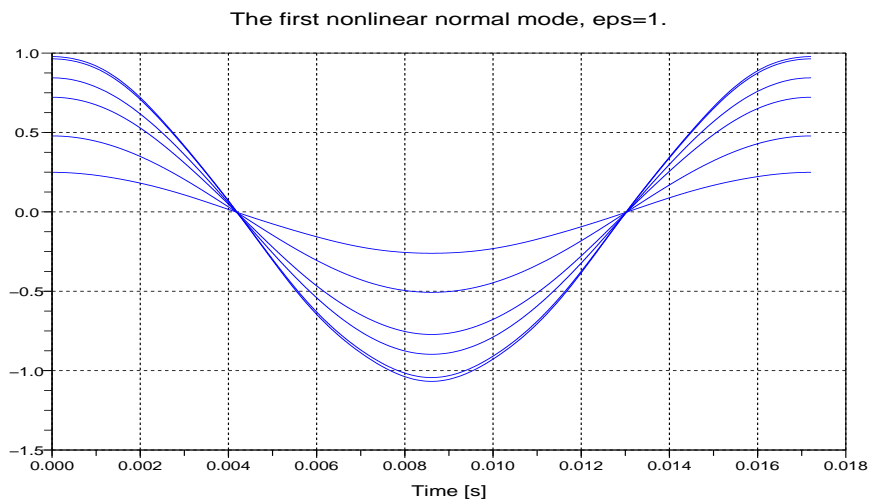


Figure 3.16. The displacements of six nodes for the first nonlinear normal mode, the period is  $T_{n2} = 0.017$  s and the corresponding frequency is  $f_{n2} = 57.62$  Hz. 75 steps in  $\epsilon$  to reach this nonlinearity, The value of the functional  $J_\epsilon$  at the last iteration is  $10^{(-5)}$  and the average time computation is 10 seconds for a calculation of the function and the gradient for ten finite elements discretization. The total CPU time is 20 hours.

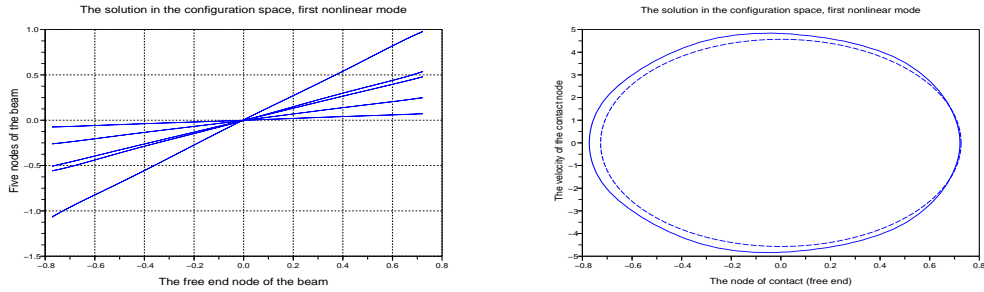


Figure 3.17. The configuration and the phase spaces for the first nonlinear normal mode for  $\epsilon = 1$ . The lines in the configuration space are not symmetric as for the linear system's lines. The ellipse in the phase space (solid line) has a small deformation comparing to the ellipse of the linear system (dashed line).

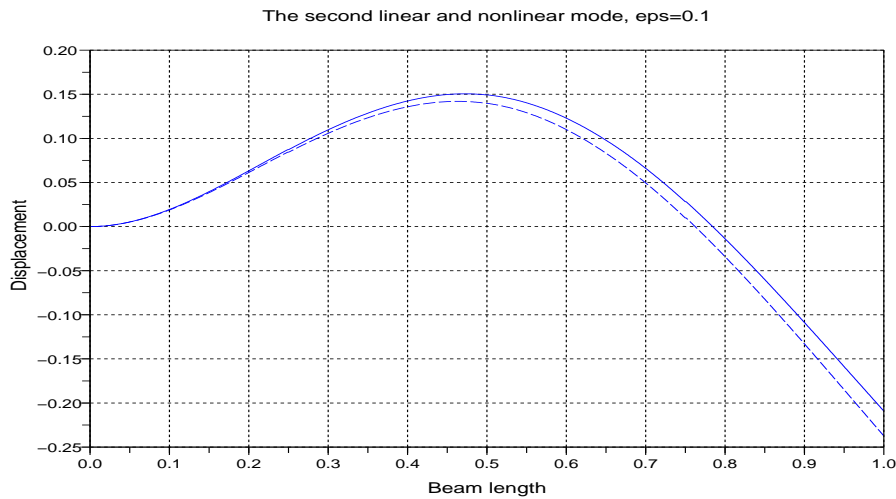


Figure 3.18. The second nonlinear normal mode of the beam with a unilateral contact (solid line) compared to the linear normal mode (dashed line) for a spring stiffness  $k_r = 107000$  N/m and for  $\epsilon = 0.1$ .

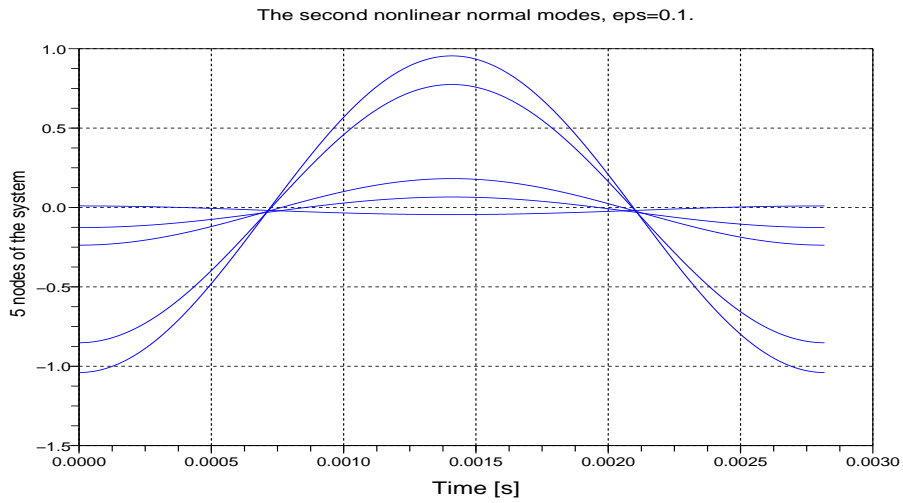


Figure 3.19. The displacements of six nodes for the second nonlinear normal mode, the period is  $T_{n2} = 0.0028$  s and the corresponding frequency is  $f_{n2} = 354.91$  Hz.

### 3.7 Conclusion and perspectives

A Numerical algorithm to compute these modes was performed and used for models with cubic and unilateral contact nonlinearity. The proof in the non smooth case of contact type is in progress. An alternative validation of the numerical algorithm via asymptotic approach was also performed and discussed in Chapter 4. The numerical algorithm was used to compute the nonlinear normal modes of the beam system with a unilateral spring presented in Chapter 1, this can help to understand better the dynamic behaviour via modal analysis. The algorithm can be improved to deal with system of large degrees of freedom;



# Chapter 4

## The method of multiple scales for a model of a unilateral contact

### 4.1 Introduction

The concept of nonlinear normal modes is discussed in Chapter 3. Since the interest is to study nonlinearities of contact type, it is necessary to validate the numerical calculation of the nonlinear normal modes in this case. The perturbation techniques can provide an alternative proof by giving analytical solutions but for small nonlinearities.

The asymptotic expansion was used to calculate the nonlinear normal modes for smooth nonlinearities [32, 33, 43]. S.Junca and B.Rousselet worked on nonlinear normal modes via Lindstedt-Poincaré technique [31], this paper is a useful support for the current work. The Lindstedt-Poincaré technique was also used to evaluate the nonlinear normal mode for piecewise linear two d-o-f system [34]. Other Ph.D. students work on different vibration problems via asymptotic approaches [44, 45]

In this chapter, We use the method of multiple scales which is efficient to find asymptotic solutions for autonomous and for forced  $n$  d-o-f system with unilateral contact [46]. The explicit solutions are proved for a time interval which depends on  $\epsilon$ . The solutions are then compared to those obtained by the numerical algorithm of Chapter 3.

Finally, a procedure to compute the nonlinear normal modes of a system with an excitation force is performed leading to experimental investigations. Therefore the different numerical methods can be validated.

The chapter is organized as follows, first the multiple scales method is used to find an analytical solution of a one d-o-f oscillator with a unilateral term under periodic excitation near the natural frequency. Then the method is applied to a  $n$  d-o-f autonomous system with unilateral contact, the analytical solution is compared to the numerical one obtained by Algorithm 3. Finally, a  $n$  d-o-f forced system with a unilateral contact is treated yielding to a direct calculation of the nonlinear normal modes.

## 4.2 One degree of freedom nonlinear forced oscillator

Consider a mass-spring model with a unilateral contact

$$\ddot{u} + \omega_0^2 u + 2\epsilon\xi\dot{u} + \epsilon u_+ = \epsilon g \cos(\omega t), \quad (4.2.1)$$

$$u(0) = a_0, \quad \dot{u}(0) = 0, \quad (4.2.2)$$

where  $\omega_0$  is the natural frequency of the linearized equation,  $\xi$  is the damping coefficient of the spring,  $\omega$  is the excitation frequency assumed to be near  $\omega_0$  and  $\epsilon$  is a real small parameter. The asymptotic expansion gives an approximate analytical solution of equation (4.2.1) which allows a deep study of the nonlinearity. The disadvantage is that this solution does not hold for large  $\epsilon$ . The method of multiple scales is used in this chapter for a one degree of freedom oscillator as well as for systems of  $n$  degrees of freedom.

### 4.2.1 The method of multiple scales - First order approximation

We consider three time scales as we will seek a solution of the first order with the remainders, the new time scales are  $T_0 = t$ ,  $T_1 = \epsilon t$  and  $T_2 = \epsilon^2 t$  where  $T_0$  represents the fast time and  $T_1$  represents the slow time and etc... The derivative with respect to  $t$  will be written as function of the derivative with respect to  $T_0$ ,  $T_1$  and  $T_2$ . The chain rule formula yields:

$$\begin{aligned} \frac{\partial}{\partial t} &= \frac{\partial}{\partial T_0} + \epsilon \frac{\partial}{\partial T_1} + \epsilon^2 \frac{\partial}{\partial T_2}, \\ \frac{\partial^2}{\partial t^2} &= \frac{\partial^2}{\partial T_0^2} + 2\epsilon \frac{\partial^2}{\partial T_0 \partial T_1} + \epsilon^2 \frac{\partial^2}{\partial T_1^2} + 2\epsilon^2 \frac{\partial^2}{\partial T_0 \partial T_2} + 2\epsilon^3 \frac{\partial^2}{\partial T_1 \partial T_2} + \epsilon^4 \frac{\partial^2}{\partial T_2^2}. \end{aligned}$$

Instead of determining the solution as a function of  $t$ , we determine it as a function of  $T_0$ ,  $T_1$  and  $T_2$ . To this end, we change the independent variable in the original equation (4.2.1) from  $t$  to  $T_0$ ,  $T_1$  and  $T_2$ .

**Proposition 4.2.1.** *The approximate solution of equation (4.2.1) of order  $\epsilon^2$  for  $t \in [0, T_\epsilon]$  with  $T_\epsilon \sim \frac{1}{\epsilon}$  is given as*

$$u^\epsilon(T_0, T_1, T_2) = u_0(T_0, T_1, T_2) + \epsilon u_1(T_0, T_1, T_2) + \mathcal{O}(\epsilon^2), \quad (4.2.3)$$

such that

$$\begin{aligned} u_0(T_0, T_1, T_2) &= a(T_1, T_2) \cos(\omega_0 T_0 + \varphi(T_1, T_2)), \\ u_1(T_0, T_1, T_2) &= -\frac{2|a(T_1, T_2)|}{\omega_0^2 \pi} \sum_{k=1}^{+\infty} \frac{(-1)^k}{(4k^2 - 1)^2} \cos(2k(\omega_0 T_0 + \varphi(T_1, T_2))) \\ &\quad + A \cos(\omega_0 T_0) - \frac{|a(T_1, T_2)|}{\omega_0^2 \pi}, \end{aligned} \quad (4.2.4)$$

where  $a$  and  $\varphi$  are a solution of system (4.2.15), and  $A$  is given as

$$A = \frac{|a|}{\omega_0^2 \pi} \left( 1 + 2 \sum_{k=1}^{+\infty} \frac{(-1)^k}{(4k^2 - 1)^2} \right).$$

We will give some useful propositions and lemma needed for the proof of Proposition 4.2.1 and for the rest of the chapter.

**Lemma 4.2.2.** [*Asymptotic expansion for  $(u + \epsilon v)_+$* ] (Junca-Rousselet [31])

Let be  $T > 0$ ,  $M > 0$ ,  $u, v$  two real valued functions defined on  $I = [0, T]$ ,

$$J_\epsilon = \{t \in I, |u(t)| \leq \epsilon M\},$$

$\mu_\epsilon(T)$  the measure of the set  $J_\epsilon$  and  $H$  be the Heaviside step function, then

$$(u + \epsilon v)_+ = (u)_+ + \epsilon H(u)v + \epsilon \chi_\epsilon(u, v), \text{ with } H(u) = \begin{cases} 1 & \text{if } u > 0 \\ 0 & \text{elsewhere} \end{cases},$$

and  $\chi_\epsilon(u, v)$  is a non negative piecewise linear function and 1-Lipschitz with respect to  $v$ , which satisfies for all  $\epsilon$ ,

if  $|v(t)| \leq M$  for any  $t \in I$ :

$$|\chi_\epsilon(u, v)| \leq |v| \leq M, \quad \int_0^T |\chi_\epsilon(u(t), v(t))| dt \leq M \mu_\epsilon(T). \quad (4.2.5)$$

**Lemma 4.2.3.** [*Order of  $\mu_\epsilon(T)$* ] (Junca-Rousselet [31])

Let  $u$  be a smooth periodic function,  $M$  be a positive constant and  $\mu_\epsilon(T)$  the measure of the set  $\{t \in I, |u(t)| \leq \epsilon M\}$ .

If  $u$  has only simple roots on  $I = [0, T]$  then for some positive  $C$ ,

$$\mu_\epsilon(T) \leq C\epsilon \times T. \quad (4.2.6)$$

More generally, if  $u$  has also double roots then

$$\mu_\epsilon(T) \leq C\sqrt{\epsilon} \times T. \quad (4.2.7)$$

**Proposition 4.2.4.** The Fourier series of  $|\cos(\omega_0 T_0 + \varphi)|$  and of  $H(\cos(\omega_0 T_0 + \varphi))$ , the Heaviside function of  $\cos(\omega_0 T_0 + \varphi)$ , are given as following, see [47] for instance,

$$|\cos(\omega_0 T_0 + \varphi)| = \frac{2}{\pi} - \frac{4}{\pi} \sum_{k=1}^{+\infty} \frac{(-1)^k}{4k^2 - 1} \cos(2k(\omega_0 T_0 + \varphi)), \quad (4.2.8)$$

$$H(\cos(\omega_0 T_0 + \varphi)) = \frac{1}{2} + \frac{2}{\pi} \sum_{k=1}^{+\infty} \frac{(-1)^k}{2k + 1} \cos((2k + 1)(\omega_0 T_0 + \varphi)). \quad (4.2.9)$$

*proof of proposition 4.2.1.*

Substituting  $u^\epsilon$  for  $u$  into (4.2.1) and taking into account the expansion of  $(u_0 + \epsilon u_1)_+$ , then equating each of the coefficients of  $\epsilon^0$  and  $\epsilon^1$  to zero, we have

$$\frac{\partial^2 u_0}{\partial^2 T_0} + \omega_0^2 u_0 = 0, \quad u_0(0) = a_0, \quad \dot{u}_0 = 0, \quad (4.2.10)$$

$$\frac{\partial^2 u_1}{\partial^2 T_0} + \omega_0^2 u_1 = g \cos(\omega t) - 2 \frac{\partial^2 u_0}{\partial T_0 \partial T_1} - 2\xi \frac{\partial u_0}{\partial T_0} - (u_0)_+, \quad u_1(0) = 0, \quad \dot{u}_1(0) = 0. \quad (4.2.11)$$

The solution of equation (4.2.10) is given as

$$u_0 = a(T_1, T_2) \cos(\omega_0 T_0 + \varphi(T_1, T_2)), \quad a(0, 0) = a_0, \quad \varphi(0, 0) = 0. \quad (4.2.12)$$

Then we use this solution in the right hand side of equation (4.2.11) to find

$$\begin{aligned} \frac{\partial^2 u_1}{\partial^2 T_0} + \omega_0^2 u_1 = & g \cos(\omega t) + 2\omega_0 \left( \frac{\partial a}{\partial T_1} + \xi a \right) \sin(\omega_0 T_0 + \varphi) \\ & + 2\omega_0 a \frac{\partial \varphi}{\partial T_1} \cos(\omega_0 T_0 + \varphi) - (a \cos(\omega_0 T_0 + \varphi))_+. \end{aligned} \quad (4.2.13)$$

The idea is to collect the terms of each frequency and then to remove the secular ones from the equation; this means that the coefficients of terms at  $\omega_0$  will be set to zero to avoid a resonance phenomena. To accomplish this, the function  $(a \cos(\omega_0 T_0 + b))_+$  is expanded as well as the frequency of excitation  $\omega$  which is near  $\omega_0$

$$\omega = \omega_0 + \epsilon \sigma,$$

where  $\sigma$  is a detuning parameter. We have

$$(a \cos(\omega_0 T_0 + \varphi))_+ = \frac{a \cos(\omega_0 T_0 + \varphi)}{2} + \frac{|a \cos(\omega_0 T_0 + \varphi)|}{2}$$

and

$$\omega T_0 = \omega_0 T_0 + \epsilon \sigma T_0 = \omega_0 T_0 + \sigma T_1,$$

using a trigonometrical formula, we get

$$\begin{aligned} g \cos(\omega T_0) &= g \cos(\omega_0 T_0 + \sigma T_1) = g \cos(\omega_0 T_0 + \varphi + \sigma T_1 - \varphi) \\ &= g \cos(\omega_0 T_0 + \varphi) \cos(\sigma T_1 - \varphi) - g \sin(\omega_0 T_0 + \varphi) \sin(\sigma T_1 - \varphi). \end{aligned}$$

Equation (4.2.13) becomes

$$\begin{aligned} \frac{\partial^2 u_1}{\partial^2 T_0} + \omega_0^2 u_1 = & \left( -g \sin(\sigma T_1 - \varphi) + 2\omega_0 \frac{\partial a}{\partial T_1} + 2\omega_0 \xi a \right) \sin(\omega_0 T_0 + \varphi) \\ & + \left( g \cos(\sigma T_1 - \varphi) + 2\omega_0 a \frac{\partial \varphi}{\partial T_1} - \frac{a}{2} \right) \cos(\omega_0 T_0 + \varphi) \\ & - \frac{|a|}{2} |\cos(\omega_0 T_0 + \varphi)|. \end{aligned} \quad (4.2.14)$$

In order to obtain a bounded solution of equation (4.2.14), the secular terms have to be removed, this yields the following differential system in  $a$  and  $\varphi$ :

$$\begin{cases} \frac{\partial a}{\partial T_1} + \xi a = \frac{g}{2\omega_0} \sin(\sigma T_1 - \varphi), \\ a \frac{\partial \varphi}{\partial T_1} = \frac{a}{4\omega_0} - \frac{g}{2\omega_0} \cos(\sigma T_1 - \varphi). \end{cases} \quad (4.2.15)$$

A change of function  $\gamma = \sigma T_1 - \varphi$  yields a simplified differential system in  $a$  and  $\gamma$

$$\begin{cases} \frac{\partial a}{\partial T_1} = -\xi a + \frac{g}{2\omega_0} \sin(\gamma), \\ \frac{\partial \gamma}{\partial T_1} = \sigma - \frac{1}{4\omega_0} + \frac{g}{2a\omega_0} \cos(\gamma). \end{cases} \quad (4.2.16)$$

We update equation (4.2.14) and obtain

$$\frac{\partial^2 u_1}{\partial^2 T_0} + \omega_0^2 u_1 = -\frac{|a|}{2} |\cos(\omega_0 T_0 + \varphi)|, \quad u_1(0) = 0, \quad \dot{u}_1 = 0. \quad (4.2.17)$$

Taking in account the Fourier expansion of  $|\cos(\omega_0 T_0 + \varphi)|$  given in (4.2.8) we get

$$\begin{aligned} u_1 = & -\frac{2|a(T_1, T_2)|}{\omega_0^2 \pi} \sum_{k=1}^{+\infty} \frac{(-1)^k}{(4k^2 - 1)^2} \cos(2k(\omega_0 T_0 + \varphi(T_1, T_2))) \\ & + A \cos(\omega_0 T_0) - \frac{|a(T_1, T_2)|}{\omega_0^2 \pi}, \end{aligned} \quad (4.2.18)$$

where

$$A = \frac{|a|}{\omega_0^2 \pi} \left( 1 + 2 \sum_{k=1}^{+\infty} \frac{(-1)^k}{(4k^2 - 1)^2} \right)$$

Note that  $T_0 = t$ ,  $T_1 = \epsilon t$  and  $T_2 = \epsilon^2 t$ ,

$$u^\epsilon = u_0(T_0, T_1, T_2) + \epsilon u_1(T_0, T_1, T_2) + \mathcal{O}(\epsilon^2).$$

Finally, we have to find the dependence of  $a$  and  $\varphi$  on  $T_2$  in order to get a bounded error of order  $\epsilon^2$ . This is a particular case of Proposition 4.5.6.  $\square$

### 4.3 One degree of freedom nonlinear autonomous oscillator

We consider a particular case of the one degree of freedom oscillator (4.2.1) for  $\xi = g = 0$ , the equation of motion becomes

$$\ddot{x} + \omega_0^2 x + \epsilon x_+ = 0, \quad x(0) = a_0, \quad \dot{x}(0) = 0. \quad (4.3.1)$$

A solution is sought in the following form

$$x^\epsilon = x^0 + \epsilon r, \quad (4.3.2)$$

the double scales method is used as we seek a solution with one term  $x^0$  and a remainder  $r$ . The derivatives are then written as follows

$$\begin{aligned}\frac{\partial}{\partial t} &= \frac{\partial}{\partial T_0} + \epsilon \frac{\partial}{\partial T_1}, \\ \frac{\partial^2}{\partial^2 t} &= \frac{\partial^2}{\partial^2 T_0} + 2\epsilon \frac{\partial^2}{\partial T_0 \partial T_1} + \epsilon^2 \frac{\partial^2}{\partial^2 T_1}.\end{aligned}$$

Equation (4.3.1) is written with the independent variables  $T_0$  and  $T_1$  as follows

$$\frac{\partial^2 x^0}{\partial^2 T_0} + \omega_0^2 x^0 = 0, \quad x^0(0) = a_0, \quad \dot{x}^0(0) = 0, \quad (4.3.3)$$

and

$$\begin{aligned}\frac{\partial^2 r}{\partial^2 T_0} + \omega_0^2 r &= -2 \frac{\partial^2 x^0}{\partial T_0 \partial T_1} - x_+^0 - \epsilon (H(x^0)r + \chi(x^0, r)) \\ &\quad - \epsilon \left( \frac{\partial^2 x^0}{\partial^2 T_1} + 2 \frac{\partial^2 r}{\partial T_0 \partial T_1} \right) - \epsilon^2 \left( \frac{\partial^2 r}{\partial^2 T_1} \right), \quad r(0) = 0, \quad \dot{r}(0) = 0.\end{aligned}$$

The right hand side of the equation of the remainder is obtained by taking into account the asymptotic expansion of  $(x^0 + \epsilon r)_+$  which is given by Lemma 4.2.2:

$$(x^0 + \epsilon r)_+ = x_+^0 + \epsilon H(x^0)r + \epsilon \chi(x^0, r), \quad (4.3.4)$$

such that  $H(x_0)$  is the Heaviside function of  $x^0$  and the remainder is solution of the following equation

$$\frac{\partial^2 r}{\partial^2 T_0} + \omega_0^2 r = S^\epsilon(T_0, T_1) + f^\epsilon(T_0, T_1) + \epsilon g^\epsilon(T_0, T_1, r), \quad r(0) = 0, \quad \dot{r}(0) = 0, \quad (4.3.5)$$

where

$$\begin{aligned}S^\epsilon(T_0, T_1) &= -2 \frac{\partial^2 x^0}{\partial T_0 \partial T_1} - x_+^0, \\ f^\epsilon(T_0, T_1, T_2) &= -\epsilon \left( \frac{\partial^2 x^0}{\partial^2 T_1} + 2 \frac{\partial^2 r}{\partial T_0 \partial T_1} + \epsilon \frac{\partial^2 r}{\partial^2 T_1} \right), \\ g^\epsilon(T_0, T_1, r) &= -\frac{(x^0 + \epsilon r)_+ - x_+^0}{\epsilon},\end{aligned}$$

The object of this section is to prove that the remainder is bounded for a time  $t \in [0, T_\epsilon]$ . Once the details of the proof are clear, the same technique will be used to prove the asymptotic solutions of the autonomous and the forced  $n$  degrees of freedom systems in the next sections.

**Proposition 4.3.1.** *If  $a$  and  $\varphi$  verify system (4.3.8), then there exists  $\epsilon_0 > 0$  and  $\gamma > 0$  such that, for  $0 < \epsilon < \epsilon_0$ , the remainder  $r$  is uniformly bounded in  $W^{2,\infty}(0, T_\epsilon)$ , where  $T_\epsilon = \frac{\gamma}{\epsilon}$ .*

*Proof.* The strategy is to remove the secular terms from the expression of  $S^\epsilon(T_0, T_1)$  to avoid a resonance phenomena; by this, we verify the first hypothesis of Lemma 4.4.5 for differential equations (1 d.d.l). Then we prove that  $f^\epsilon(T_0, T_1)$  and  $g^\epsilon(T_0, T_1, r)$  verify the second and the third hypothesis.

**Step 1: removing secular terms from  $S^\epsilon(T_0, T_1)$  and extracting the conditions on the coefficients.**

The solution of equation (4.3.3) is given by

$$x^0 = a(T_1) \cos(\omega_0 T_0 + \varphi(T_1)), \quad a(0) = a_0, \quad \varphi(0) = 0. \quad (4.3.6)$$

Then  $S^\epsilon$  is given as follows

$$S^\epsilon = -2 \frac{\partial^2 x^0}{\partial T_0 \partial T_1} - x_+^0 = 2 \frac{\partial a}{\partial T_1} \omega_0 \sin(\omega_0 T_0 + \varphi) + 2a\omega_0 \frac{\partial \varphi}{\partial T_1} \cos(\omega_0 T_0 + \varphi) - \frac{a \cos(\omega_0 T_0 + \varphi)}{2} - \frac{|a \cos(\omega_0 T_0 + \varphi)|}{2}. \quad (4.3.7)$$

By collecting the coefficient of  $\sin(\omega_0 T_0 + \varphi)$  and  $\cos(\omega_0 T_0 + \varphi)$  and setting them to zero, we get a system of differential equations on  $a$  and  $\varphi$

$$\begin{cases} 2 \frac{\partial a}{\partial T_1} \omega_0 = 0, & a(0) = a_0, \\ 2a\omega_0 \frac{\partial \varphi}{\partial T_1} - \frac{a}{2} = 0, & \varphi(0) = 0. \end{cases} \quad (4.3.8)$$

The solution is given as  $a = a_0$  and  $\varphi = \frac{1}{4\omega_0} T_1$ .

Then  $S^\epsilon(T_0, T_1) = -\frac{|a_0 \cos(\omega_0 T_0 + \frac{1}{4\omega_0} T_1)|}{2}$  which is not resonant and bounded (see Fourier series of  $|\cos|$ ), but it is  $\epsilon$  dependent.

**Step 2: writing the differential equation as function of the independent variable  $t$ .**

We write all the remaining terms as function of the independent variable  $t$  after moving the derivative of  $r$  to the left hand side of the differential equation in  $r$ , we have

$$\frac{\partial^2 r}{\partial t^2} + \omega_0^2 r = \tilde{S}^\epsilon(t) + \tilde{f}^\epsilon(t) + \epsilon \tilde{g}^\epsilon(t, r), \quad r(0) = 0, \quad \dot{r}(0) = 0, \quad (4.3.9)$$

where

$$\begin{aligned} \tilde{S}^\epsilon(t) &= -\frac{|a_0 \cos(\omega_0 + \epsilon \frac{t}{4\omega_0})|}{2}, \\ \tilde{f}^\epsilon(t) &= -\epsilon \left( \frac{\partial^2 x^0}{\partial T_1^2} \right) = \epsilon \frac{a_0}{16\omega_0^2} \cos(\omega_0 + \frac{\epsilon}{4\omega_0})t, \\ \tilde{g}^\epsilon(t, r) &= -\frac{(x^0 + \epsilon r)_+ - x_+^0}{\epsilon}, \end{aligned}$$

**Step 3: verifying the hypothesis of Lemma 4.4.5.**

$\tilde{S}^\epsilon(t)$  does not contain any term at the frequency  $\omega_0$  (there is no terms in  $\cos(\omega_0 t)$  or  $\sin(\omega_0 t)$ ),

this is done since we have removed the secular terms from the expression of  $S^\epsilon$ , this is also true if  $\epsilon = 0$ .

$\tilde{f}^\epsilon(t)$  is bounded. Moreover, there exists  $C$  such that  $\int_0^T |\tilde{f}_\epsilon(t)| dt \leq C\epsilon T$ .

We still have to deal with  $\tilde{g}$ , the function  $x_+$  is 1-Lipschitz then easily we have

$$|\tilde{g}^\epsilon(t, r)| = \left| -\frac{(x^0 + \epsilon r)_+ - x_+^0}{\epsilon} \right| \leq |r|.$$

then for all  $R > 0$ :  $M_R = \sup_{\epsilon \in (0,1), t > 0, r < R} |\tilde{g}^\epsilon(t, r)| = R < \infty$ . Lemma 4.4.5 provides the proof. □

**Corollary 4.3.2.** *The conditions which ensure an approximate solution of equation (4.3.1) with a bounded error are  $a = a_0$  and  $\varphi = \frac{1}{4\omega}T_1 = \frac{\epsilon}{4\omega}t$ . This gives the following solution for  $x^0$*

$$x^0(t) = a_0 \cos\left(\omega + \frac{\epsilon}{4\omega}\right)t.$$

and  $x = x^0 + \epsilon r$  such as  $\|r\|_{W^{2,\infty}(0,T_\epsilon)} \leq C$ .

### 4.3.1 A stationary approximate solution [Permanent regime]

The steady state solutions are important for large sets of mechanical problems as they show the behaviour of the system for a long time. The steady solution does not depend on the initial conditions as the damping term  $\xi$  will reduce its effect. It depends only on the excitation force and the parameters of the system. To get an approximate steady state solution of equation (4.2.1), the amplitude of the solution and the phase difference have to be constant thus  $\frac{\partial a}{\partial T_1} = 0$  and  $\frac{\partial \gamma}{\partial T_1} = 0$ .

**Proposition 4.3.3.** *The frequency response equation which puts in evidence the dependence of the response magnitude on the frequency is given as*

$$a^2 = \frac{g^2}{4\omega_0^2 \left( \xi^2 + \left( \sigma - \frac{1}{4\omega_0} \right)^2 \right)}. \quad (4.3.10)$$

*a is defined as a function of  $\sigma$  hence the solution is stable and there is not a jump phenomenon for this kind of nonlinearity. This feature is discussed in Section 4.3.2.*

*Proof.* When  $a$  and  $\varphi$  are constant then system (4.2.16) becomes

$$\begin{cases} -\xi a + \frac{g}{2\omega_0} \sin(\gamma) = 0, \\ \sigma - \frac{1}{4\omega_0} + \frac{g}{2a\omega_0} \cos(\gamma) = 0. \end{cases} \quad (4.3.11)$$

A simple calculation gives the magnitude of the stationary solution as function of the natural frequency and the damping coefficient, thus

$$a^2 = \frac{g^2}{4\omega_0^2 \left( \xi^2 + \left( \sigma - \frac{1}{4\omega_0} \right)^2 \right)}.$$

□

**Proposition 4.3.4.** *A steady state solution is given as*

$$\begin{aligned} u^\epsilon(t) = & a \cos(\omega t - \gamma) + \epsilon \left( A \cos(\omega_0 t) - \frac{|a|}{\omega_0^2 \pi} \right) \\ & - \epsilon \left( \frac{2|a|}{\omega_0^2 \pi} \sum_{k=1}^{+\infty} \frac{(-1)^k}{(4k^2 - 1)^2} \cos(2k(\omega t - \gamma)) \right), \end{aligned} \quad (4.3.12)$$

where  $\omega = \omega_0 + \epsilon\sigma$ ,  $a$  and  $\gamma$  satisfy relation (4.3.11).

*Proof.* The stationary solution can be obtained from solution (4.4.13) by taking into account system (4.3.11), i.e.  $a$  does not depend on the time, neither  $\gamma$ . Moreover, the solution has the same frequency as the force excitation with a phase delay  $\gamma$ . The first term  $u_0$  can be expressed as

$$u_0 = a \cos(\omega_0 T_0 + \varphi) = a \cos(\omega_0 T_0 + \sigma T_1 - \gamma) = a \cos(\omega_0 t + \epsilon\sigma t - \gamma) = a \cos(\omega t - \gamma).$$

The same technique is applied to  $u_1$ , the proof is then accomplished. □

### 4.3.2 Stability of the approximate solution

One important feature of nonlinear system is the stability of the solution, see [48] for instance.

**Proposition 4.3.5.** *The solution of a nonlinear differential system is stable if the eigenvalues of linearized system have negative real parts.*

**Proposition 4.3.6.** *The solution of system (4.2.16) is stable and the Jacobian matrix of the linearized system is given as*

$$\begin{bmatrix} -\xi & a(\frac{1}{4\omega_0} - \sigma) \\ -\frac{1}{a}(\frac{1}{4\omega_0} - \sigma) & -\xi \end{bmatrix}. \quad (4.3.13)$$

*Proof.* Let us denote

$$\begin{cases} g_1 = -\xi a + \frac{g}{2\omega_0} \sin(\gamma), \\ g_2 = \sigma - \frac{1}{4\omega_0} + \frac{g}{2a\omega_0} \cos(\gamma). \end{cases} \quad (4.3.14)$$

The partial derivative of  $g_1$  and  $g_2$  with respect to  $a$  and  $\gamma$  can be expressed as:

$$\begin{aligned} \partial_a g_1 &= -\xi, & \partial_\gamma g_1 &= \frac{g}{2\omega_0} \cos(\gamma), \\ \partial_a g_2 &= -\frac{g}{2a^2\omega_0} \cos(\gamma), & \partial_\gamma g_2 &= -\frac{g}{2a\omega_0} \sin(\gamma). \end{aligned}$$

We evaluate this partial derivative at the critical point ( $g_1 = 0$  and  $g_2 = 0$ ), we can easily find

$$\begin{aligned} \partial_a g_1 &= -\xi, & \partial_\gamma g_1 &= a(\frac{1}{4\omega_0} - \sigma), \\ \partial_a g_2 &= -\frac{1}{a}(\frac{1}{4\omega_0} - \sigma), & \partial_\gamma g_2 &= -\xi. \end{aligned}$$

Therefore the Jacobian matrix has two negative eigenvalues since its trace is negative and its determinant is positive, this can prove the stability of the system.  $\square$

### 4.3.3 Numerics

We present here a comparison between the numerical steady state solution of equation (4.2.1) and the analytical solution (4.3.12); the results showed good agreement. Figure 4.1 shows the frequency contents of the numerical solution for  $\epsilon = 0.1$  and for  $\xi = 1$ , the frequency axis is normalized by the excitation frequency  $\frac{\omega}{2\pi}$ . The solution is at the same excitation frequency with the presence of even harmonics. This is in agreement with the analytical solution. The numerical and the analytical displacements are shown in Figure 4.2, good agreement is found with a small shift when the displacement is positive, this can be produced as  $\epsilon$  is not small enough. Figure 4.3 shows the displacements for  $\omega = 1.1$  and  $\epsilon = 0.01$ , good agreement is found.

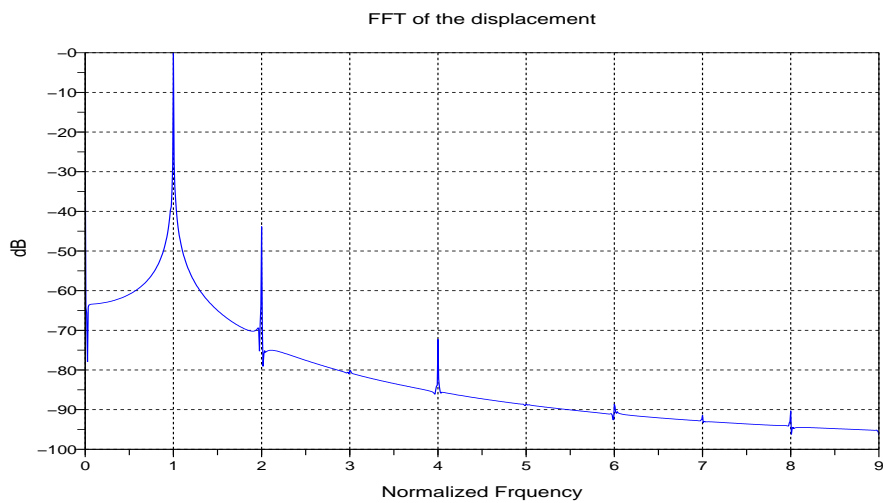


Figure 4.1. The frequency contents of the steady state solution for  $\epsilon = 0.1$ ,  $\xi = 1$  and  $\omega = 1.1$ . the frequency axis is normalized by the frequency of excitation, the response contains peaks corresponding to the excitation frequency and to its even harmonic.

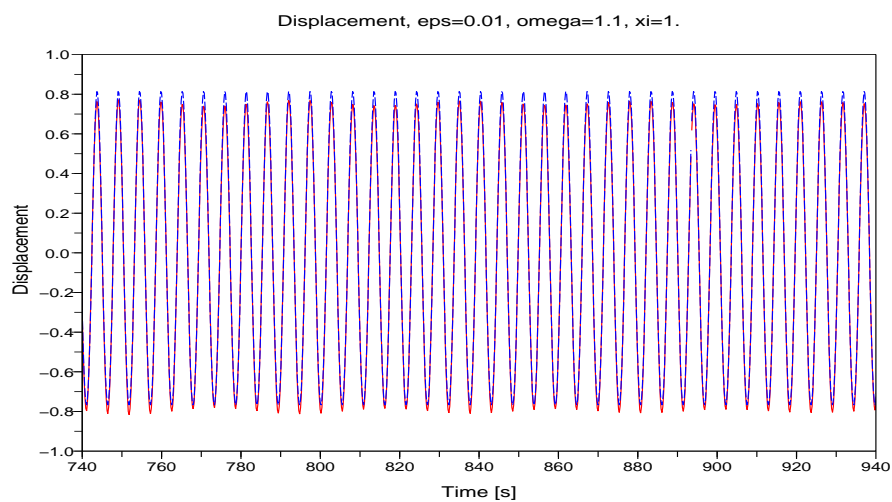


Figure 4.2. The numerical solution (solid line) and the explicit solution (dashed line) for  $\epsilon = 0.1$ ,  $\xi = 1$  and  $\omega = 1.1$ . The two solutions are close but a small difference appear when the displacement is positive.

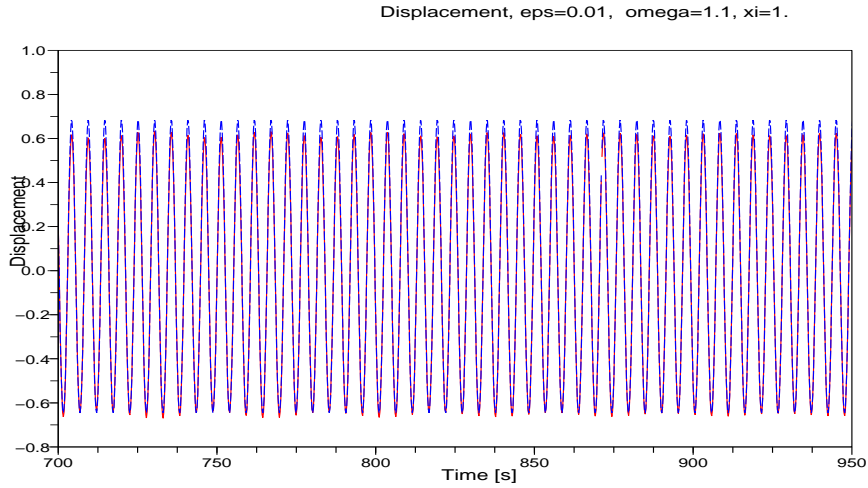


Figure 4.3. The numerical solution (solid line) and the explicit solution (dashed line) for  $\epsilon = 0.01$ ,  $\xi = 1$  and  $\omega = 1.1$ . The two solutions feet very well.

## 4.4 Nonlinear normal mode of systems with unilateral contact

The motivation of this study is to calculate the nonlinear normal modes of an undamped autonomous system with a unilateral contact. This method is also developed to prove the existence of the nonlinear normal modes for a nonlinearity of contact type. It is an alternative to the proof presented in Chapter 3. We also compare the solution obtained by Algorithm 2 of Chapter 3 with the analytical solution obtained by the multiple scales method.

Consider the nonlinear autonomous undamped system written in the real space

$$M\ddot{Y} + KY + \epsilon F(Y) = 0, \quad (4.4.1)$$

$$(F(Y))_{i=1,\dots,n} = \begin{cases} 0 & \text{if } i \neq r, \\ (Y_r)_+ & \text{if } i = r. \end{cases}$$

The choice of this model is not arbitrary, it can be a model of a beam with a unilateral contact as in Chapter 1 or a mass-spring model with one unilateral spring as in Chapter 3; hence  $\epsilon$  is a small parameter representing a spring stiffness. It is a restrictive case of nonlinearity but a change of the mass and the stiffness matrices can be done to model many situations of systems with unilateral contact and with different boundary conditions.

### 4.4.1 Equation of motion in the eigenvector space

The system is written in the eigenvectors basis, let  $(\phi_i)_{i=1,\dots,n}$  and  $(\omega_i)_{i=1,\dots,n}$  be the generalized eigenvectors and eigenvalues of  $M$  and  $K$  respectively,  $\phi$  is the basis transformation matrix and  $\Omega^2 = \text{diag}(\omega_i^2)_{i=1,\dots,n}$ .  $\phi$  is chosen such that  ${}^t\phi M \phi = I_n$  and  ${}^t\phi K \phi = \Omega^2$ , The

basis change then yields the following differential system:

$$\ddot{X} + \Omega^2 X + \epsilon f(X) = 0, \quad (4.4.2)$$

where  $f(X) = {}^t \phi F(\phi X)$ . The special form of the nonlinearity in  $Y$  takes the following form in  $X$ :

$$(f(X))_{i=1,\dots,n} = \left( \phi_{ri} \left( \sum_{j=1}^n \phi_{rj} X_j \right) \right)_{+} \Big|_{i=1,\dots,n}.$$

For convenience, system (4.4.2) is written componentwise to obtain

$$\ddot{X}_i + \omega_i^2 X_i + \epsilon \phi_{ri} \left( \sum_{j=1}^n \phi_{rj} X_j \right)_{+} = 0, \quad \forall i \in \{1, \dots, n\}. \quad (4.4.3)$$

#### 4.4.2 The method of multiple scales

This method is introduced in Section 4.2.1. As we are seeking a solution of three terms, we have then to consider three time scales  $T_0$ ,  $T_1$ , and  $T_2$  such that  $T_0 = t$ ,  $T_1 = \epsilon t$  and  $T_2 = \epsilon^2 t$ . The derivation operator with respect to the independent variable  $t$  is then written as function of the other scales:

$$\begin{aligned} \frac{\partial}{\partial t} &= \frac{\partial}{\partial T_0} + \epsilon \frac{\partial}{\partial T_1} + \epsilon^2 \frac{\partial}{\partial T_2}, \\ \frac{\partial^2}{\partial^2 t} &= \frac{\partial^2}{\partial^2 T_0} + 2\epsilon \frac{\partial^2}{\partial T_0 \partial T_1} + \epsilon^2 \frac{\partial^2}{\partial^2 T_1} + 2\epsilon^2 \frac{\partial^2}{\partial T_0 \partial T_2} + 2\epsilon^3 \frac{\partial^2}{\partial T_1 \partial T_2} + \epsilon^4 \frac{\partial^2}{\partial^2 T_2}. \end{aligned}$$

A solution of system (4.4.3) is sought in the following form

$$X_i^\epsilon = X_i^0 + \epsilon X_i^1 + \epsilon^2 r_i, \quad \forall i \in \{1, \dots, n\}, \quad (4.4.4)$$

where  $r_i$  is the remainder. Using the same technique as in Section 4.2.1, equation (4.4.3) is written with the independent variables  $T_0$ ,  $T_1$  and  $T_2$  as follows

**Proposition 4.4.1.**  $\forall i \in \{1, \dots, n\}$ , the terms  $X_i^0$  and  $X_i^1$  are solutions of the following differential equations respectively

$$\frac{\partial^2 X_i^0}{\partial^2 T_0} + \omega_i^2 X_i^0 = 0, \quad (4.4.5)$$

$$\frac{\partial^2 X_i^1}{\partial^2 T_0} + \omega_i^2 X_i^1 = -2 \frac{\partial^2 X_i^0}{\partial T_0 \partial T_1} - \phi_{ri} \left( \sum_{j=1}^n \phi_{rj} X_j^0 \right)_{+}, \quad (4.4.6)$$

and the remainder  $r_i$  is a solution of the following differential equation

$$\begin{aligned} \frac{\partial^2 r_i}{\partial^2 T_0} + \omega_i^2 r_i &= S_i(T_0, T_1, T_2) + f_i^\epsilon(T_0, T_1, T_2) + \epsilon g_i^\epsilon(T_0, T_1, T_2, r_j), \\ r_i(0) &= 0, \quad \dot{r}_i(0) = 0, \end{aligned} \quad (4.4.7)$$

where

$$\begin{aligned}
S_i(T_0, T_1, T_2) &= -\frac{\partial^2 X_i^0}{\partial T_1^2} - 2\frac{\partial^2 X_i^1}{\partial T_0 \partial T_1} - 2\frac{\partial^2 X_i^0}{\partial T_0 \partial T_2} - \phi_{ri} H(u)v, \\
f_i^\epsilon(T_0, T_1, T_2) &= \epsilon \left( -\frac{\partial^2 X_i^1}{\partial T_1^2} - 2\frac{\partial^2 X_i^0}{\partial T_1 \partial T_2} - 2\epsilon \frac{\partial^2 X_i^1}{\partial T_1 \partial T_2} - 2\epsilon \frac{\partial^2 X_i^1}{\partial T_0 \partial T_2} - \epsilon \frac{\partial^2 X_i^0}{\partial^2 T_2} - \epsilon^2 \frac{\partial^2 X_i^1}{\partial^2 T_2} \right) \\
&\quad - \phi_{ri} \chi(u, v) - \left( 2\epsilon \frac{\partial^2 r_i}{\partial T_0 \partial T_1} + \epsilon^2 \frac{\partial^2 r_i}{\partial^2 T_1} + 2\epsilon^2 \frac{\partial^2 r_i}{\partial T_0 \partial T_2} + 2\epsilon^3 \frac{\partial^2 r_i}{\partial T_1 \partial T_2} + \epsilon^4 \frac{\partial^2 r_i}{\partial^2 T_2} \right), \\
g_i^\epsilon(T_0, T_1, T_2, r^j) &= -\phi_{ri} \frac{[(u + \epsilon v + \epsilon^2 w)_+ - (u + \epsilon v)_+]}{\epsilon^2}.
\end{aligned}$$

such that  $u = \phi_{r1} X_1^0$ ,  $v = \sum_j^n \phi_{rj} X_j^1$ ,  $w = \sum_j^n \phi_{rj} r_j$ .

*Proof.* We substitute (4.4.4) in equation (4.4.3) and collect the remaining term after identifying the terms of order  $\epsilon^0$  and  $\epsilon^1$ , we obtain easily the equations of  $X_i^0$  and  $X_i^1$ . The equation of  $r_i$  can be found by writing all the remaining terms of order  $\epsilon^2$  and more,

$$\begin{aligned}
\frac{\partial^2 r_i}{\partial^2 T_0} + \omega_i^2 r_i &= -\frac{\partial^2 X_i^0}{\partial T_1^2} - 2\frac{\partial^2 X_i^1}{\partial T_0 \partial T_1} - 2\frac{\partial^2 X_i^0}{\partial T_0 \partial T_2} - \phi_{ri} H(u)(v + \epsilon w) - \phi_{ri} \chi(u, v + \epsilon w) \\
&\quad + \epsilon \left( -\frac{\partial^2 X_i^1}{\partial T_1^2} - 2\frac{\partial^2 X_i^0}{\partial T_1 \partial T_2} - 2\epsilon \frac{\partial^2 X_i^1}{\partial T_1 \partial T_2} - 2\epsilon \frac{\partial^2 X_i^1}{\partial T_0 \partial T_2} - \epsilon \frac{\partial^2 X_i^0}{\partial^2 T_2} - \epsilon^2 \frac{\partial^2 X_i^1}{\partial^2 T_2} \right) \\
&\quad - \left( 2\epsilon \frac{\partial^2 r_i}{\partial T_0 \partial T_1} + \epsilon^2 \frac{\partial^2 r_i}{\partial^2 T_1} + 2\epsilon^2 \frac{\partial^2 r_i}{\partial T_0 \partial T_2} + 2\epsilon^3 \frac{\partial^2 r_i}{\partial T_1 \partial T_2} + \epsilon^4 \frac{\partial^2 r_i}{\partial^2 T_2} \right).
\end{aligned}$$

On the other hand, we have

$$\begin{aligned}
\chi_\epsilon(u, v + \epsilon w) &= \frac{(u + \epsilon v + \epsilon^2 w)_+ - [(u)_+ + H(u)(\epsilon v + \epsilon^2 w)]}{\epsilon} \\
&= \frac{(u + \epsilon v)_+ - [(u)_+ + \epsilon H(u)v]}{\epsilon} + \frac{(u + \epsilon v + \epsilon^2 w)_+ - (u + \epsilon v)_+}{\epsilon} \\
&\quad - \epsilon H(u)w \\
&= \chi_\epsilon(u, v) - \epsilon H(u)w + \epsilon \tilde{g}_\epsilon(T_0, T_1, T_2, w),
\end{aligned}$$

with

$$\tilde{g}_\epsilon(T_0, T_1, T_2, w) = \frac{[(u + \epsilon v + \epsilon^2 w)_+ - (u + \epsilon v)_+]}{\epsilon^2},$$

By taking in account that

$$\chi_\epsilon(u, v + \epsilon w) + \epsilon H(u)w = \chi_\epsilon(u, v) + \epsilon \tilde{g}_\epsilon(T_0, T_1, T_2, w)$$

and separating the terms we get Expression 4.4.7. □

### 4.4.3 Nonlinear normal mode of the autonomous system with unilateral contact

Until now, we didn't mentioned any information about the initial conditions of the system to be solved. In order to obtain a periodic solution, the initial conditions will be determined in order to obtain a periodic solution of the system of a period to be determined, i.e. a nonlinear normal mode of the system. This method is an alternative to the algorithm presented in Chapter 3 for unilateral nonlinearity; it is preferable to come back to that Chapter for detailed definitions and formulation of the nonlinear normal modes. Finding a nonlinear normal modes of system (4.4.2) is equivalent to search for initial conditions and a period which ensure a periodic solution of the system. Hence, the unknown are  $(a_i)_{i=1,\dots,n}$  and a period  $T$  such as

$$X^\epsilon(T) = X^\epsilon(0), \quad \dot{X}^\epsilon(T) = \dot{X}^\epsilon(0),$$

with the initial conditions:

$$\begin{cases} X_1^\epsilon(0) = X_1^0(0) + \epsilon X_1^1(0) = a_0 + \epsilon a_1, & \dot{X}_1^\epsilon(0) = 0, \\ X_i^\epsilon(0) = X_i^0(0) + \epsilon X_i^1(0) = \epsilon a_i, & \dot{X}_i^\epsilon(0) = 0, \quad \forall i \in \{2, \dots, n\}. \end{cases} \quad (4.4.8)$$

$a_0$  is a real number, the conditions above correspond to the nonlinear mode denoted by 1, the same technique can be reproduced to find the initial conditions needed to obtain the other nonlinear normal modes without any restriction. The system is then written with the corresponding initial conditions,

$$\frac{\partial^2 X_1^0}{\partial T_0^2} + \omega_1^2 X_1^0 = 0, \quad X_1^0(0) = a_0, \quad \dot{X}_1^0 = 0, \quad (4.4.9)$$

$$\frac{\partial^2 X_1^1}{\partial T_0^2} + \omega_1^2 X_1^1 = -2 \frac{\partial^2 X_1^0}{\partial T_0 \partial T_1} - \phi_{r1} \left( \sum_{j=1}^n \phi_{rj} X_j^0 \right)_+, \quad X_1^1(0) = a_1, \quad \dot{X}_1^1 = 0. \quad (4.4.10)$$

and  $\forall i \in \{2, \dots, n\}$

$$\frac{\partial^2 X_i^0}{\partial T_0^2} + \omega_i^2 X_i^0 = 0, \quad X_i^0(0) = 0, \quad \dot{X}_i^0 = 0, \quad (4.4.11)$$

$$\frac{\partial^2 X_i^1}{\partial T_0^2} + \omega_i^2 X_i^1 = -2 \frac{\partial^2 X_i^0}{\partial T_0 \partial T_1} - \phi_{ri} \left( \sum_{j=1}^n \phi_{rj} X_j^0 \right)_+, \quad X_i^1(0) = a_i, \quad \dot{X}_i^1 = 0. \quad (4.4.12)$$

Note that the initial conditions corresponding to  $X_1^0$  is not zero but the others are, this is normal since we are seeking the "first" normal mode, this means that the initial conditions vector is tangent to the "first" eigenvector.

The strategy is to use equations (4.4.9) and (4.4.10) to find the period of the normal mode with its harmonics then to use equations (4.4.11) and (4.4.12) to determine the initial conditions  $(a_i)_{i=2,\dots,n}$ . The fact that equation (4.4.11) has a trivial solution  $X_i^0 = 0, \forall i \in \{2, \dots, n\}$  simplifies the calculation.

**Proposition 4.4.2.** *The solution of equations (4.4.9) and (4.4.10) are respectively*

$$X_1^0(T_0, T_1, T_2) = a \cos(\omega_1 T_0 + \varphi),$$

$$X_1^1(T_0, T_1, T_2) = -\frac{\phi_{r1}|\phi_{r1}a|}{\omega_1^2\pi} - \frac{2\phi_{r1}|\phi_{r1}a|}{\omega_1^2\pi} \sum_{k=1}^{+\infty} \frac{(-1)^k}{(4k^2 - 1)^2} \cos(2k(\omega_1 T_0 + \varphi))$$

$$+ A_1 \cos(\omega_1 T_0),$$

where  $a = a(T_2)$ ,  $\varphi = \frac{\phi_{r1}^2}{4\omega_1} T_1 + \varphi_1(T_2)$  and  $A_1 = a_1 + \frac{\phi_{r1}|\phi_{r1}a|}{\omega_1^2\pi} + \frac{2\phi_{r1}|\phi_{r1}a|}{\omega_1^2\pi} \sum_{k=1}^{+\infty} \frac{(-1)^k}{(4k^2 - 1)^2}$ .  $a(T_2)$  and  $\varphi_1(T_2)$  will be determined later in order to get a bounded error.

*Proof.* The proof consists in solving equations (4.4.9) and (4.4.10) to get  $X_1^0$  and  $X_1^1$ . The classical solution of (4.4.9) is given as

$$X_1^0(T_0) = a(T_1, T_2) \cos(\omega_1 T_0 + \varphi(T_1, T_2)), \quad a(0, 0) = a_0, \quad \varphi_0(0, 0) = 0. \quad (4.4.13)$$

$a$  and  $\varphi$  are function of  $T_1$  and  $T_2$  and they should be calculated in order to get a bounded solution of equation (4.4.10). Equation (4.4.11) has a trivial solution  $X_i^0 = 0, \forall i \in \{2, \dots, n\}$ , we update equation (4.4.10) and get

$$\frac{\partial^2 X_1^1}{\partial^2 T_0} + \omega_1^2 X_1^1 = 2 \frac{\partial a}{\partial T_1} \omega_1 \sin(\omega_1 T_0 + \varphi) + 2a\omega_1 \frac{\partial \varphi}{\partial T_1} \cos(\omega_1 T_0 + \varphi)$$

$$- \frac{\phi_{r1}^2 a \cos(\omega_1 T_0 + \varphi)}{2} - \phi_{r1} \frac{|\phi_{r1} a \cos(\omega_1 T_0 + \varphi)|}{2}. \quad (4.4.14)$$

By collecting the secular terms and equating them to zero, we get the following system of partial differential equations

$$\begin{cases} 2 \frac{\partial a}{\partial T_1} \omega_1 = 0, & a(0, 0) = a_0, \\ 2a\omega_1 \frac{\partial \varphi}{\partial T_1} - \frac{\phi_{r1}^2 a}{2} = 0, & \varphi(0, 0) = 0. \end{cases} \quad (4.4.15)$$

A simple calculation yields  $a = a(T_2)$  and  $\varphi = \frac{\phi_{r1}^2}{4\omega_1} T_1 + \varphi_1(T_2)$ . We still need to calculate  $X_1^1(T_0, T_1, T_2)$  from equation (4.4.14) after removing the secular terms

$$\frac{\partial^2 X_1^1}{\partial^2 T_0} + \omega_1^2 X_1^1 = -\phi_{r1} \frac{|\phi_{r1} a \cos(\omega_1 T_0 + \varphi)|}{2}, \quad X_1^1(0) = a_1, \quad \dot{X}_1^1(0) = 0. \quad (4.4.16)$$

This equation is similar to equation (4.2.17) then the solution is given as,

$$X_1^1(T_0, T_1, T_2) = -\frac{\phi_{r1}|\phi_{r1}a|}{\omega_1^2\pi} - \frac{2\phi_{r1}|\phi_{r1}a|}{\omega_1^2\pi} \sum_{k=1}^{+\infty} \frac{(-1)^k}{(4k^2 - 1)^2} \cos(2k(\omega_1 T_0 + \varphi))$$

$$+ A_1 \cos(\omega_1 T_0),$$

where  $A_1 = a_1 + \frac{\phi_{r1}|\phi_{r1}a|}{\omega_1^2\pi} + \frac{2\phi_{r1}|\phi_{r1}a|}{\omega_1^2\pi} \sum_{k=1}^{+\infty} \frac{(-1)^k}{(4k^2 - 1)^2}$ , This ends the proof.  $\square$

Finally  $(a_i)_{i=1,\dots,n}$  have to be determined in order to obtain the initial condition vector which yields a periodic solution of period  $T$ .

**Proposition 4.4.3.** *The initial conditions  $(a_i)_{i=1,\dots,n}$  which ensure an approximate periodic solution of system (4.4.2) of period  $T$  are given as follows*

$$\begin{aligned} a_1 &= -\frac{\phi_{r1}|\phi_{r1}a|}{\omega_1^2\pi} - \frac{2\phi_{r1}|\phi_{r1}a|}{\omega_1^2\pi} \sum_{k=1}^{+\infty} \frac{(-1)^k}{(4k^2-1)^2} \\ a_i &= -\frac{\phi_{ri}|\phi_{r1}a|}{\omega_i^2\pi} - \frac{2\phi_{ri}|\phi_{r1}a|}{\pi} \sum_{k=1}^{+\infty} \frac{(-1)^k}{(4k^2-1)} \frac{1}{(\omega_i^2-4k^2\omega_1^2)} \\ &\quad - \frac{\phi_{ri}\phi_{r1}a}{2(\omega_i^2-\omega_1^2)}, \quad \forall i \in \{2, \dots, n\}. \end{aligned} \quad (4.4.17)$$

*Proof.* We set  $A_1$  to zero in Proposition 4.4.2, this can give directly  $a_1$ .

Consider once again equation (4.4.12) by updating  $X_i^0 = 0, \forall i \in \{2, \dots, n\}$ , and  $X_1^0 = a \cos(\omega_1 T_0 + \varphi)$  we obtain

$$\frac{\partial^2 X_i^1}{\partial^2 T_0} + \omega_i^2 X_i^1 = -\frac{\phi_{ri}\phi_{r1}a \cos(\omega_1 T_0 + \varphi)}{2} - \frac{\phi_{ri}|\phi_{r1}a \cos(\omega_1 T_0 + \varphi)|}{2}, \quad (4.4.18)$$

$$X_i^1(0) = a_i, \quad \dot{X}_i^1 = 0. \quad (4.4.19)$$

By using the same technique as before we get the solution in the following form

$$\begin{aligned} X_i^1 &= -\frac{\phi_{ri}|\phi_{r1}a|}{\omega_i^2\pi} - \frac{2\phi_{ri}|\phi_{r1}a|}{\pi} \sum_{k=1}^{+\infty} \frac{(-1)^k}{(4k^2-1)} \frac{1}{(\omega_i^2-4k^2\omega_1^2)} \cos(2k(\omega_1 T_0 + \varphi)) \\ &\quad + A_i \cos(\omega_i T_0) - \frac{\phi_{ri}\phi_{r1}a}{2(\omega_i^2-\omega_1^2)} \cos(\omega_1 T_0 + \varphi), \end{aligned} \quad (4.4.20)$$

with

$$A_i = a_i + \frac{\phi_{ri}|\phi_{r1}a|}{\omega_i^2\pi} + \frac{2\phi_{ri}|\phi_{r1}a|}{\pi} \sum_{k=1}^{+\infty} \frac{(-1)^k}{(4k^2-1)} \frac{1}{(\omega_i^2-4k^2\omega_1^2)} + \frac{\phi_{ri}\phi_{r1}a}{2(\omega_i^2-\omega_1^2)},$$

$(A_i)_{i=2,\dots,n}$  has to be set to zero to ensure a periodic solution for all  $(X_i^1)_{i=2,\dots,n}$  of period  $T$  therefore

$$\begin{aligned} a_i &= -\frac{\phi_{ri}|\phi_{r1}a|}{\omega_i^2\pi} - \frac{2\phi_{ri}|\phi_{r1}a|}{\pi} \sum_{k=1}^{+\infty} \frac{(-1)^k}{(4k^2-1)} \frac{1}{(\omega_i^2-4k^2\omega_1^2)} \\ &\quad - \frac{\phi_{ri}\phi_{r1}a}{2(\omega_i^2-\omega_1^2)}. \end{aligned} \quad (4.4.21)$$

□

*Remark 4.4.4.* The functions  $a(T_2)$  and  $\varphi_1(T_2)$  are not defined until now, they have to verify additional conditions in order to obtain a bounded solution. These additional conditions come from the hypothesis which should be verified by the source term of the equation of the remainders 4.4.7.

#### 4.4.4 Bounds on the remainders

The approximate solutions are valid for small  $\epsilon$ , it is important to study the remainders of these solutions in order to find the conditions which ensure a good approximation, i.e. the necessary and sufficient conditions to have bounded errors. We will prove that the remainders are bounded on a time interval which depends on  $\epsilon$ , this can be done by writing the differential equations which involve the remainders with the approximate solutions. We have to prove that the source term of these equations satisfies the hypothesis of the following lemma proved in [31].

**Lemma 4.4.5. [Bounds for large time for systems](Junca-Rousselet [31])**

Let  $w_\epsilon = (w_1^\epsilon, \dots, w_N^\epsilon)$  be the solution of the following system:

$$\begin{cases} (\lambda_1)^2 (w_k^\epsilon)'' + (\lambda_k)^2 w_k^\epsilon = S_k(s) + f_k^\epsilon(s) + \epsilon g_k^\epsilon(s; w_\epsilon), \\ w_k^\epsilon(0) = 0, \quad (w_k^\epsilon)'(0) = 0, \quad k = 1, \dots, N. \end{cases} \quad (4.4.22)$$

If source terms satisfy the following conditions where  $M > 0$ ,  $C > 0$  are fixed constants :

1. non resonance conditions with  $S_k(s)$  are  $2\pi$ -periodic functions and  $|S_k(s)| \leq M$ ,

(a)  $S_1(s)$  is orthogonal to  $e^{\pm is}$ , i.e.  $\int_0^{2\pi} S_1(s) e^{\pm is} ds = 0$ ,

(b)  $\lambda_k, \lambda_1$  are  $\mathbb{Z}$  independent for all  $k \neq 1$ ,

2.  $|f_k^\epsilon| \leq M$  and for all  $T$ ,  $\int_0^T |f_\epsilon(s)| ds \leq C\epsilon T$  (resp  $C\sqrt{\epsilon}T$ ),

3. for all  $R > 0$ :  $M_R = \max_k \sup_{\epsilon \in (0,1), s > 0, w_1^2 + \dots + w_N^2 < R^2} |g_k^\epsilon(s; u)| < \infty$ ,

then, there exists  $\epsilon_0 > 0$  and  $\gamma > 0$  such that, for  $0 < \epsilon < \epsilon_0$ ,  $w_\epsilon$  is uniformly bounded in  $W^{2,\infty}(0, T_\epsilon)$ , where  $T_\epsilon = \frac{\gamma}{\epsilon}$  ( resp  $\frac{\gamma}{\sqrt{\epsilon}}$ ).

**Proposition 4.4.6.** if  $\varphi_1(T_2) = -\frac{\phi_{r_1}^4}{16\omega_1^3} T_2$  and  $a(T_2) = a_0$  then there exists  $\epsilon_0 > 0$  and  $\gamma > 0$  such that, for  $0 < \epsilon < \epsilon_0$ , the remainder  $(r_i)_{i=1,\dots,n}$  is uniformly bounded in  $W^{2,\infty}(0, T_\epsilon)$ , where  $T_\epsilon = \frac{\gamma}{\epsilon}$ .

*Proof.* The same strategy as in the proof of Proposition 4.3.1 is used, it consists to remove the secular terms from the expression of  $S_1(T_0, T_1, T_2)$  to avoid a resonance phenomena; then we write all the remaining terms as function of the independent variable  $t$ . By this, we verify the first hypothesis of Lemma 4.4.5. Then we prove that  $f_i^\epsilon(t)$  and  $g_i^\epsilon(t, r^1, \dots, r^n)$  verify the second and the third hypothesis.

**Step 1: removing secular term from  $S_1(T_0, T_1, T_2)$ .**

We write again the differential equation which involves the remainders with the other terms,

$$\begin{aligned} \frac{\partial^2 r_i}{\partial^2 T_0} + \omega_i^2 r_i &= S_i(T_0, T_1, T_2) + f_i^\epsilon(T_0, T_1, T_2) + \epsilon g_i^\epsilon(T_0, T_1, T_2, r_j), \\ r_i(0) &= 0, \quad \dot{r}_i(0) = 0, \end{aligned} \quad (4.4.23)$$

where

$$S_1(T_0, T_1, T_2) = -\frac{\partial^2 X_1^0}{\partial^2 T_1} - 2\frac{\partial^2 X_1^1}{\partial T_0 \partial T_1} - 2\frac{\partial^2 X_1^0}{\partial T_0 \partial T_2} - \phi_{r1} H(u)v,$$

$u = \phi_{r1} X_1^0, v = \sum_{j=1}^n \phi_{rj} X_j^1$ . The solution of equation (4.4.9) is given as

$$X_1^0 = a(T_2) \cos(\omega_1 T_0 + \frac{\phi_{r1}^2}{4\omega_1} T_1 + \varphi_1(T_2)), \quad a(0) = a_0, \quad \varphi_1(0) = 0. \quad (4.4.24)$$

$\varphi_1(T_2)$  will be determined in order to obtain non resonant terms in the expression of  $S_1$ .  $v$  does not contain any resonant terms, i.e. any term in  $\cos(\omega_1 T_0)$  or  $\sin(\omega_1 T_0)$ , this is obtained by construction.  $H(u)$  also does not contain any resonant terms (see equation (4.2.9)). We still have

$$-\frac{\partial^2 X_i^0}{\partial^2 T_1} - 2\frac{\partial^2 X_i^0}{\partial T_0 \partial T_2}$$

which can have secular terms. A simple calculation gives:

$$\begin{aligned} -\frac{\partial^2 X_i^0}{\partial^2 T_1} - 2\frac{\partial^2 X_i^0}{\partial T_0 \partial T_2} &= a\left(\frac{\partial \varphi}{\partial T_1}\right)^2 \cos(\omega_1 T_0 + \varphi) \\ &+ \frac{\partial a}{\partial T_2} \omega_1 \sin(\omega_1 T_0 + \varphi) + a\omega_1 \frac{\partial \varphi_1}{\partial T_2} \cos(\omega_1 T_0 + \varphi). \end{aligned} \quad (4.4.25)$$

The coefficients of the resonant terms in the expression of  $S_1$  have to be set to zero to ensure the first hypothesis of the lemma:

$$\begin{cases} \frac{\partial a}{\partial T_2} = 0, & a(0) = a_0, \\ a\omega_1 \frac{\partial \varphi_1}{\partial T_2} + a\left(\frac{\partial \varphi}{\partial T_1}\right)^2 = 0, & \varphi_1(0) = 0. \end{cases} \quad (4.4.26)$$

The solution is then given as  $a = a_0$  and  $\varphi_1 = -\frac{1}{\omega_1} \left(\frac{\partial \varphi}{\partial T_1}\right)^2 T_2 = -\frac{\phi_{r1}^4}{16\omega_1^3} T_2$ .

### Step 2: writing the differential equation as function of the independent variable $t$ .

Right now, we express all the terms of  $S_i$ ,  $f_i^\epsilon$  and  $g_i^\epsilon$  as function of the independent variable  $t$ . We also move the terms in  $r_i$  to the left hand side of the equation to find a differential equation in  $t$ :

$$\frac{\partial^2 r_i}{\partial^2 t} + \omega_i^2 r_i = \tilde{S}_i(t) + \tilde{f}_i^\epsilon(t) + \epsilon g_i^\epsilon(t, r_j), \quad r_i(0) = 0, \quad \dot{r}_i(0) = 0, \quad (4.4.27)$$

$$\tilde{S}_i(t) = -2\frac{\partial^2 X_i^1}{\partial T_0 \partial T_1} - \phi_{ri} H(u)v,$$

$$\begin{aligned} \tilde{f}_i^\epsilon(t) &= \epsilon \left( -\frac{\partial^2 X_i^1}{\partial T_1^2} - 2\frac{\partial^2 X_i^0}{\partial T_1 \partial T_2} - 2\epsilon \frac{\partial^2 X_i^1}{\partial T_1 \partial T_2} - 2\epsilon \frac{\partial^2 X_i^1}{\partial T_0 \partial T_2} - \epsilon \frac{\partial^2 X_i^0}{\partial^2 T_2} - \epsilon^2 \frac{\partial^2 X_i^1}{\partial^2 T_2} \right) \\ &- \phi_{ri} \chi(u, v), \end{aligned}$$

$$g_i^\epsilon(t, r^j) = -\phi_{ri} \frac{[(u + \epsilon v + \epsilon^2 w)_+ - (u + \epsilon v)_+]}{\epsilon^2}.$$

**Step 3: verifying the hypothesis of Lemma 4.4.5.**

$\tilde{S}_1 = -2 \frac{\partial^2 X_1^1}{\partial T_0 \partial T_1} - \phi_{r1} H(u)v$ , it does not contain any resonant term and it can be expressed as function of  $t$ .

$\tilde{f}_i^\epsilon(t)$  involves terms in cosine and sine as well as the function  $\chi(u, v)$ , it can be expressed as function of  $t$  since all the terms are known. Then  $\tilde{f}_i^\epsilon$  is bounded as it is written as a finite sum of bounded terms; the function  $\chi(u, v)$  verifies Lemma 4.2.2 and Lemma 4.2.3 then there exists  $C$  such that  $\int_0^T |\tilde{f}_i^\epsilon(s)| ds \leq C\epsilon T$ .

Finally  $w = \sum_{j=1}^n \phi_{rj} r_j$  and  $u_+$  is 1-Lipschitzian then there exists  $C_i, \forall i \in \{1, \dots, n\}$  such that

$$|g_i^\epsilon(t, r^1, \dots, r^n)| = \left| -\phi_{ri} \frac{[(u + \epsilon v + \epsilon^2 w)_+ - (u + \epsilon v)_+]}{\epsilon^2} \right| \leq C_i |r|$$

then for all  $R > 0$ :  $M_R = \max_k \sup_{\epsilon \in (0,1), t > 0, r_1^2 + \dots + r_n^2 < R^2} |g_k^\epsilon(t; u)| < \infty$ . The proof is then accomplished by the direct use of Lemma 4.4.5.  $\square$

**Corollary 4.4.7.** *The approximate solution of system 4.4.3 of order  $\epsilon$  is given as follows*

$$X_1(t) = a_0 \cos \left( \omega_1 + \epsilon \frac{\phi_{r1}^2}{4\omega_1} - \epsilon^2 \frac{\phi_{r1}^4}{16\omega_1^3} \right) t - \epsilon \frac{\phi_{r1} |\phi_{r1} a|}{\omega_1^2 \pi} \epsilon \left( -\frac{2\phi_{r1} |\phi_{r1} a|}{\omega_1^2 \pi} \sum_{k=1}^{+\infty} \frac{(-1)^k}{(4k^2 - 1)^2} \cos \left( 2k \left( \omega_1 + \epsilon \frac{\phi_{r1}^2}{4\omega_1} - \epsilon^2 \frac{\phi_{r1}^4}{16\omega_1^3} \right) t \right) \right),$$

and for  $i \in \{2, \dots, n\}$

$$X_i(t) = -\epsilon \frac{2\phi_{ri} |\phi_{r1} a|}{\pi} \sum_{k=1}^{+\infty} \frac{(-1)^k}{(4k^2 - 1)} \frac{1}{(\omega_i^2 - 4k^2 \omega_1^2)} \cos \left( 2k \left( \omega_1 + \epsilon \frac{\phi_{r1}^2}{4\omega_1} - \epsilon^2 \frac{\phi_{r1}^4}{16\omega_1^3} \right) t \right) - \epsilon \frac{\phi_{ri} |\phi_{r1} a|}{\omega_i^2 \pi} - \epsilon \frac{\phi_{ri} \phi_{r1} a}{2(\omega_i^2 - \omega_1^2)} \cos \left( \omega_1 + \epsilon \frac{\phi_{r1}^2}{4\omega_1} - \epsilon^2 \frac{\phi_{r1}^4}{16\omega_1^3} \right) t,$$

The approximate period is then given by

$$T = \frac{2\pi}{\omega_1 + \epsilon \frac{\phi_{r1}^2}{4\omega_1} - \epsilon^2 \frac{\phi_{r1}^4}{16\omega_1^3}} \quad (4.4.28)$$

### 4.4.5 Comparison between the numerical solutions and the asymptotic expansions

We present a comparison of the numerical solutions given by Algorithm 2 and the asymptotic expansions discussed in this chapter. We apply both methods to compute the nonlinear normal modes of the discrete system (4.4.29) with the unilateral contact. Note that the asymptotic expansion is applied to system (4.4.2) where the matrices  $M$  and  $K$  are arbitrary and the unilateral contact could be at any point.

### Mass-spring model with a unilateral spring

Consider the discrete model of six mass-springs with only a unilateral contact presented in Section 3.6.2 of Chapter 3 (see Figure 3.7).

$$\ddot{X} + KX + \tilde{\epsilon}F(X) = 0, \quad (4.4.29)$$

Where  $\tilde{\epsilon} = \epsilon k_r$ ,  $k_r$  is the spring stiffness and  $\epsilon$  is a positive number,  $X = [X_1, \dots, X_6]$ ,  $K = \text{tridiag}(-1, 2, -1)$  of size  $6 \times 6$  and  $(F(X))_i = (X_5)_+ \delta_{5i}$ . The natural frequencies and their corresponding periods are given in Table 4.1. We will show the first and the fourth nonlinear normal modes for a small  $\epsilon$  in the time domain and the initial conditions in the space domain, the results are compared to the numerical solutions obtained by Algorithm 2 of Chapter 3.

Figures 4.4 and 4.6 show respectively the initial conditions vector which ensure the fourth and the first nonlinear normal modes calculated by the asymptotic expansion and by the numerical algorithm, the results show good agreement for  $\epsilon = 0.02$  and  $k_r = 1$ . Figures 4.5 and 4.7 show the fourth and the first nonlinear normal modes respectively for  $\epsilon = 0.02$  and  $k_r = 1$  also calculated by the asymptotic expansion and by the numerical algorithm.

<b>Frequencies</b> $f_i$	0.07 Hz	0.138 Hz	0.198 Hz	0.248 Hz	0.286 Hz	0.31 Hz
<b>Periods</b> $T_i$	14.11s	7.24s	5.03 s	4.03 s	3.48s	3.22 s

Table 4.1. The natural frequencies of the linearized system with their corresponding periods.

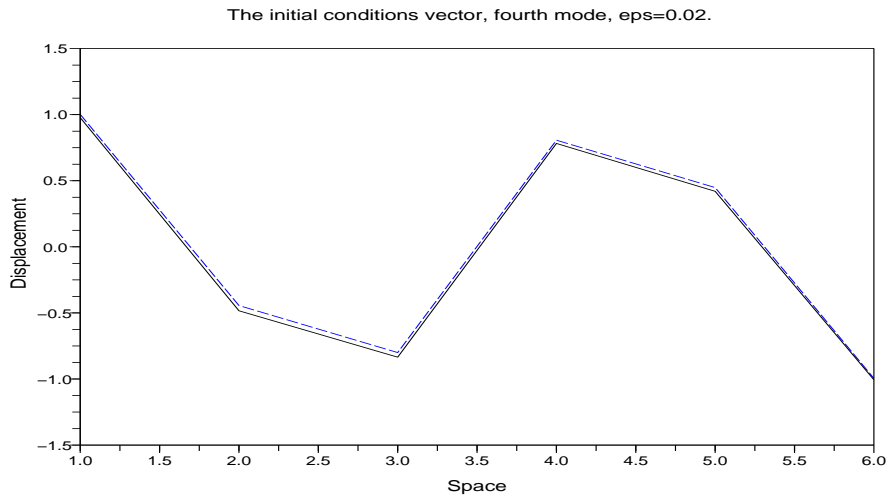


Figure 4.4. The initial condition vector which ensures the fourth nonlinear normal mode by asymptotic expansion (solid line) and by the numerical algorithm (dashed line) for  $\epsilon = 0.02$ .

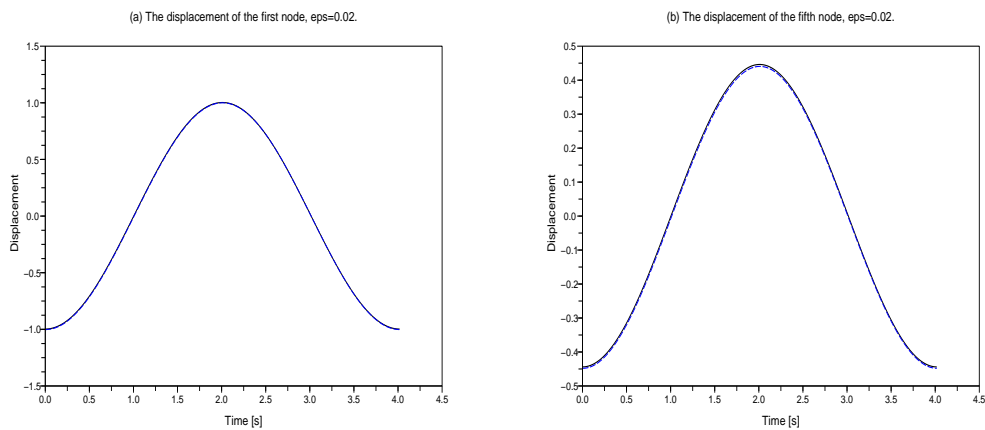


Figure 4.5. The displacement calculated by asymptotic expansion (solid line) and by the numerical algorithm (dashed line) of the first node (a) and the fifth node (b) for  $\epsilon = 0.02$ .

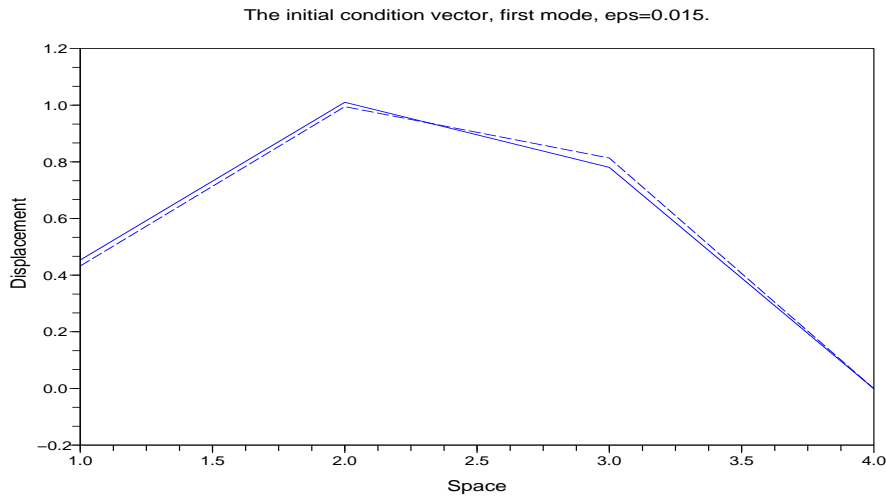


Figure 4.6. The initial condition vector which ensures the first nonlinear normal mode by asymptotic expansion (solid line) and by the numerical algorithm (dashed line) for  $\epsilon = 0.015$ .

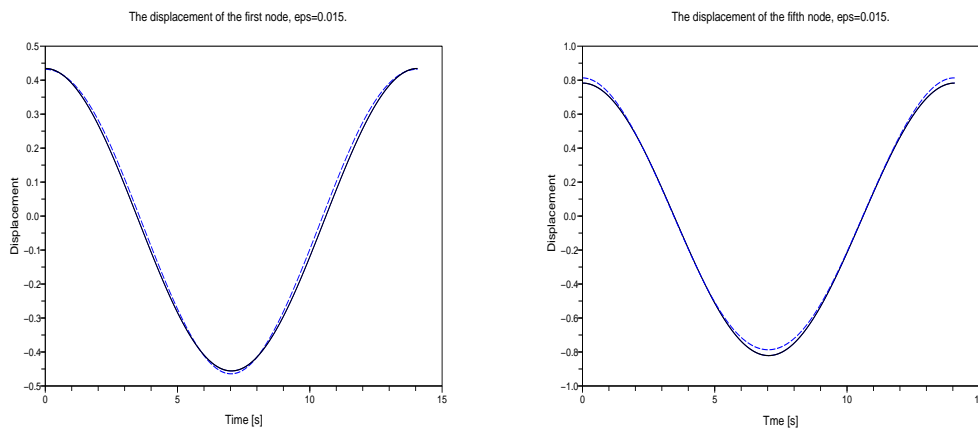


Figure 4.7. The displacement calculated by asymptotic expansion (solid line) and by the numerical algorithm (dashed line) of the first node (a) and the fifth node (b) for  $\epsilon = 0.015$ .

#### 4.4.6 Nonlinear normal mode of a beam with a unilateral spring

The main interest is to study the behaviour of a beam striking a one sided spring and to understand the effect of this unilateral contact to the linear normal modes of the beam via asymptotic expansion. To realize this, we have to determine the mass and the stiffness matrices of the beam and incorporate the unilateral spring into the finite element model at a chosen point. We will present results for a cantilever beam with a unilateral spring at the free end and for a clamped-clamped beam with a unilateral spring in the middle. A spring stiffness is fixed to  $k_r = 107000$  N/m which corresponds to the stiffness of a rubber, it is high comparing to the stiffness of the beam in flexion. Refer to Chapter 1 and to [11] for more details about the physical properties and about the equations of both cases.

##### Cantilevered beam

The model is discussed in Chapter 1 with an experimental validation and a scheme of the mechanical system. The nonlinear normal modes of this beam are found by the use of the multiple scales method and they are compared to the linear normal modes to see the effect of the unilateral spring. Figures 4.8, 4.9 and 4.10 show the three first nonlinear normal modes respectively compared to their corresponding linear normal modes. the results are in agreement with those obtained by Algorithm 2 and presented in Section 3.6.3.

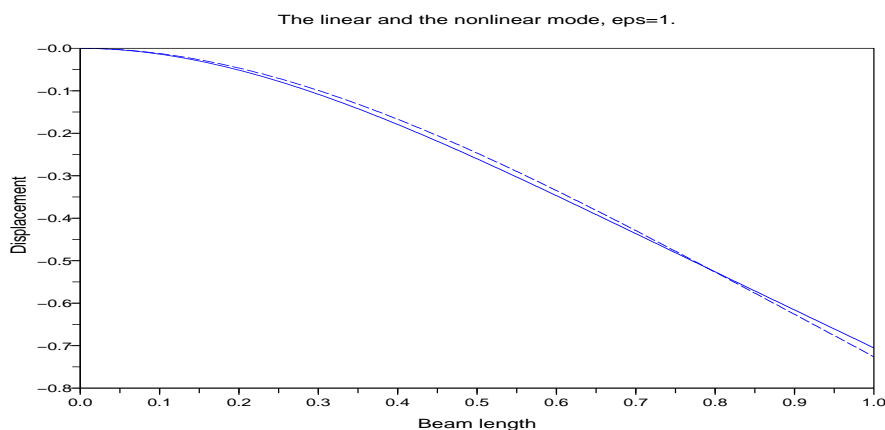


Figure 4.8. The first nonlinear normal mode (solid line) compared to the corresponding linear normal mode (dashed line) for  $k_r = 107000$  N/m and for  $\epsilon = 1$ . The spring is localized at the free end of the beam.

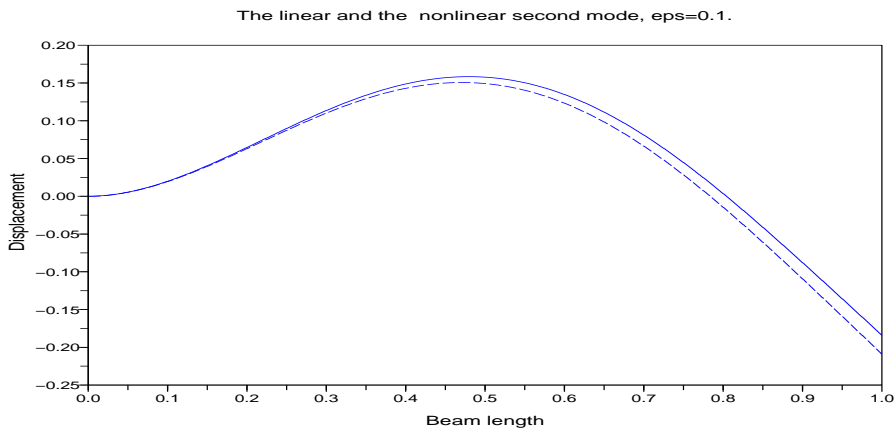


Figure 4.9. The second nonlinear normal mode (solid line) compared to the corresponding linear normal mode (dashed line) for  $k_r = 107000 \text{ N/m}$  and for  $\epsilon = 0.1$ . The spring is localized at the free end of the beam.

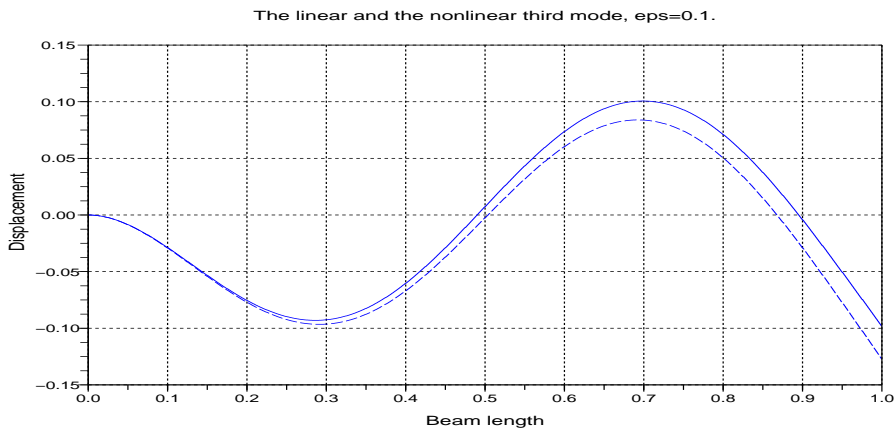


Figure 4.10. The third nonlinear normal mode (solid line) compared to the corresponding linear normal mode (dashed line) for  $k_r = 107000 \text{ N/m}$  and for  $\epsilon = 0.1$ . The spring is localized at the free end of the beam.

### Clamped-Clamped beam

A change of the boundary conditions and of the spring position leads to a clamped-clamped Euler-Bernoulli beam with unilateral contact in the middle of the beam, this model is studied numerically in [12]. We present a calculation of its nonlinear normal modes in the space domain, i.e. the initial conditions vector which yields a periodic solution of the system. Figures 4.11 and 4.12 show the second and the third nonlinear normal modes compared to the linear one for a spring stiffness of  $k_r = 107000$  N/m and for  $\epsilon = 1$ .

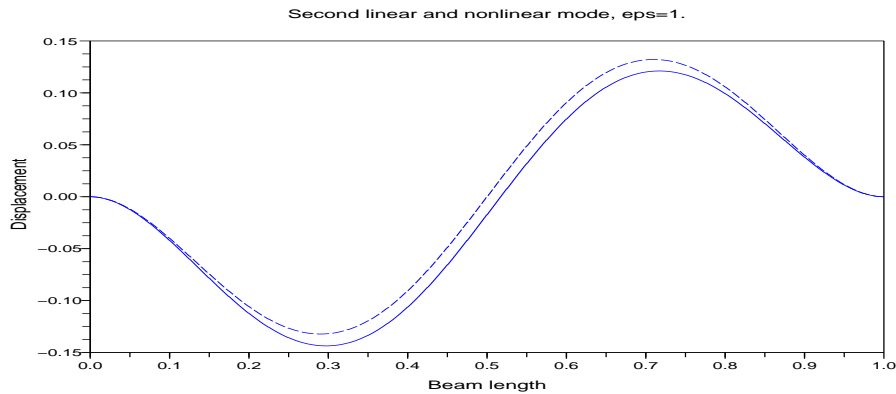


Figure 4.11. The second nonlinear normal mode (solid line) compared to the corresponding linear normal mode (dashed line) for  $k_r = 107000$  N/m and for  $\epsilon = 1$ . The spring is localized in the middle of the beam.

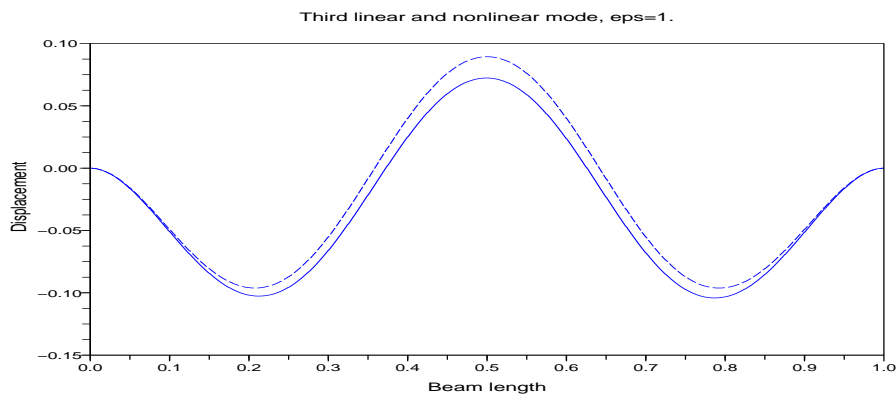


Figure 4.12. The third nonlinear normal mode (solid line) compared to the corresponding linear normal mode (dashed line) for  $k_r = 107000$  N/m and for  $\epsilon = 1$ . The spring is localized in the middle of the beam.

## 4.5 Nonlinear normal modes and forced systems

The aim of the study is to provide efficient tools to deal with nonlinearities encountered in mechanical engineering from different points of view. The concept of nonlinear normal modes was then introduced with different methods to compute them. All these methods use the initial condition arguments to ensure a periodic solution. Unfortunately an experimental validation of these methods is far from being realizable because it is impossible to excite a mechanical system with a special modal form of initial conditions. In this section, we study the feasibility of such experimental validation. We will introduce a force excitation and see if we can find the nonlinear normal modes. We use the same notation as Section 4.4. We consider the following differential system written in the eigenvector space

$$\ddot{X} + \Omega^2 X + \epsilon C \dot{X} + \epsilon f(X) = \epsilon(G^1 + \epsilon G^2) \cos(\omega t), \quad (4.5.1)$$

where  $C$  is a diagonal damping matrix  $(C_{ii})_{i=1,\dots,n}$ ,  $G^1 = (G_i^1)_{i=1,\dots,n}$ ,  $G^2 = (G_i^2)_{i=1,\dots,n}$  and

$$\omega = \omega_1 + \epsilon\sigma,$$

$\sigma$  is a detuning parameter. We are dealing with the nonlinear normal mode denoted 1 as in previous sections. The multiple scales method will also be used with the same notation for the time derivatives. Finally, the system is written componentwise to obtain  $\forall i \in \{1, \dots, n\}$ :

$$\ddot{X}_i + \omega_i^2 X_i + \epsilon C_{ii} \dot{X}_i + \epsilon \phi_{ri} \left( \sum_{j=1}^n \phi_{rj} X_j \right)_+ = \epsilon(G_i^1 + \epsilon G_i^2) \cos(\omega t). \quad (4.5.2)$$

An approximate solution is sought as the first two terms of the asymptotic expansion

$$X_i^\epsilon = X_i^0 + \epsilon X_i^1 + \mathcal{O}(\epsilon^2).$$

### 4.5.1 Multiple scales expansion of forced system with unilateral contact

The object is to determine initial conditions  $a_i, \forall i \in \{2, \dots, n\}$  in order to obtain a periodic solution of system (4.5.2). The triple scales method yields the following equations:

$$\frac{\partial^2 X_i^0}{\partial T_0^2} + \omega_i^2 X_i^0 = 0, \quad (4.5.3)$$

$$\frac{\partial^2 X_i^1}{\partial T_0^2} + \omega_i^2 X_i^1 = -2 \frac{\partial^2 X_i^0}{\partial T_0 \partial T_1} - \phi_{ri} \left( \sum_{j=1}^n \phi_{rj} X_j^0 \right)_+ - C_{ii} \frac{\partial X_i^0}{\partial T_0} + G_i^1 \cos(\omega T_0), \quad (4.5.4)$$

with the initial conditions:

$$\begin{cases} X_1^\epsilon(0) = X_1^0(0) + \epsilon X_1^1(0) = a_0 + \epsilon a_1, & \dot{X}_1^\epsilon(0) = 0, \\ X_i^\epsilon(0) = X_i^0(0) + \epsilon X_i^1(0) = \epsilon a_i, & \dot{X}_i^\epsilon(0) = 0, \quad \forall i \in \{2, \dots, n\}. \end{cases} \quad (4.5.5)$$

Note that  $\forall i \in \{2, \dots, n\}$  equation (4.5.3) has a trivial solution  $X_i^0 = 0$  since  $X_i^0(0) = 0$ . However  $X_1^0 = a(T_1, T_2) \cos(\omega_1 T_0 + \varphi(T_1, T_2))$  as  $X_1^0(0) = a_0$  and  $\dot{X}_1^0(0) = 0$ . By updating equation (4.5.4), we have

$$\frac{\partial^2 X_i^1}{\partial T_0^2} + \omega_i^2 X_i^1 = -\phi_{ri}(\phi_{r1} X_1^0)_+ + G_i^1 \cos(\omega T_0), \quad \forall i \in \{2, \dots, n\}. \quad (4.5.6)$$

**Proposition 4.5.1.** *The initial conditions  $a_i, \forall i \in \{2, \dots, n\}$  needed to ensure a periodic solution of system (4.5.2) are equal to those defined in proposition 4.4.3 if  $G_i^1 = 0, \forall i \in \{2, \dots, n\}$ . This means that systems (4.5.2) and (4.4.2) have the same normal mode if the first order term of the excitation force  $G_1^1$  is tangent to the eigenvector of the linearized system.*

*Proof.* The proof consists in showing that if  $G_i^1 = 0, \forall i \in \{2, \dots, n\}$ , then the equations which define  $a_i, \forall i \in \{2, \dots, n\}$  for system (4.5.2) are equivalent to the equation defining the initial condition  $a_i$  for system (4.4.2). This is immediate since equation (4.5.6) is equivalent to equation (4.4.18) after setting  $G_i^1 = 0, \forall i \in \{2, \dots, n\}$ .  $\square$

We still need to solve equation (4.5.4) for  $i = 1$  to find the period of the solution

$$\frac{\partial^2 X_1^1}{\partial T_0^2} + \omega_1^2 X_1^1 = -2 \frac{\partial^2 X_1^0}{\partial T_0 \partial T_1} - \phi_{r1} \left( \sum_{j=1}^n \phi_{rj} X_j^0 \right)_+ - C_{11} \frac{\partial X_1^0}{\partial T_0} + G_1^1 \cos(\omega T_0), \quad (4.5.7)$$

The same technique as in Section 4.2.1 is used, it consists in removing the secular terms from the right hand side of the equation. For convenience we denote by  $\xi = \frac{C_{11}}{2}, g = G_1$  and  $\gamma = \sigma T_1 - \varphi$

**Proposition 4.5.2.** *The first order term of the solution  $X_1^1$  is given as,*

$$X_1^1 = -\frac{\phi_{r1} |\phi_{r1} a|}{\omega_1^2 \pi} - \frac{2\phi_{r1} |\phi_{r1} a|}{\omega_1^2 \pi} \sum_{k=1}^{+\infty} \frac{(-1)^k}{(4k^2 - 1)^2} \cos(2k(\omega_1 T_0 + \sigma T_1 - \gamma)) + A_1 \cos(\omega_1 T_0), \quad (4.5.8)$$

where

$$A_1 = a_1 + \frac{\phi_{r1} |\phi_{r1} a|}{\omega_1^2 \pi} + \frac{2\phi_{r1} |\phi_{r1} a|}{\omega_1^2 \pi} \sum_{k=1}^{+\infty} \frac{(-1)^k}{(4k^2 - 1)^2},$$

$a$  and  $\gamma$  are solution of the following differential system,

$$\begin{cases} \frac{\partial a}{\partial T_1} = -\xi a + \frac{g}{2\omega_1} \sin(\gamma), & a(0, 0) = a_0, \\ \frac{\partial \gamma}{\partial T_1} = \sigma - \frac{\phi_{r1}^2}{4\omega_1} + \frac{g}{2a\omega_1} \cos(\gamma) & \gamma(0, 0) = 0. \end{cases} \quad (4.5.9)$$

*Proof.* Substituting  $X_1^0 = a(T_1, T_2) \cos(\omega_1 T_0 + \varphi(T_1, T_2)), \xi = \frac{C_{11}}{2}, g = G_1$  and

$$(\phi_{r1} a(T_1, T_2) \cos(\omega_1 T_0 + \varphi(T_1, T_2)))_+ = -\frac{\phi_{r1} a \cos(\omega_1 T_0 + \varphi)}{2} - \frac{|\phi_{r1} a \cos(\omega_1 T_0 + \varphi)|}{2}$$

in equation (4.5.7) and factorizing we have

$$\begin{aligned}
\frac{\partial^2 X_1^1}{\partial^2 T_0} + \omega_1^2 X_1^1 &= \left( -g \sin(\sigma T_1 - \varphi) + 2\omega_1 \frac{\partial a}{\partial T_1} + 2\omega_1 \xi a \right) \sin(\omega_1 T_0 + \varphi) \\
&\quad \left( g \cos(\sigma T_1 - \varphi) + 2\omega_1 a \frac{\partial \varphi}{\partial T_1} - \frac{\phi_{r1}^2 a}{2} \right) \cos(\omega_1 T_0 + \varphi) \\
&\quad - \frac{\phi_{r1} |\phi_{r1} a \cos(\omega_1 T_0 + \varphi)|}{2}, \quad X_1^1(0) = a_1, \quad \dot{X}_1^1(0) = 0.
\end{aligned} \tag{4.5.10}$$

By setting the secular terms to zeros and denoting by  $\gamma = \sigma T_1 - \varphi$  we directly get system (4.5.9) and the following differential equation

$$\frac{\partial^2 X_1^1}{\partial^2 T_0} + \omega_1^2 X_1^1 = -\frac{\phi_{r1} |\phi_{r1} a \cos(\omega_1 T_0 + \varphi)|}{2}, \quad X_1^1(0) = a_1, \quad \dot{X}_1^1(0) = 0, \tag{4.5.11}$$

where the solution is given in the proof of proposition 4.4.2 □

## 4.5.2 Bounds on the remainder

As in the previous section, we will study the remainder of the approximate solution to ensure that it is bounded and then to prove our asymptotic solutions. The equation which relies the remainder and the approximate solution can be obtained by substituting the following approximate solution in equation (4.5.2):

$$X^\epsilon = X_i^0 + \epsilon X_i^1 + \epsilon^2 r_i, \quad \forall i \in \{1, \dots, n\}. \tag{4.5.12}$$

**Proposition 4.5.3.** *The remainder  $r_i$  is then solution of the following differential equation*

$$\begin{aligned}
\frac{\partial^2 r_i}{\partial^2 T_0} + \epsilon \frac{\partial r_i}{\partial T_0} + \omega_i^2 r_i &= S_i(T_0, T_1, T_2) + f_i^\epsilon(T_0, T_1, T_2) + \epsilon g_i^\epsilon(T_0, T_1, T_2, r_j), \\
r_i(0) &= 0, \quad \dot{r}_i(0) = 0,
\end{aligned} \tag{4.5.13}$$

where

$$\begin{aligned}
S_i(T_0, T_1, T_2) &= -\frac{\partial^2 X_i^0}{\partial^2 T_1} - 2 \frac{\partial^2 X_i^1}{\partial T_0 \partial T_1} - 2 \frac{\partial^2 X_i^0}{\partial T_0 \partial T_2} - C_{ii} \frac{\partial X_i^0}{\partial T_1} - C_{ii} \frac{\partial X_i^1}{\partial T_0} \\
&\quad + G_i^2 \cos(\omega T_0) - \phi_{ri} H(u)v, \\
f_i^\epsilon(T_0, T_1, T_2) &= \epsilon \left( -\frac{\partial^2 X_i^1}{\partial T_1^2} - 2 \frac{\partial^2 X_i^0}{\partial T_1 \partial T_2} - 2\epsilon \frac{\partial^2 X_i^1}{\partial T_1 \partial T_2} - 2\epsilon \frac{\partial^2 X_i^1}{\partial T_0 \partial T_2} - \epsilon \frac{\partial^2 X_i^0}{\partial^2 T_2} - \epsilon^2 \frac{\partial^2 X_i^1}{\partial^2 T_2} \right) \\
&\quad \epsilon \left( -C_{ii} \frac{\partial X_i^1}{\partial T_1} - C_{ii} \frac{\partial X_i^0}{\partial T_2} - \epsilon C_{ii} \frac{\partial X_i^1}{\partial T_2} \right) - \phi_{ri} \chi(u, v) \\
&\quad - \left( 2\epsilon \frac{\partial^2 r_i}{\partial T_0 \partial T_1} + \epsilon^2 \frac{\partial^2 r_i}{\partial^2 T_1} + 2\epsilon^2 \frac{\partial^2 r_i}{\partial T_0 \partial T_2} + 2\epsilon^3 \frac{\partial^2 r_i}{\partial T_1 \partial T_2} + \epsilon^4 \frac{\partial^2 r_i}{\partial^2 T_2} + \epsilon \frac{\partial r_i}{\partial T_1} + \epsilon^2 \frac{\partial r_i}{\partial T_2} \right), \\
g_i^\epsilon(T_0, T_1, T_2, r^1, \dots, r^n) &= -\phi_{ri} \frac{[(u + \epsilon v + \epsilon^2 w)_+ - (u + \epsilon v)_+]}{\epsilon^2}.
\end{aligned}$$

such that  $u = \phi_{r1} X_1^0$ ,  $v = \sum_j^n \phi_{rj} X_j^1$  and  $w = \sum_j^n \phi_{rj} r_j$ .

The proof is similar to the proof of Proposition 4.4.1. The following Lemma is needed to proof that the remainder is bounded, it is a general case of Lemma 6.3 of [31] where a damping term is added.

**Lemma 4.5.4. [Bounds for large time ]**

Let  $w_\epsilon$  be a solution of

$$\begin{cases} w_\epsilon'' + \epsilon w_\epsilon' + w_\epsilon = S(s) + f_\epsilon(s) + \epsilon g_\epsilon(s, w_\epsilon), \\ w_\epsilon(0) = 0, \quad w_\epsilon'(0) = 0. \end{cases} \quad (4.5.14)$$

If source terms satisfy the following conditions where  $M > 0$ ,  $C > 0$  are fixed constants :

1.  $S(s)$  is a  $2\pi$ -periodic function orthogonal to  $e^{\pm is}$ , and  $|S(s)| \leq M$  for all  $s$ ,

2.  $|f_\epsilon| \leq M$  and for all  $T$ ,  $\int_0^T |f_\epsilon(s)| ds \leq C\epsilon T$  (resp.  $C\sqrt{\epsilon}T$ ),

3. for all  $R > 0$ :  $M_R = \sup_{\epsilon \in (0,1), s > 0, R > |u|} |g_\epsilon(s, u)| < \infty$ ,

that is to say that  $g_\epsilon(s, u)$  is locally bounded with respect to  $u$  independently from  $\epsilon \in (0, 1)$  and  $s \in (0, +\infty)$ ,

then, there exists  $\epsilon_0 > 0$  and  $\gamma > 0$  such that, for  $0 < \epsilon < \epsilon_0$ ,  $w_\epsilon$  is uniformly bounded in  $W^{2,\infty}(0, T_\epsilon)$ , where  $T_\epsilon = \frac{\gamma}{\epsilon}$  (resp.  $\frac{\gamma}{\sqrt{\epsilon}}$ ).

Notice that  $f_\epsilon$  and  $g_\epsilon$  are not necessarily continuous. But in previous sections the right hand side is globally continuous, i.e.  $S + f_\epsilon + \epsilon g_\epsilon(\cdot, w_\epsilon)$  is continuous, so, in this case,  $w_\epsilon$  is  $C^2$ .

*Proof.* First we remove the non resonant periodic source term. Second, we get  $L^\infty$  bound for  $w_\epsilon$  and  $w_\epsilon'$  with an energy estimate. Third, with equation (4.5.14), we get an uniform estimate for  $w_\epsilon''$  in  $L^\infty(0, T_\epsilon)$  and the  $W^{2,\infty}$  regularity.

Step 1: remove  $S$

It suffices to write  $w_\epsilon = w_1 + w_2^\epsilon$  where  $w_1$  solves the linear problem:

$$w_1'' + \epsilon w_1' + w_1 = S(s), \quad w_1(0) = 0, \quad w_1'(0) = 0. \quad (4.5.15)$$

$w_1$  and  $w_1'$  are uniformly bounded in  $L^\infty(0, +\infty)$  since there is no resonance.

More precisely,  $w_1 = F(s) + Ae^{-\frac{\epsilon}{2}s} \cos\left(\frac{\sqrt{4-\epsilon^2}}{2}s\right) + Be^{-\frac{\epsilon}{2}s} \sin\left(\frac{\sqrt{4-\epsilon^2}}{2}s\right)$ , where  $F$  is  $2\pi$  periodic.  $F$  is obtained by Fourier expansion without harmonic  $n = \pm 1$  since  $S$  is never resonant:

$$F(s) = \sum_{n \neq \pm 1} \frac{c_n}{1 - n^2 + i\epsilon n} e^{ins} \quad \text{with} \quad S(s) = \sum_{n \neq \pm 1} c_n e^{ins}. \quad (4.5.16)$$

$F$  is uniformly bounded, with Cauchy-Schwarz inequality set  $C_0^2 = \sum_{n \neq \pm 1} |n^2 - 1 - i\epsilon n|^{-2}$ ,

we obtain:

$$\|F\|_{L^\infty} \leq \sum_{n \neq \pm 1} \frac{|c_n|}{|n^2 - 1 - i\epsilon n|} \leq C_0 \|S\|_{L^2(0, 2\pi)} \leq C_0 \|S\|_{L^\infty(0, 2\pi)}. \quad (4.5.17)$$

Similarly, set  $D_0^2 = \sum_{n \neq \pm 1} n^2 |n^2 - 1 - i\epsilon n|^{-2}$ , we have  $\|F'\|_{L^\infty} \leq D_0 \|S\|_{L^\infty(0, 2\pi)}$ .

Furthermore,  $0 = w_1(0) = F(0) + A$ , and  $0 = (w_1)'(0) = F'(0) + B$ , then,  $A$  and  $B$  are well defined.  $w_1$  is also bounded, i.e. there exists  $M_1 > 0$  such that  $\|w_1\|_{W^{1, \infty}(0, +\infty)} \leq M_1$ . Notice that from equation (4.5.15),  $w_1$  belongs in  $W^{2, \infty}$ .

Then we get an equation similar to (4.5.14) for  $w_2^\epsilon$  with  $S \equiv 0$  and the same assumption for the same  $f_\epsilon$  and the new  $g_\epsilon$ :  $\bar{g}_\epsilon(s, w) = g_\epsilon(s, w_1 + w)$ .

$$\begin{cases} (w_2^\epsilon)'' + (w_2^\epsilon)' + (w_2^\epsilon) = f_\epsilon(s) + \epsilon \bar{g}_\epsilon(s, w_2^\epsilon), \\ (w_2^\epsilon)(0) = 0, \quad (w_2^\epsilon)'(0) = 0. \end{cases} \quad (4.5.18)$$

### Step 2: energy estimate

Second, we get an energy estimate for  $w_2^\epsilon$ . We fix  $R > 0$  such that  $R$  is greater than the uniform bound  $M_1$  obtained for  $w_\epsilon^1$ ,  $R = M_1 + \rho$  with  $\rho > 0$ . Let us define

$$2E(s) = ((w_2^\epsilon)'(s))^2 + (w_2^\epsilon(s))^2 + \epsilon \frac{1}{2} \int_0^s ((w_2^\epsilon)')^2 dt, \quad \bar{E}(s) = \sup_{0 < \tau < s} E(\tau), \quad (4.5.19)$$

and  $T_\epsilon$  be the first time  $T > 0$  such that  $2\bar{E}(T) \geq \rho^2$ , i.e.  $\rho$  estimates the size of  $(w_2^\epsilon)$  and  $(w_2^\epsilon)'$ .

Multiplying the differential equation (4.5.18) by  $(w_2^\epsilon)'$ , we have for all  $s < T < T_\epsilon(\rho)$  the following inequalities since  $\sup_{0 < \tau < s} |(w_2^\epsilon)'(\tau)| \leq \sqrt{2\bar{E}(s)}$ , and  $\int_0^s |f_\epsilon(s)| ds \leq C\epsilon T$ ,

$$\begin{aligned} E(s) &= \int_0^s f_\epsilon(\tau) (w_2^\epsilon)'(\tau) d\tau + \epsilon \int_0^s \bar{g}_\epsilon(\tau, (w_2^\epsilon)(\tau)) (w_2^\epsilon)'(\tau) d\tau, \\ &\leq C\epsilon s \sqrt{2\bar{E}(s)} + \epsilon s M_R \sqrt{2\bar{E}(s)}, \\ \bar{E}(T) &\leq C\epsilon T \sqrt{2\bar{E}(T)} + \epsilon T M_R \sqrt{2\bar{E}(T)}, \\ \epsilon T &\geq \frac{\sqrt{\bar{E}(T)}/2}{M_R + C}. \end{aligned} \quad (4.5.20)$$

Notice that if  $2\bar{E}(T) < \rho^2$  for all  $T > 0$  then  $T_\epsilon = +\infty$ . The critical case is when  $T_\epsilon$  is finite and  $\bar{E}(T)$  approaches  $\rho^2/2$  when  $T$  goes to  $T_\epsilon(\rho)$ . Thus we have  $T_\epsilon \geq \frac{\rho}{2\epsilon(M_R + C)}$

and  $E(t) \leq \frac{\rho^2}{2}$  for  $t \leq T_\epsilon = \frac{\gamma}{\epsilon}$  with  $\gamma = \frac{\rho}{2(M_R + C)}$ .

The proof is similar when  $\int_0^s |f_\epsilon(\tau)| d\tau \leq C\sqrt{\epsilon}T$  then  $T_\epsilon \geq \frac{\rho}{2\sqrt{\epsilon}(\sqrt{\epsilon}M_R + C)}$ .  $\square$

**Lemma 4.5.5. [Bounds for large time for systems]**

Let  $w_\epsilon = (w_1^\epsilon, \dots, w_N^\epsilon)$  be the solution of the following system:

$$\begin{cases} (\lambda_1)^2 (w_k^\epsilon)'' + \epsilon (w_k^\epsilon)' + (\lambda_k)^2 w_k^\epsilon = S_k(s) + f_k^\epsilon(s) + \epsilon g_k^\epsilon(s; w_\epsilon), \\ w_k^\epsilon(0) = 0, \quad (w_k^\epsilon)'(0) = 0, \quad k = 1, \dots, N. \end{cases} \quad (4.5.21)$$

If source terms satisfy the following conditions where  $M > 0, C > 0$  are fixed constants :

1. non resonance conditions with  $S_k(s)$  are  $2\pi$ -periodic functions and  $|S_k(s)| \leq M$ ,

(a)  $S_1(s)$  is orthogonal to  $e^{\pm is}$ , i.e.  $\int_0^{2\pi} S_1(s) e^{\pm is} ds = 0$ ,

(b)  $\lambda_k, \lambda_1$  are  $\mathbb{Z}$  independent for all  $k \neq 1$ ,

2.  $|f_k^\epsilon| \leq M$  and for all  $T$ ,  $\int_0^T |f_\epsilon(s)| ds \leq C\epsilon T$  or  $C\sqrt{\epsilon}T$ ,

3. for all  $R > 0$ :  $M_R = \max_k \sup_{\epsilon \in (0,1), s > 0, w_1^2 + \dots + w_N^2 < R^2} |g_k^\epsilon(s; u)| < \infty$ ,

then, there exists  $\epsilon_0 > 0$  and  $\gamma > 0$  such that, for  $0 < \epsilon < \epsilon_0$ ,  $w_\epsilon$  is uniformly bounded in  $W^{2,\infty}(0, T_\epsilon)$ , where  $T_\epsilon = \frac{\gamma}{\epsilon}$  ( resp  $\frac{\gamma}{\sqrt{\epsilon}}$ ).

*Proof.* The proof of this Lemma is inspired from the proof of Lemma 4.4.5, see Lemma 6.4 of [31] for technical details.  $\square$

**Proposition 4.5.6.** If  $a$  and  $\gamma$  verify system 4.5.22 and 4.5.9 then There exists  $\epsilon_0 > 0$  and  $\gamma > 0$  such that, for  $0 < \epsilon < \epsilon_0$ , the remainder  $(r_i)_{i=1,\dots,n}$  is uniformly bounded in  $W^{2,\infty}(0, T_\epsilon)$ , where  $T_\epsilon = \frac{\gamma}{\epsilon}$ .

*Proof.* The proof is similar to the proof of Proposition 4.4.6. The nonlinear terms  $f_i^\epsilon$  and  $g_i^\epsilon$  verify the second and the third conditions of Lemma 4.5.4 after moving the derivative of  $r_i$  to the left hand side . We have to find the conditions on  $S_1$  which ensure a bounded solution, i.e. we have to remove the secular terms. To do this, we set  $G_1^2$  to zero, it is not a restrictive case since the term of first order of the excitation force is not zero ( $G_1^1 \neq 0$ ).  $S_1$  is then given as

$$S_1(T_0, T_1, T_2) = -\frac{\partial^2 X_i^0}{\partial T_1^2} - 2\frac{\partial^2 X_i^1}{\partial T_0 \partial T_1} - 2\frac{\partial^2 X_i^0}{\partial T_0 \partial T_2} - C_{ii} \frac{\partial X_i^0}{\partial T_1} - C_{ii} \frac{\partial X_i^1}{\partial T_0} - \phi_{ri} H(u) v$$

$X_1^1$  does not contains any term at the frequency  $\omega_1$  if we take  $A_1 = 0$  in Proposition 4.5.2.  $v$  does not also have any resonant term as well as  $H(u)$ . We still have

$$-\frac{\partial^2 X_i^0}{\partial T_1^2} - 2\frac{\partial^2 X_i^0}{\partial T_0 \partial T_2} - 2\zeta \frac{\partial X_i^0}{\partial T_1}$$

which can have secular terms. A simple calculation gives:

$$\begin{aligned}
& -\frac{\partial^2 X_i^0}{\partial^2 T_1} - 2\frac{\partial^2 X_i^0}{\partial T_0 \partial T_2} - 2\xi \frac{\partial X_i^0}{\partial T_1} = \\
& \left( -\frac{\partial^2 a}{\partial^2 T_1} + a\left(\sigma - \frac{\partial \gamma}{\partial T_1}\right)^2 + 2a\frac{\partial \gamma}{\partial T_2}\omega_1 - 2\xi\frac{\partial a}{\partial T_1} \right) \cos(\omega_1 T_0 + \sigma T_1 - \gamma) \\
& + \left( 2\left(\frac{\partial a}{\partial T_1} + \xi a\right)\left(\sigma - \frac{\partial \gamma}{\partial T_1}\right) + a\frac{\partial^2 \gamma}{\partial^2 T_1} + 2\frac{\partial a}{\partial T_2}\omega_1 \right) \sin(\omega_1 T_0 + \sigma T_1 - \gamma)
\end{aligned}$$

The coefficients of the secular terms in the expression of  $S_1$  have to be set to zero to ensure the first hypothesis of the lemma:

$$\begin{cases} 2a\frac{\partial \gamma}{\partial T_2}\omega_1 = \frac{\partial^2 a}{\partial^2 T_1} - a\left(\sigma - \frac{\partial \gamma}{\partial T_1}\right)^2 + 2\xi\frac{\partial a}{\partial T_1}, & \gamma(0,0) = 0, \\ 2\frac{\partial a}{\partial T_2}\omega_1 = -2\left(\frac{\partial a}{\partial T_1} + \xi a\right)\left(\sigma - \frac{\partial \gamma}{\partial T_1}\right) - a\frac{\partial^2 \gamma}{\partial^2 T_1}, & a(0,0) = 0. \end{cases} \quad (4.5.22)$$

This conditions should be added to the conditions of system 4.5.9 to ensure a bounded solution. □

### 4.5.3 Approximate steady state solution

A stationary solution for system (4.5.9) can be found for  $\frac{\partial a}{\partial T_1} = 0$  and  $\frac{\partial \gamma}{\partial T_1} = 0$ , this yields the following frequency response equation:

$$a^2 = \frac{g^2}{4\omega_1^2 \left( \xi^2 + \left( \sigma - \frac{\phi_{r1}^2}{4\omega_1} \right)^2 \right)} \quad (4.5.23)$$

The steady state solution is then given as

$$\begin{aligned}
X_1^0 &= a \cos(\omega t - \gamma), \\
X_1^1 &= -\frac{\phi_{r1}|\phi_{r1}a|}{\omega_1^2 \pi} - \frac{2\phi_{r1}|\phi_{r1}a|}{\omega_1^2 \pi} \sum_{k=1}^{+\infty} \frac{(-1)^{k+1}}{(4k^2 - 1)^2} \cos(2k(\omega t - \gamma)) + A_1 \cos(\omega_1 t).
\end{aligned}$$

This shows that the steady state solution has the same period as the excitation force with a phase delay in addition to the harmonics generated by the nonlinear term. It is in agreement with the solution of the single degree of freedom oscillator calculated for equation (4.2.1). Note that the frequency of the response depends only on the frequency of the excitation force. This is true as the damping matrix reduces the effect of the natural frequencies of the system being excited by the force when time goes to infinity.

#### 4.5.4 Stability of the approximate solution

The steady state solution of equation (4.2.1) was stable. The same technique shows that the solution of system (4.5.1) is also stable. We will just calculate the Jacobian corresponding to system (4.5.9) which is given as follows

$$\begin{bmatrix} -\xi & a_0(\frac{\phi_{r1}}{4} - \sigma) \\ -\frac{1}{a_0}(\frac{\phi_{r1}}{4} - \sigma) & -\xi \end{bmatrix}. \quad (4.5.24)$$

It has negative eigenvalues since its trace is negative and its determinant is positive, refer to the first section for more details.

#### 4.5.5 Alternative Calculation of the nonlinear normal modes with an excitation force

The amplitude of the steady state response depends only on the excitation frequency and magnitude, it does not depend on the initial conditions. This amplitude is given in the frequency response in equation (4.5.23). When this amplitude is maximum, it puts in evidence a resonance phenomena, the solution stays bounded due to the damping term. We deduce that this amplitude is maximum for a  $\sigma$  value which corresponds to the period of the nonlinear normal mode of the autonomous system (4.4.28).

**Proposition 4.5.7.** *The amplitude  $a$  of the response is maximum if  $\sigma = \frac{\phi_{r1}^2}{4\omega_1}$  and then the excitation frequency which leads to a nonlinear normal mode is*

$$\omega = \omega_1 + \epsilon\sigma = \omega_1 + \epsilon\frac{\phi_{r1}^2}{4\omega_1}.$$

*It corresponds to the first order approximation of the nonlinear normal mode of the autonomous system (4.4.28)*

*Proof.* We differentiate  $a$  in equation (4.5.23) with respect to  $\sigma$ , we find easily

$$\frac{\partial a}{\partial \sigma} = \frac{-g(\sigma - \frac{\phi_{r1}^2}{4\omega_1})}{2\omega_1 \left( \xi^2 + (\sigma - \frac{\phi_{r1}^2}{4\omega_1})^2 \right)^{\frac{3}{2}}},$$

which shows that  $a$  is maximum when  $\sigma = \frac{\phi_{r1}^2}{4\omega_1}$ . □

This proposition opens the door to the experimental validation, but not completely: the excitation force used for the calculation of an analytical solution has a special form, it is of first order in the direction of the first eigenvector with components of order  $\epsilon$  on the other eigenvectors. This form is not workable experimentally and the experiments are more suitable for a punctual excitation in the real space which leads to non zero components on all the eigenvectors. The problem can then be treated by exciting the system with a force which has components on all the eigenvectors, this can complicate the calculation of an analytical

solution. But the choice of the form of the excitation force is not capital as the choice of the excitation frequency! If all components of the system are excited by a frequency near an eigenfrequency, only the component which corresponds to this frequency will have a large solution and the other solutions will be neglected. This aspect is not proved mathematically but we have done numerical simulations to confirm this idea. We give a procedure to find a nonlinear normal mode using an excitation force:

1. Define the level of the nonlinearity  $\epsilon$ .
2. Define which nonlinear normal mode to be found.
3. Find the nonlinear frequency of the system. This can be done by three methods using: A Frequency sweep, the numerical algorithm of Chapter 3 or the approximate period by multiple scales of the autonomous system.
4. Excite the system on a point at this frequency for long time to establish the permanent regime.
5. Extract a time solution long a period of excitation, this is an approximation of the nonlinear normal mode.
6. The displacement of the nodes can be obtained in the space domain, this gives the deflexion mode shapes of the structure.

The method use the integration of a nonlinear differential system, it is then simple to be used in term of computation time and implementation.

### 4.5.6 Numerical results of a cantilever beam with a unilateral elastic contact

We apply the procedure described above to find the first two approximate nonlinear normal modes of a the cantilevered beam system studied in Section 4.4.6. The beam is under a punctual harmonic excitation. Figure 4.13 shows the first nonlinear normal mode of the beam, the excitation frequency is calculated using the approximate period of the autonomous system:  $\omega = \omega_1 + \epsilon \frac{\phi_{r1}^2}{4\omega_1}$ . The nonlinear frequency is 77.58 Hz and the linear one is 52.7 Hz, and that is for a stiffness  $k_r = 107000$  N/m and for  $\epsilon = 5$ . Figure 4.15 shows the time steady state solution for 50 periods of the first nonlinear normal mode. Figure 4.14 shows the first deflexion mode shape of the beam for two time points corresponding to a period of excitation. Figure 4.16 shows the second nonlinear normal mode in the time domain for  $k_r = 107000$  N/m and for  $\epsilon = 5$ . The nonlinear frequency is 340 Hz and the linear one is 328.5 Hz. Figure 4.18 shows the time steady state solution for 50 periods of the second nonlinear normal mode. The second deflexion mode shape is also plotted in Figure 4.17.

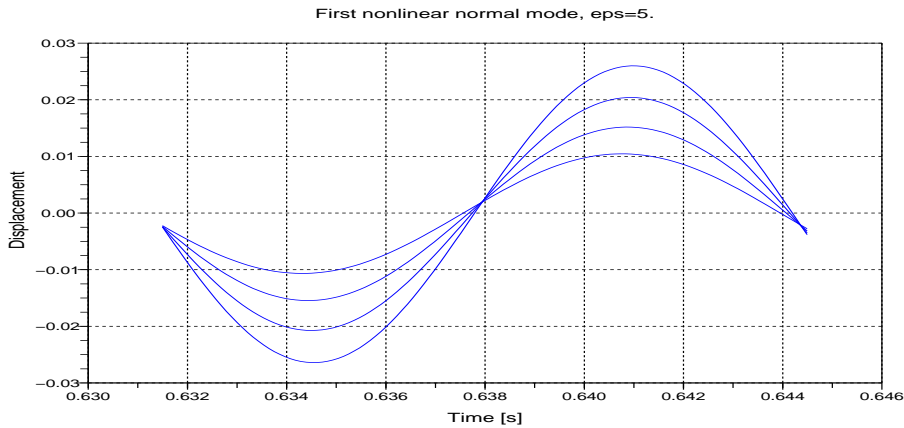


Figure 4.13. The first approximate nonlinear normal mode, the nonlinear frequency is 77.58 Hz for  $\epsilon = 5$  and  $k_r = 107000$  N/m.

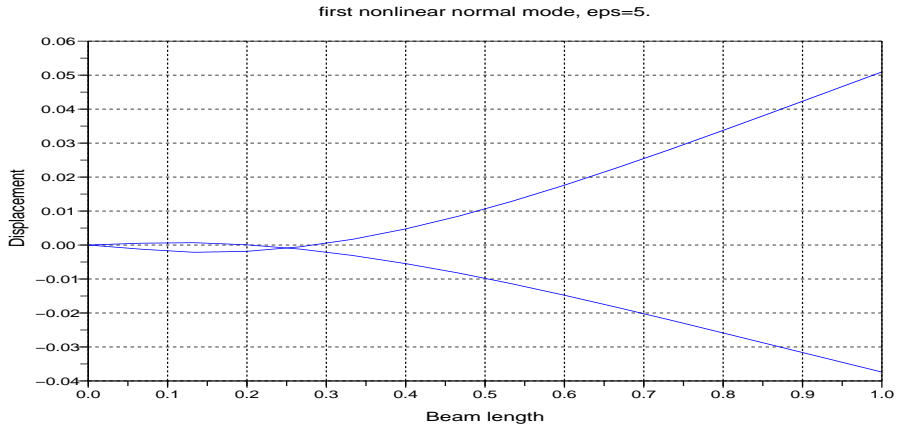


Figure 4.14. The first deflexion mode shape for two time points

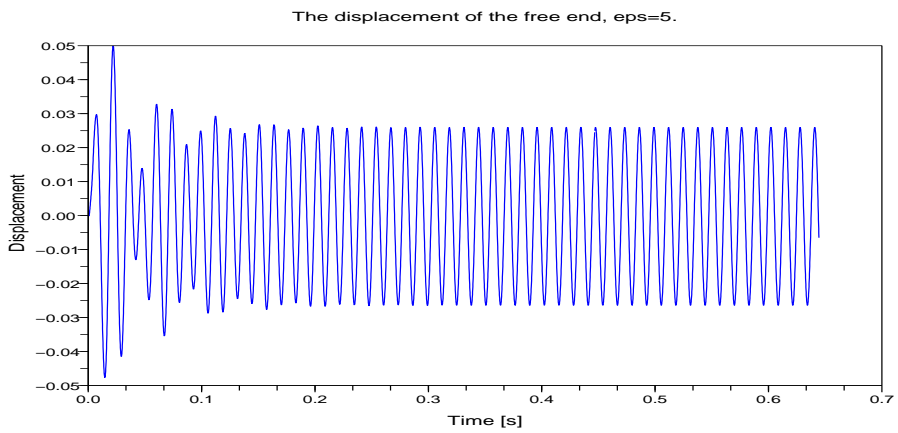


Figure 4.15. The displacement of the last node for 50 nonlinear periods for an excitation at the first nonlinear mode

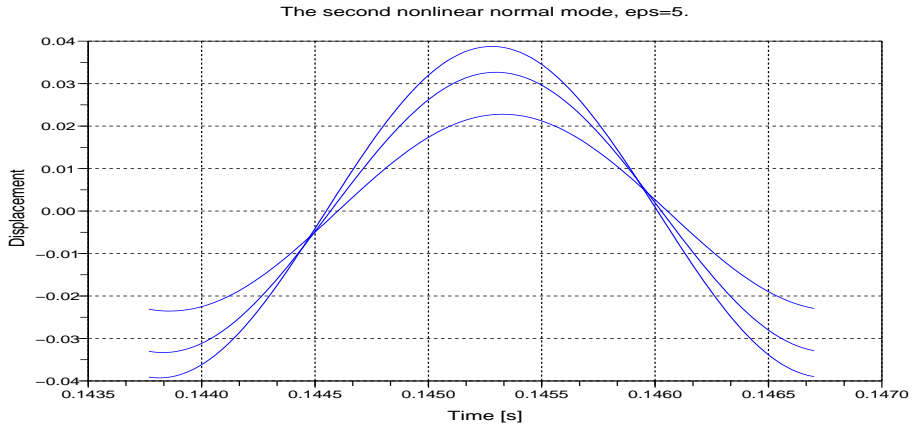


Figure 4.16. The second approximate nonlinear normal mode, the nonlinear frequency is 340 Hz for  $\epsilon = 5$  and  $k_r = 107000$  N/m.

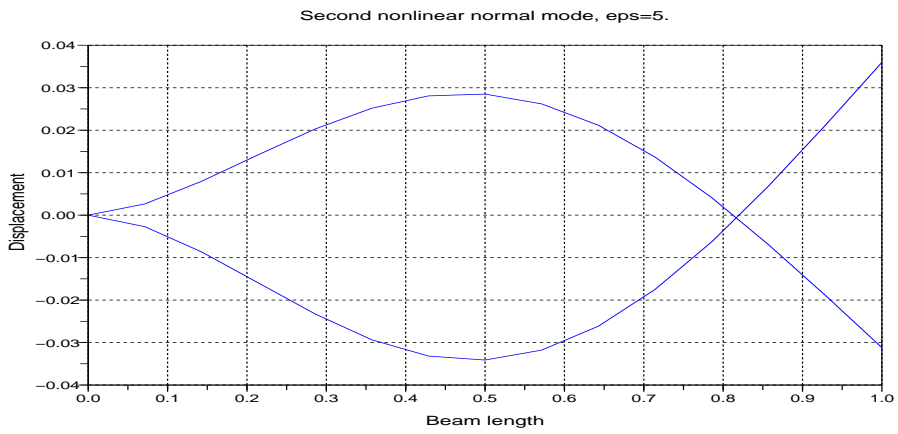


Figure 4.17. The second deflexion mode shape for two time points

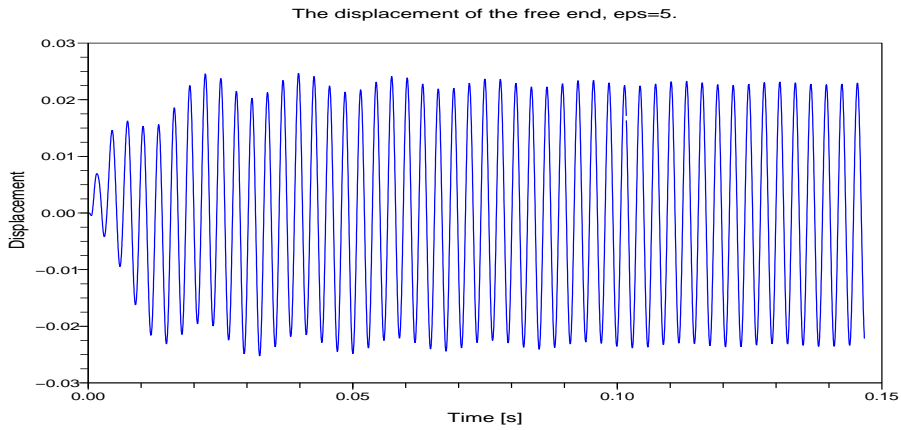


Figure 4.18. The displacement of the last node for 50 nonlinear periods for an excitation at the second nonlinear mode

## 4.6 conclusion

The multiple scales method has been used to calculate the nonlinear normal modes of mechanical system with a unilateral contact. All the asymptotic solutions are proved for a time intervals  $[0, T\epsilon]$  with  $T\epsilon \sim \frac{1}{\epsilon}$ . The methods has also been used for system with a force excitation in presence of a damping term. The results are compared to the numerical solutions computed using the algorithm of Chapter 3, very good agreement is found. A simple procedure to compute the nonlinear normal modes of a system using a harmonic excitation is described, this can be usefull for an experimental validation of the different described methods.



# General conclusion

Two major parts were discussed in the present thesis, the first one dealt with a model of a cantilever beam with a unilateral elastic contact under periodic excitation; The second part dealt with the nonlinear normal modes.

The first part consists on Chapters 1 and 2, we have presented a model of a beam sticking a snubber at the free end in three possible configurations: a simple contact, a contact with pre-stress and a contact with backlash. The whole system was under a support vibrations or a punctual excitation force. The models were validated with experimental sequences for the three configurations, a good agreement was found in all cases. This simple model was developed to predict the responses of satellite solar arrays in presence of bumpers during the launch phase.

The developed model can then predict the responses of the structure for different range of excitations, this can help to understand the effect of the unilateral contact to the whole dynamics. The nonlinear normal modes are a natural extension of the linear normal modes to nonlinear mechanical systems. We have proved the existence of these modes in the differentiable case using the implicit functions theorem which yielded a constructive way. An algorithm was also performed to compute the nonlinear normal modes of nonlinear mechanical systems. This algorithm required a gradient computation which was also done. This work was presented in Chapter 3.

In chapter 4, an asymptotic method were used to evaluate the nonlinear normal modes and to compute periodic solutions for mechanical systems with a unilateral elastic contact. The solution was compared to those obtained by the numerical algorithm of Chapter 3. It gave then an analytical validation of the numerical method. This perturbation technique was used also to compute the nonlinear normal modes of forced systems. The nonlinear modes give then an access to the modal analysis of the mechanical system studied in the first part of the thesis.



# Bibliography

- [1] G. Lebeau and M. Schatzman. A wave problem in a half-space with a unilateral constraint at the boundary. *Journal of Differential Equations*, 53(3):309 – 361, 1984.
- [2] M. Schatzman. Uniqueness and continuous dependence on data for one-dimensional impact problems. *Mathematical and Computer Modelling*, 28(4-8):1 – 18, 1998. Recent Advances in Contact Mechanics.
- [3] C. Pozzolini and A. Léger. A stability result concerning the obstacle problem for a plate. *Journal de Mathématiques Pures et Appliquées*, 90(6):505 – 519, 2008.
- [4] A. Léger and C. Pozzolini. Sur la zone de contact entre une plaque élastique et un obstacle rigide. *Comptes Rendus Mécanique*, 335(3):144 – 149, 2007.
- [5] J. H. Bonsel, R. H. B. Fey, and H. Nijmeijer. Application of a dynamic vibration absorber to a piecewise linear beam system. *Nonlinear Dynamics*, 37:227–243, 2004.
- [6] R.H.B. Fey and F.P.H. van Liempt. Sine sweep and steady-state response of a simplified solar array model with nonlinear elements. *International conference on Structural Dynamics Modelling*, pages 201 – 210, 2002.
- [7] E. L. B. van de Vorst, M. F. Heertjes, D. H. van Campen, A. de Kraker, and R. H. B. Fey. Experimental and numerical analysis of the steady state behaviour of a beam system with impact. *Journal of Sound and Vibration*, 212(2):321 – 336, 1998.
- [8] J. A. Turner. Non-linear vibrations of a beam with cantilever-hertzian contact boundary conditions. *Journal of Sound and Vibration*, 275(1-2):177 – 191, 2004.
- [9] D. Stancioiu, H. Ouyang, and J. E. Mottershead. Vibration of a beam excited by a moving oscillator considering separation and reattachment. *Journal of Sound and Vibration*, 310(4-5):1128 – 1140, 2008.
- [10] C.N. Bapat. Exact solution of stable periodic one contact per n cycles motion of a damped linear oscillator contacting a unilateral elastic stop. *Journal of Sound and Vibration*, 314(3-5):803 – 820, 2008.
- [11] H. Hazim, N. Ferguson, and B. Rousselet. The dynamics of a beam with a local unilateral elastic contact. Submitted, <http://hal.archives-ouvertes.fr/hal-00445688/en/>, 2009.

- [12] H. Hazim and B. Rousselet. Finite Elements for a Beam System With Nonlinear Contact Under Periodic Excitation. In *Ultrasonic wave propagation in non homogeneous media*, page 149, France, 2008.
- [13] H. Hazim and B. Rousselet. Frequency sweep for a beam system with local unilateral contact modeling satellite solar arrays. In *Tendances des applications mathématiques en Tunisie, Algérie, Maroc Tendances des applications mathématiques en Tunisie, Algérie, Maroc*, page 541, Maroc, 2009. <http://hal-unice.archives-ouvertes.fr/hal-00418507/en/>.
- [14] H. Hazim, B. Rousselet, and N. Ferguson. Numerical And Experimental Study For A Beam System With Local Unilateral Contact Modelling Satellite Solar Arrays. In *The 11th European Spacecraft Structures, Materials and Mechanical Testing Conference (ECSSMMT 11)*, Toulouse, France, 2009. <http://hal-unice.archives-ouvertes.fr/hal-00418509/en/>.
- [15] S. Bellizzi and R. Bouc. A new formulation for the existence and calculation of non-linear normal modes. *Journal of Sound and Vibration*, 287(3):545 – 569, 2005.
- [16] D. Jiang, C. Pierre, and S. W. Shaw. Large-amplitude non-linear normal modes of piecewise linear systems. *Journal of Sound and Vibration*, 272(3-5):869 – 891, 2004.
- [17] G. Kerschen, M. Peeters, J.C. Golinval, and A.F. Vakakis. Nonlinear normal modes, part i: A useful framework for the structural dynamicist. *Mechanical Systems and Signal Processing*, 23(1):170 – 194, 2009. Special Issue: Non-linear Structural Dynamics.
- [18] S. W. Shaw and C. Pierre. Non-linear normal modes and invariant manifolds. *Journal of Sound and Vibration*, 150(1):170 – 173, 1991.
- [19] S. Junca and B. Rousselet. Asymptotic expansions of vibrations with small unilateral contact. In *Ultrasonic wave propagation in non homogeneous media*. Springer, 2008.
- [20] B. Rousselet. Non linear vibrations for non destructive testings, ode models. In *Advances in geomaterials and structures*, pages 245–254, 2008.
- [21] G. Vanderborck B. Rousselet. Non destructive control of cables: O.d.e. models of non linear vibrations. In *Variational Formulations in Mechanics : Theory and Applications - A Workshop dedicated to the 60th Birthday of Professor Raül A. Feijoo; 3-5/9/2006*. LNCC, Petropolis, Bresil, 2006.
- [22] B. Rousselet and G. Vanderborck. Non destructive testing with non linear vibroacoustic. In Rassineux Ohayon, Grellier, editor, *Septième colloque national en Calcul de structures*, volume 2, pages 603–608. Hermes, 2005.
- [23] Scilab. A free software. Available at <http://www.scilab.org/>, 2009.
- [24] M Gérardin. *Théorie des vibrations: applications à la dynamique des structures*. Masson Paris, second edition, 1996.

- [25] R. M. Rosenberg. Steady-state forced vibrations. *International Journal of Non-Linear Mechanics*, 1(2):95 – 108, 1966.
- [26] R. M. Rosenberg. The normal modes of non-linear n-degree-of-freedom systems. *Journal of applied Mechanics*, 30:7–14, 1962.
- [27] R.H. Rand. A direct method for non-linear normal modes. *International Journal of Non-Linear Mechanics*, 9(5):363 – 368, 1974.
- [28] A. F. Vakakis. Non-linear normal modes (nnms) and their applications in vibration theory: an overview. *Mechanical Systems and Signal Processing*, 11(1):3 – 22, 1997.
- [29] E. Pesheck, C. Pierre, and S. W. Shaw. A new galerkin-based approach for accurate non-linear normal modes through invariant manifolds. *Journal of Sound and Vibration*, 249(5):971 – 993, 2002.
- [30] G.Iooss and E.Lombardi. Approximate invariant manifolds up to exponentially small terms. *Journal of Differential Equations*, 248(6):1410 – 1431, 2010.
- [31] S. Junca and B. Rousselet. The method of strained coordinates for vibrations with weak unilateral springs. preprint <http://hal-unice.archives-ouvertes.fr/hal-00395351>.
- [32] A. H. Nayfeh and S. A. Nayfeh. Nonlinear normal modes of a continuous system with quadratic nonlinearities. *Journal of Vibration and Acoustics*, 117(2):199–205, 1995.
- [33] A. H. Nayfeh, C. Chin, and S. A. Nayfeh. Nonlinear normal modes of a cantilever beam. *Journal of Vibration and Acoustics*, 117(4):477–481, 1995.
- [34] F.Vestroni, A.Luongo, and A.Paolone. A perturbation method for evaluating nonlinear normal modes of a piecewise linear two-degrees-of-freedom system. *Nonlinear Dynamics*, Volume 54(11):379 – 393, 2008.
- [35] S. Bellizzi and R. Bouc. A new formulation for the existence and calculation of non-linear normal modes. *Journal of Sound and Vibration*, 287(3):545 – 569, 2005.
- [36] R. Arquier, S. Bellizzi, R. Bouc, and B. Cochelin. Two methods for the computation of nonlinear modes of vibrating systems at large amplitudes. *Computers & Structures*, 84(24-25):1565 – 1576, 2006. *Non-linear Dynamics of Structures and Mechanical Systems*.
- [37] S. Bellizzi, P. Guillemain, and R. Kronland-Martinet. Identification of coupled non-linear modes from free vibration using time-frequency representations. *Journal of Sound and Vibration*, 243(2):191 – 213, 2001.
- [38] S. Bellizzi and R. Bouc. An amplitude-phase formulation for nonlinear modes and limit cycles through invariant manifolds. *Journal of Sound and Vibration*, 300(3-5):896 – 915, 2007.

- [39] M. Peeters, R. Vigié, G. Sérandour, G. Kerschen, and J.-C. Golinval. Nonlinear normal modes, part ii: Toward a practical computation using numerical continuation techniques. *Mechanical Systems and Signal Processing*, 23(1):195 – 216, 2009. Special Issue: Non-linear Structural Dynamics.
- [40] G. Birkhoff and G-C. Rota. *Ordinary differential equations*. Introductions to Higher Mathematics. Boston-New York-Chicago: Ginn and Company, VII, 318 p., 1962.
- [41] A. L. Dontchev and T. Zolezzi. *Well-posed optimization problems*, volume 1543 of *Lecture Notes in Mathematics*. Springer-Verlag, Berlin, 1993.
- [42] F. H. Clarke. *Optimization and nonsmooth analysis*, volume 5 of *Classics in Applied Mathematics*. Society for Industrial and Applied Mathematics (SIAM), Philadelphia, PA, second edition, 1990.
- [43] A. H. Nayfeh, C. Chin, and S. A. Nayfeh. On nonlinear normal modes of systems with internal resonance. *Journal of Vibration and Acoustics*, 118(3):340–345, 1996.
- [44] Anouar Gasmi. Méthode de la moyenne et de double échelle pour un système de corde en vibration non linéaire. <http://hal-unice.archives-ouvertes.fr/hal-00418570/PDF/gasmi27avril.pdf>.
- [45] Ben Brahim N. and B. Rousselet. Vibration d’une barre avec une loi de comportement localement non linéaire. In *Tendances des applications mathématiques en Tunisie, Algerie, Maroc Tendances des applications mathématiques en Tunisie, Algerie, Maroc*, page 479, Maroc, 2009.
- [46] A. H. Nayfeh. *Introduction to perturbation techniques*. Wiley-Interscience [John Wiley & Sons], New York, 1981. A Wiley-Interscience Publication.
- [47] R. E. Edwards. *Fourier series: a modern introduction. Vol. II*. Holt, Rinehart and Winston, Inc., New York, 1967.
- [48] Ju. L. Dalec’kiĭ and M. G. Kreĭn. *Stability of solutions of differential equations in Banach space*. American Mathematical Society, Providence, R.I., 1974. Translated from the Russian by S. Smith, Translations of Mathematical Monographs, Vol. 43.

## **Vibrations d'une poutre avec un ressort unilatéral. Solutions périodiques. Modes non-linéaires**

### **Résumé**

La thèse est composée de deux parties présentées en quatre chapitres. La première partie traite de la modélisation, des simulations et des validations expérimentales d'un modèle de poutre en contact avec un ressort linéaire unilatéral sous une excitation périodique. C'est un modèle mécanique simplifié d'un panneau solaire d'une satellite et d'une cale élastique en phase de lancement. Le système est soumis à une excitation harmonique du support sous forme d'une accélération imposée ou d'une force ponctuelle. Le modèle est validé expérimentalement par des séquences d'essais sur une poutre en aluminium en contact avec une cale en Solithane. Les résultats montrent une cohérence avec les solutions numériques obtenues. La deuxième partie est centrée sur les modes normaux non-linéaires des systèmes mécaniques. Une nouvelle formulation est présentée pour trouver ces modes comme zéros d'une application non-linéaire. Un algorithme utilisant des algorithmes existants, basé sur la continuité des solutions périodiques, est développé pour le calcul des modes normaux.

La technique de développement asymptotique par échelles multiples pour le calcul des solutions analytiques approchées d'une équation différentielle avec un terme unilatéral est introduit. On utilise ensuite cette technique pour le calcul des modes normaux non-linéaires d'un système autonome à un nombre  $n$  de degrés de liberté avec un contact unilatéral. On traite aussi le cas d'un système forcé, on conjecture ainsi que l'on obtient une procédure simple pour le calcul des modes non linéaires. L'ensemble fournit donc des outils mathématiques validés pour le calcul des modes non-linéaires du système traité dans la première partie de la thèse.

## **Vibrations of a beam with a unilateral spring. Periodic solutions. Nonlinear normal modes**

### **Abstract**

The thesis consists of two parts presented in four chapters. The first one deals with the modelling, the simulations and the experimental validations of a beam model with a unilateral linear spring under a periodic excitation. It is a simplified mechanical model of a satellite solar array and an elastic bumper during the launch stage. The system is under a harmonic excitation given as an imposed acceleration or a punctual force. The model is validated with experimental sequences on an aluminum beam in contact with a Solithane bumper. The results show a good agreement with the numerical simulations. The second part is focused on the nonlinear normal modes of mechanical systems. A new formulation is then presented to find these modes as zeros of a nonlinear mapping. An algorithm based on the continuation of periodic solutions is performed using existent algorithms. The perturbation technique using multiple scales method for the calculation of approximate analytical solutions of a differential equation with a unilateral term is introduced. We use then this technique for the calculation of the nonlinear normal modes of  $n$  degrees of freedom autonomous system with a unilateral contact. We also deal with the case of forced systems, thus we obtain a simple procedure for the calculation of the nonlinear normal modes. All these techniques provide different validated mathematical tools for a modal analysis of the mechanical system treated in the first part of the thesis.